

Research Plan for Spin Physics at RHIC

February 11, 2005

Abstract

In this report we present the research plan for the RHIC spin program. The report covers 1) the science of the RHIC spin program in a world-wide context; 2) the collider performance requirements for the RHIC spin program; 3) the detector upgrades required, including timelines; 4) time evolution of the spin program.

Authors

Christine Aidala^a, Mei Bai^b, Leslie Bland^b, Alessandro Bravar^b, Gerry Bunce^{b,c}, Mickey Chiu^d, Abhay Deshpande^{c,e}, Douglas Fields^{c,f}, Wolfram Fischer^b, Yoshinori Fukao^{g,h}, Yuji Goto^{c,h}, Matthias Grosse Perdekamp^{c,d}, Wlodek Guryn^b, Masanori Hirai^h, David Kawall^{c,i}, Edward Kistenev^b, Stefan Kretzer^{b,c}, Akio Ogawa^b, Kensuke Okada^c, Jianwei Qiu^j, Greg Rakness^{b,k}, Vladimir Rykov^h, Naohito Saito^g, Hal Spinka^l, Marco Stratmann^m, Kazutaka Sudoh^h, Bernd Surrowⁿ, Atsushi Taketani^{c,h}, Michael Tannenbaum^b, Manabu Togawa^{g,h}, Larry Trueman^b, Fleming Videbaek^b, Steve Vigdor^o, Werner Vogelsang^{b,c}, Yasushi Watanabe^{c,h}

(see next page for institutions)

^a Columbia University

^b Brookhaven National Laboratory

^c RIKEN-BNL Research Center

^d University of Illinois at Urbana-Champaign

^e State University of New York at Stony Brook

^f University of New Mexico

^g Kyoto University, Japan

^h RIKEN, Japan

ⁱ University of Massachusetts at Amherst

^j Iowa State University

^k Pennsylvania State University

^l Argonne National Laboratory

^m University of Regensburg, Germany

ⁿ Massachusetts Institute of Technology

^o Indiana University and Indiana University Cyclotron Facility

Contents

1	Executive Summary	4
2	The science case for RHIC Spin	9
2.1	Synopsis of results from polarized DIS	11
2.2	Compelling questions in spin physics	13
2.3	Unpolarized pp scattering	16
2.4	Probing the spin structure of the nucleon in polarized pp collisions	19
2.5	Exploring the gluon contribution to the proton spin	22
2.6	Global Analysis	29
2.7	W production at RHIC	31
2.7.1	Introduction	31
2.7.2	Basic concepts of W production	32
2.7.3	Experimental aspects on W production at RHIC	36
2.8	Transverse spin structure	38
2.9	What else is going on around the world?	48
2.9.1	COMPASS experiment at CERN	48
2.9.2	HERMES experiment at DESY	49
2.9.3	Nucleon Spin related experiments at Jefferson Laboratory	50
2.10	Elastic Scattering of polarized high energy protons	50
2.11	Search for Physics beyond the Standard Model	52
2.12	Connection to eRHIC	54
2.12.1	Direct Connections	55
2.12.2	Indirect Spin Connections	55
3	Accelerator performance	57
3.1	Polarization limitations	58
3.2	Luminosity limitations	59

3.3	Polarimetry	59
3.4	Long-term perspective	61
4	Experiments	63
4.1	PHENIX	63
4.1.1	PHENIX Central Arms	64
4.1.2	Muon Arms	65
4.1.3	PHENIX Local Polarimetry and Relative Luminosity Detectors	66
4.1.4	PHENIX DAQ and Computing	68
4.1.5	PHENIX Detector upgrades	69
4.2	STAR	72
4.2.1	Recent spin-related upgrades	72
4.2.2	Future STAR upgrades relevant to the spin physics program	75
4.3	Other experiments	80
4.3.1	PP2PP	80
4.3.2	BRAHMS	80
4.3.3	Jet Target Experiment	82
4.3.4	Large Acceptance New RHIC Detector	82
5	Spin plan schedule	84
5.1	10 physics weeks	84
5.2	5 physics weeks	85
6	Summary	87
7	Appendix: the charge from DOE	89

1 Executive Summary

An action item from the June 30-July 1, 2004 DOE Office of Nuclear Physics Science and Technology Review of the Brookhaven National Laboratory (BNL) Relativistic Heavy Ion Collider (RHIC) written Report, dated September 13, 2004, was that "*BNL should prepare a document that articulates its research plan for the RHIC spin physics program. A copy should be submitted to DOE by January 31, 2005.*" This document is submitted to the DOE Office of Nuclear Physics on behalf of the Laboratory, in response to that action item.

We provide here a plan that addresses: 1) the science of the RHIC spin program in a world-wide context; 2) the collider performance requirements for the RHIC spin program; 3) the detector upgrades required, including timelines; 4) time evolution of the spin program. The RHIC Spin Plan Group was charged to formulate the plan by Thomas Kirk, BNL Associate Director for High Energy and Nuclear Physics. The charge is given in the appendix.

The importance of the study of nucleon spin to nuclear physics and the anticipated contribution of RHIC is discussed in the first section of this report. Spin plays a central role in our theory of the strong interactions, *Quantum Chromodynamics* or QCD, and to understand spin phenomena in QCD will help to understand QCD itself. Nucleons, protons and neutrons, are built from quarks and the QCD force-carrier, gluons. *Unpolarized* deep inelastic scattering (DIS) experiments, scattering high energy electrons and muons from nucleons, first discovered quarks in the 1960s, and then over the next 30 years, DIS experiments exquisitely verified the QCD prediction for the energy dependence of the scattering. This was a triumph of QCD. *Polarized* deep inelastic scattering experiments then showed that the quarks in the nucleons carry only about 20% of the nucleon spin, a major surprise. The remaining 80% must be carried by the gluon spin and by orbital angular momentum of the quarks and gluons in the nucleon. Experiments with polarization at RHIC will probe the proton spin in new profound ways. A particular strength of the RHIC spin program is to measure the gluon contribution to the proton spin. A second emphasis will be a clean, elegant measurement of the quark and anti-quark polarizations, sorted by quark flavor, through parity-violating production of W bosons. RHIC will also probe the structure of transversely polarized protons, which may be related to the orbital angular momentum of the quarks and gluons in the proton. To contribute to the understanding of nucleon structure and the nature of confinement of the quarks and gluons inside the nucleons is the primary goal of the spin physics program at RHIC.

The key points of this report are emphasized in the following three figures.

Science. In Figure 1, we show the sensitivity that we expect for measurements of gluon polarization in the proton. RHIC will measure this with a number of probes, which will test our understanding of the underlying physics, and produce a robust result for this key measurement. The expected sensitivity of the ongoing DIS experiment at CERN, COMPASS, is also shown. Measuring the gluon polarization is a worldwide quest, and RHIC will provide the most sensitive and definitive results.

The figure shows expected results for both high cross section processes (left panel, jets), and for the more theoretically precise but lower cross section process of direct photon production. Pion and jet probes will give important results earlier in the program with lower luminosity and polarization, with one result from the 2003 run already published, and it is anticipated that results

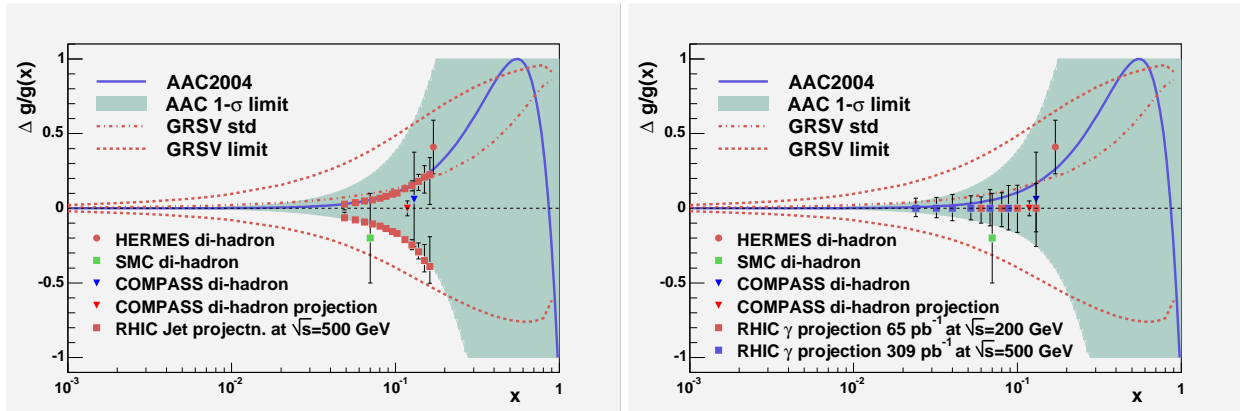


Figure 1: Plot of the gluon polarization, $\Delta g/g$, vs. x , the fraction of the proton momentum carried by the gluon. The curves in both panels show the gluon polarizations from two analyses [1, 2] of polarized deeply-inelastic scattering data [3]. The left panel shows STAR sensitivities from jet production at $\sqrt{s} = 500$ GeV, and the right panel shows projections for PHENIX for direct-photon production at 200 and 500 GeV. Results and projections from existing fixed target deep inelastic scattering experiment di-hadron data [4, 5, 6] are also shown. Experiments measure the beam helicity asymmetry A_{LL} . Its conversion to $\Delta g/g$ requires a global analysis. This plot represents an example of sensitivity to $\Delta g/g$ of the different experiments.

from the 2005 run will greatly constrain the gluon polarization. The direct photon channel (right panel) most directly measures the gluon polarization. This "golden channel" requires high luminosity and high polarization. We have a robust theoretical understanding of the reactions that we will use to probe the proton spin structure, with confirmed predictions of cross sections from next-to-leading order QCD.

Fig. 1 also shows the importance of both 200 and 500 GeV running. 200 GeV running gives sensitivity to about half of the expected integral contribution of gluons to the proton spin. Sensitivity to much of the remainder requires access to lower momentum fractions that will be probed in the 500 GeV runs. With running at the two energies, a large gluon polarization, consistent with the gluon carrying most of the spin of the proton, would be precisely measured.

In Figure 2, we show the expected sensitivity to anti-quark polarization, sorted by flavor. This is a direct measurement by observing the parity violating production of W bosons, with RHIC running at $\sqrt{s}=500$ GeV. RHIC will provide definitive measurements, where only model-dependent results presently exist from DIS. This will be an exciting result, addressing how it is that the combination of quark and anti-quarks in the proton carry little of the proton spin. The focus on the dependence of the spin structure on antiquark flavor will provide a profound test of the mechanisms for producing the sea of quark-antiquark pairs that strongly influences nucleon structure.

Experiment Upgrades for W Program To accomplish the W measurements, both STAR and PHENIX must upgrade their detectors. STAR requires additional precision forward tracking to unambiguously determine the charge sign of the ~ 40 GeV electrons for $W \rightarrow e^\pm + \nu$. This will be proposed in 2006, for completion for the 2010 run, at an estimated cost of \$5M. PHENIX requires additional triggering for selection of the $W \rightarrow \mu^\pm + \nu$ decays out of the expected 10

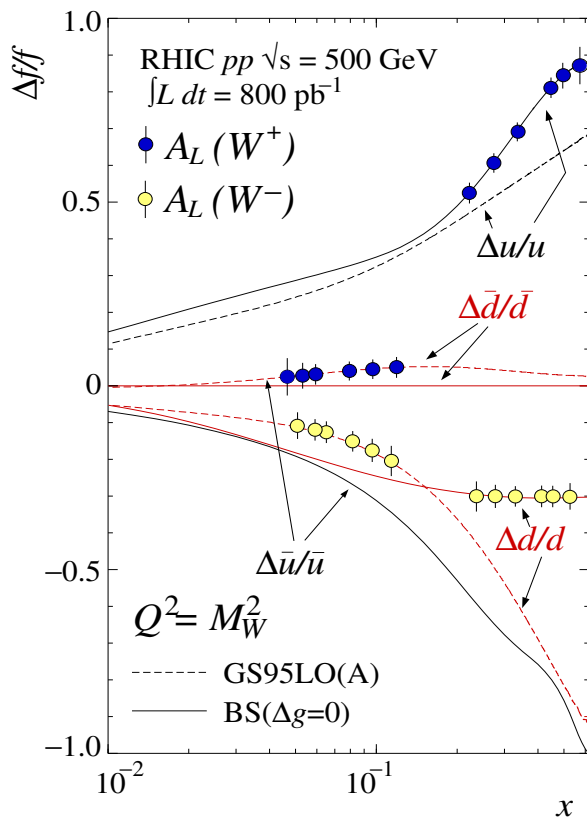


Figure 2: *Quark and antiquark polarization in the proton, $\Delta f/f(x)$, vs. $\log x$ with models [7, 8] for u , d , \bar{u} and \bar{d} ; with expected uncertainties for RHIC. x is the fraction of the proton momentum carried by the quark/antiquark.*

million collisions per second for the 500 GeV running. This is being proposed this year, for completion for the 2009 run, at an estimated cost of \$3.3M.

Accelerator Requirements and Time Evolution To accomplish these important physics goals, we need high polarization, high luminosity, and significant running at both $\sqrt{s}=200$ GeV (the present spin program energy) and at $\sqrt{s}=500$ GeV (RHIC at the full heavy ion rigidity). The present level of polarization is 45% and we expect to reach the target of 70% in 2006 for 200 GeV running. We plan to develop the polarization for 500 GeV running over the next several years, and expect to reach the target of 70% in time for the 500 GeV program in 2009. The minimum and maximum expected luminosities per year are shown in Figure 3, with three bands. The first band begins in 2005, and displays the integrated luminosity with time for 10 weeks of physics running per year, for 200 GeV. The 200 GeV run continues to mid-2009, when we show the changeover to 500 GeV. This change is dictated by reaching the target luminosity goal shown on the figure for 200 GeV. The target is the basis of the sensitivities shown in Fig. 1.

Beginning mid-2009, we switch to 500 GeV. Both W physics and gluon polarization physics will be pursued. This is shown reaching the target in 2012, with 10 physics weeks per year. This, then, gives the sensitivities shown in Figures 1 and 2.

Figure 3 also shows a band for running spin for 5 physics weeks per year, taken as 10 weeks every two years to reduce end effects. The band shows only 200 GeV running because, even by

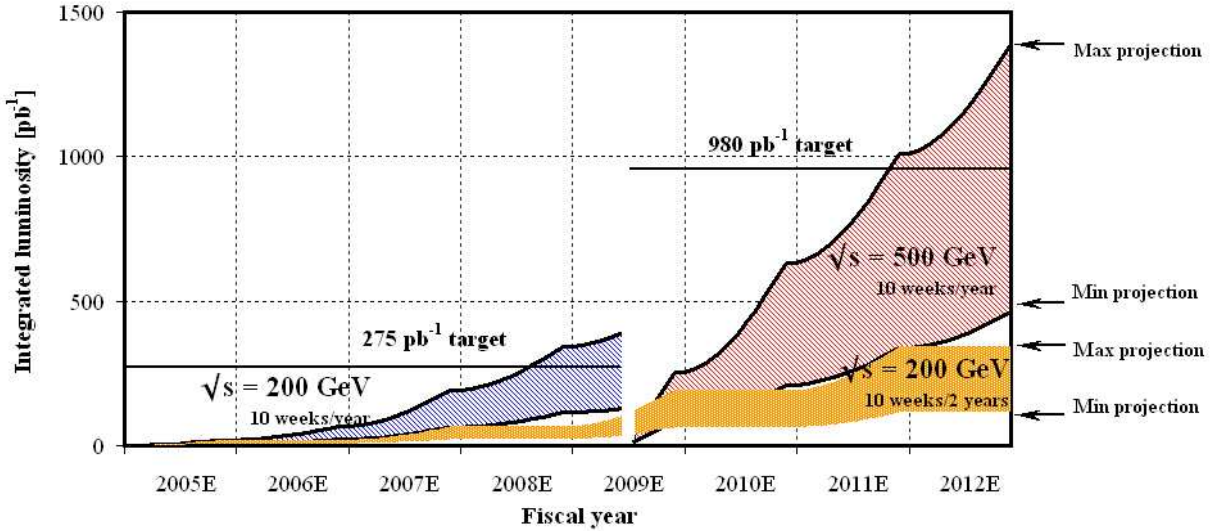


Figure 3: Minimum and maximum projected integrated luminosity through FY2012. Delivered luminosity numbers are given for one of two interaction points. For the scenario with 10 weeks of physics operation per year, the assumed energy is $\sqrt{s}=200$ GeV until mid-FY2009, and 500 GeV thereafter. For the scenario with 10 weeks every other year, the assumed energy is 200 GeV throughout the entire period.

2012, we will not have accumulated the target luminosity for gluon polarization measurements. To complete the program as we have shown it requires running to at least 2019.

Responding to the charge to the spin planning group (see appendix), we considered just two running scenarios, 5 and 10 spin physics weeks per year. These indicate "the physics goals that can be met over a period of years without involving the Group in difficult funding and cost scenarios that are not central to the calculation of physics accomplishments over time."

The 10 week per year scenario shown in Fig. 3 includes the assumption that the detector upgrades for STAR and PHENIX for the W program are accomplished by 2010, and is therefore "technically driven". This is the preferred scenario from BNL.

The 5 week per year scenario, shown also in Fig. 3, requires at least 6 years of running at each energy to accomplish the definitive measurements of gluon polarization and anti-quark polarization shown in Figures 1 and 2. Thus, for example, by 2012 one would not yet have constrained well the total gluon contribution to the proton spin, and would not have begun to probe the sea quark polarizations. Such a slow and inefficient approach would seriously degrade the impact of the RHIC spin program.

The 5 week per year plan would be a most difficult and unfortunate scenario, with RHIC poised to answer these major questions on nucleon structure. With this scenario, not only will the answers be very slow in coming, but the community of world-class accelerator physicists, experimenters, and theorists that drive the program, reaching already state of the art polarization and luminosity, and with remarkable physics output, will not be challenged to their capacities and these teams will be difficult to maintain.

By achieving the measurement sensitivities shown in Figures 1 and 2, RHIC will contribute major new understanding to the structure of the protons and neutrons that make up the known

matter in the universe, and to our understanding of the theory of the strong interaction, Quantum Chromodynamics. This work will qualitatively change our understanding of the nuclear force, contributing to a field developed through major breakthroughs in theory, including the discovery of asymptotic freedom in QCD that received the 2004 Nobel Prize in Physics, and in experiment, with the discoveries of quarks, precision confirmation of predicted scaling violations, and the spin surprise that the quarks carry very little of the nucleon spin.

The body of the report provides the details for the program described above. The report also includes other exciting science areas, such as planned studies (and an already published measurement) on transverse spin, which may access orbital angular momentum. A number of heavy ion driven (or with spin) upgrades, based on a detector R&D program supported since FY 2003 as part of the RHIC operations budget, also offer exciting spin physics opportunities, and these are described in the Experiments section of the report.

2 The science case for RHIC Spin

Spin is one of the most fundamental concepts in physics, deeply rooted in Poincaré invariance and hence in the structure of space-time itself. All elementary particles we know today carry spin, among them the particles that are subject to the strong interactions, the spin-1/2 quarks and the spin-1 gluons. Spin, therefore, plays a central role also in our theory of the strong interactions, *Quantum Chromodynamics (QCD)*, and to understand spin phenomena in QCD will help to understand QCD itself. To contribute to this understanding is the primary goal of the spin physics program at RHIC.

It is a remarkable property of QCD, known as *confinement*, that quarks and gluons are not seen in isolation, but only bound to singlet states of the strong “color” charge they carry. At the heart of investigating confinement in QCD is the study of the inner structure of strongly-interacting particles in nature that are composed of quarks and gluons. Among these, the proton and neutron are clearly special as they make up all nuclei and hence most of the visible mass in the universe. Their detailed study is therefore of fundamental interest. The proton and neutron also carry spin-1/2, which immediately brings the central role of spin in nucleon structure to the fore. It is worth recalling that the discovery of the fact that the proton has structure— and hence really the birth of strong interaction physics— was due to spin, through the measurement of a very unexpected “anomalous” magnetic moment of the proton by O. Stern and collaborators in 1933 [9]. Today, after decades of ever more detailed studies of nucleon structure, a prime question is how the proton spin-1/2 is composed of the average spins and orbital angular momenta of quarks and gluons inside the proton. Polarization has become an essential tool in the investigation of the strong interactions through nucleon structure.

Quarks were originally introduced simply based on symmetry considerations [10], in an attempt to bring order into the large array of strongly-interacting particles observed in experiment. In order to satisfy the Pauli exclusion principle for baryons such as the Δ^{++} or the Ω^- which are made up of three quarks of the same flavor, the spin-1/2 quarks had to carry a new quantum number [11], later termed “color”. A modern rendition of Rutherford’s experiment has shown us that quarks are real. This experiment is the deeply-inelastic scattering (DIS) of electrons (or, later, muons) off the nucleon, a program that was started in the late 1960’s at SLAC [12]. A high-energy electron interacts with the nucleon, via exchange of a highly virtual photon. For virtuality of $\sqrt{Q^2} > 1$ GeV distances < 0.2 fm are probed in the proton. The proton breaks up in the course of the interaction. The early DIS results compelled an interpretation as elastic scattering of the electron off pointlike, spin-1/2, constituents of the nucleon [13, 14], carrying fractional electric charge. These constituents, called “partons” were subsequently identified with the quarks. The existence of gluons was proved indirectly from a missing $\sim 50\%$ contribution [15] to the proton momentum not accounted for by the quarks. Later on, direct evidence for gluons was found in three-”jet” production in electron-positron annihilation [16]. From observed angular distributions of the jets it became clear that gluons have spin one [17].

The so successful parton interpretation of DIS assumed that partons are practically free (i.e., non-interacting) on the short time scales set by the high virtuality of the exchanged photon. This implied that the underlying theory of the strong interactions must actually be relatively weak on short time or, equivalently, distance scales [18]. In a groundbreaking development, Gross, Wilczek and Politzer showed in 1973 that the non-abelian theory “QCD” of quarks and gluons,

which had just been developed a few months earlier [19], possessed this remarkable feature of “asymptotic freedom” [20], a discovery for which they were awarded the 2004 Nobel Prize for Physics. The interactions of partons at short distances, while weak in QCD, were then predicted to lead to visible effects in the experimentally measured DIS structure functions known as “scaling violations” [21]. These essentially describe the response of the partonic structure of the proton to the resolving power of the virtual photon, set by its virtuality Q^2 . It has arguably been *the* triumph of QCD that the predicted scaling violations have been observed experimentally and verified with great precision. Deeply-inelastic scattering thus paved the way for our theory of the strong interactions, QCD.

Over the following two decades or so, studies of nucleon structure became ever more detailed and precise. Partly this was due to increased luminosities and energies of lepton machines, eventually culminating in the HERA ep collider. Also, hadron colliders entered the scene. It was realized that, again thanks to asymptotic freedom, the partonic structure of the nucleon seen in DIS is universal in the sense that it can also be studied in very inelastic reactions in proton-proton scattering [22, 23, 24]. This offered the possibility to learn about other aspects of nucleon structure (and hence, QCD), for instance about its gluon content which is not primarily accessed in DIS. Being known with more precision, nucleon structure also became a tool in the search of new physics, the outstanding example perhaps being the discovery of the W^\pm and Z bosons at CERN’s Sp \bar{p} S collider [25]. The Tevatron collider today and LHC in the near future are continuations of this theme.

A further milestone in the study of the nucleon was the advent of *polarized* electron beams in the early seventies [26]. This later on allowed to perform DIS measurements with *polarized* lepton beam and nucleon target [27], offering for the first time the possibility to study whether for example quarks and antiquarks have on average preferred spin directions inside a spin-polarized nucleon. The program of polarized DIS has been continuing ever since and has been an enormously successful branch of particle physics. Its single most important result is the finding that quark and antiquark spins provide very little – only about $\sim 20\%$ – of the proton spin [3, 28]. In parallel, starting from the mid 1970’s, there also was a very important line of research on polarization phenomena in hadron-hadron reactions in fixed-target kinematics. In particular, unexpectedly large single-transverse spin asymmetries were seen [29, 30, 31] which, as will be discussed later, may tell us about further fundamental spin-related properties of the nucleon, but have defied a complete understanding in QCD so far.

In the context of the exploration of nucleon structure achieved so far, it is clear that the RHIC spin program is the logical continuation. Very much in the spirit of the unpolarized hadron colliders in the 1980’s, RHIC enters the field to start from where polarized DIS has taken us so far. Here, too, asymptotic freedom of QCD, accessible because of the high energy of RHIC’s polarized beams, is the tool to investigate the partonic structure of the proton. Experiments with polarization at RHIC will probe the proton spin in new profound ways [32], complementary to polarized DIS. We will learn about the polarization of gluons in the proton and about details of the flavor structure of the polarized quark and antiquark distributions. RHIC will probe the structure of transversely polarized protons, and we hope to unravel the origin of the transverse-spin asymmetries mentioned above. RHIC will also investigate polarization phenomena in high-energy *elastic* scattering of protons, an equally uncharted area of QCD. Finally, if circumstances are very favorable, knowledge gathered about the spin structure of the proton could conceivably be used to turn RHIC into a discovery machine for New Physics, or a machine that probes the

chiral structure, inaccessible in unpolarized pp collisions, of new interactions possibly to be found at the LHC.

The field of nucleon structure thrives on the complementarity of information obtained in lepton-nucleon and nucleon-nucleon scattering. We shall see examples of this throughout this report. We see a collider with polarized electrons and protons as the next logical step after RHIC in our quest to explore the spin structure of the nucleon and spin phenomena in QCD.

After a brief review of where we currently stand in this field, the subsequent sections will address the most exciting aspects of the RHIC spin physics program in more detail.

2.1 Synopsis of results from polarized DIS

Spin physics at RHIC has been motivated by the exciting results from the experimental program on polarized DIS over the last ~ 30 years [3]. Most of the DIS measurements were performed with longitudinal polarization of the lepton beam and the nucleon target. The difference of cross sections for the case where the lepton and nucleon have aligned spins or opposite spins then gives access to the spin-dependent structure function $g_1(x, Q^2)$ of the nucleon. Here Q^2 is as before the virtuality of the exchanged photon, and x is the Bjorken variable, $x = Q^2/(2P \cdot q)$ with P and q the nucleon and photon momenta, respectively. The left part of Fig. 4 shows a recent compilation [33] of the world data on $g_1(x, Q^2)$. Information from both proton and neutron targets is available. The importance of g_1 lies in the fact that it has a simple interpretation in the parton model, equivalent to considering the lepton-nucleon interaction as a scattering of polarized leptons off polarized free partons. In the parton model, and including the dominant part of the QCD scaling violations mentioned above, g_1 may be written as

$$g_1(x, Q^2) = \frac{1}{2} \sum_q e_q^2 [\Delta q(x, Q^2) + \Delta \bar{q}(x, Q^2)] . \quad (1)$$

Here the Δq , $\Delta \bar{q}$ are the helicity distribution functions of quarks and antiquarks in the nucleon. For example,

$$\Delta q(x, Q^2) = q^+(x, Q^2) - q^-(x, Q^2) \quad (2)$$

counts the number densities of quarks with the same helicity as the nucleon, minus opposite. It contains information on the *spin* structure of the proton. The kinematic Bjorken variable x is identified with the proton momentum fraction carried by the struck quark. The Q^2 -dependence of the parton distributions is precisely the dependence on the “resolving power” mentioned earlier, quantitatively predictable in QCD perturbation theory, thanks to asymptotic freedom. It is also known as Q^2 -“evolution” of the parton distributions [34]. Physically, it expresses the fact that as Q^2 increases one has higher resolution of the partons, so that it is more likely that a struck quark has radiated one or more gluons so that it is effectively resolved into several partons, each with lower momentum fraction. Similarly, a struck quark may have originated from a gluon splitting into a quark-antiquark pair. This picture explains another remarkable feature of the DIS scaling violations: the Q^2 -dependence of the quark densities, and hence of the structure function $g_1(x, Q^2)$, is partly driven by the *gluon* density in the proton, despite the fact that the gluon density does not appear in Eq. (1). The polarized “helicity” gluon density is defined in analogy with Eq. (2) as

$$\Delta g(x, Q^2) = g^+(x, Q^2) - g^-(x, Q^2) . \quad (3)$$

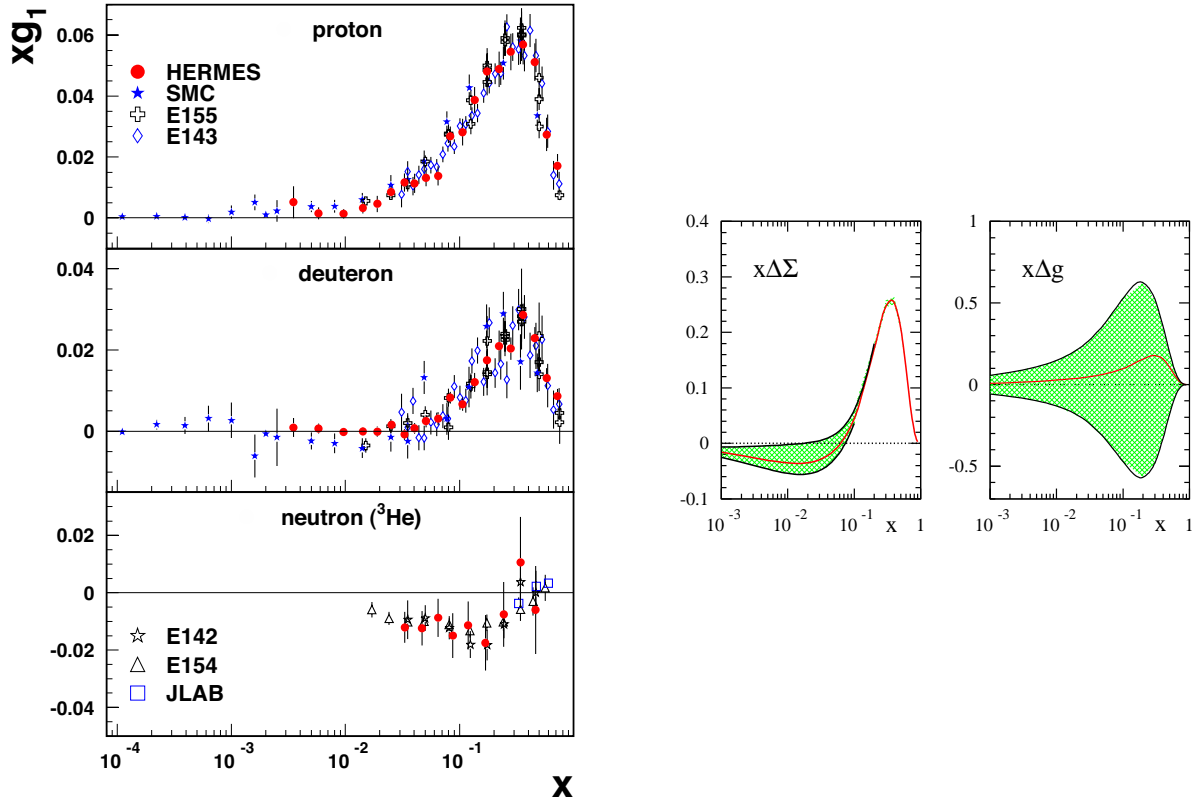


Figure 4: *Left: data on the spin structure function xg_1 , as compiled and shown in [33]. Right: results from an analysis [2] of polarized DIS in terms of spin-dependent nucleon parton densities $\Delta\Sigma(x, Q^2)$ and $\Delta g(x, Q^2)$ at $Q^2 = 1 \text{ GeV}^2$. $\Delta\Sigma$ is the total quark and antiquark helicity distribution (see Eq. (4)) and Δg the gluon helicity distribution defined in Eq. (3). The shaded bands represent a range of distributions found consistent with polarized DIS data in [2].*

Thus scaling violations in polarized DIS allow, in principle, to determine not only the $\Delta q + \Delta\bar{q}$ combinations for various flavors, but also Δg .

Extensive analyses of polarized-DIS data in terms of the polarized parton distributions have been performed by several groups, taking into account a “state-of-the-art” theoretical framework that includes additional non-leading (“higher-order”) corrections to the framework described above [1, 2, 8, 35, 36]. One result, taken from [2], is shown in the right part of Fig. 4. The results refer to a Q^2 scale of 1 GeV^2 , which is a typical scale from which perturbative evolution as described above could be used to calculate the distributions at higher Q^2 . The first panel shows the sum of all polarized quark and antiquark distributions,

$$\Delta\Sigma = \Delta u + \Delta\bar{u} + \Delta d + \Delta\bar{d} + \Delta s + \Delta\bar{s} \quad (4)$$

as a function of x . As can be seen, it is known to a fair accuracy, except at the lower x , where we have indicated by a shaded band a range of $\Delta\Sigma(x)$ that was found to be consistent with the polarized-DIS data in Ref. [2]. The right-hand plot displays the polarized gluon density Δg . Evidently, we know very little about gluon polarization in the nucleon. The latter result is not surprising: as we pointed out earlier, the only information on Δg from polarized DIS comes from scaling violations. Since all experiments performed so far have been with fixed targets, the available energy, and hence the reach in Q^2 , have been very limited, resulting in a virtually unconstrained Δg .

It has been possible to extrapolate the results shown in Fig. 4 to $x \rightarrow 0$. There are important insights into nucleon structure that could be gained from this. First of all, there is a venerable sum rule by Bjorken [37] – that actually predates QCD – which remarkably relates the integrals over all x of the high- Q^2 DIS polarized structure functions for the proton and the neutron to the decay constant $g_A \approx 1.273$ in low-energy neutron β -decay:

$$\int_0^1 dx (g_1^p(x, Q^2) - g_1^n(x, Q^2)) = \frac{1}{6}g_A + \mathcal{O}(\alpha_s(Q^2)) , \quad (5)$$

where we have indicated that there are perturbative-QCD corrections to the relation, known to very high accuracy. This sum rule, which was the original motivation for performing measurements in polarized DIS, has been verified experimentally at the 10% level [3].

Using further information from baryon β -decays, it was also possible to determine the x -integral over the combination $\Delta\Sigma$ shown in Fig. 4. This has resulted in one of the most renowned – and debated – results in recent Nuclear and Particle Physics [28]. The importance of the integral of $\Delta\Sigma$, also known as the nucleon “axial charge”, lies in the fact that it yields the average of all *quark and antiquark helicity contributions to the proton helicity*:

$$\langle S_q \rangle = \frac{1}{2} \int_0^1 \Delta\Sigma(x, Q^2) dx . \quad (6)$$

This follows from the definition of the spin-dependent quark distribution functions in Eq. (2); the factor 1/2 is because quarks carry spin-1/2. Experimentally [3],

$$\langle S_q \rangle \approx 0.1 , \quad (7)$$

with an error of about 50%. Despite its large error, the fact that $\langle S_q \rangle \ll 0.5$ implies that very little of the proton spin is carried by that of the quarks. This result is in striking contrast with predictions from constituent quark models and has therefore been dubbed “proton spin crisis”. Even though the identification of nucleon with parton helicity is not a prediction of QCD, such models have enjoyed success in describing hadron magnetic moments and spectroscopy. In any case, polarized DIS teaches us that we must look elsewhere for the proton spin!

2.2 Compelling questions in spin physics

The results from polarized inclusive DIS clearly called for further investigation of the nucleon spin. What are first of all the other candidates for carrying the nucleon spin? An examination of angular momentum in QCD equates the spin-1/2 of the proton by contributions from quark spins, gluon spins, and quark and gluon orbital angular momenta [38, 39, 40]:

$$\frac{1}{2} = \langle S_q \rangle + \langle S_g \rangle + \langle L_q \rangle + \langle L_g \rangle . \quad (8)$$

We have suppressed a dependence of each of the terms on the resolution scale Q^2 . The gluon spin contribution is directly obtained from the gluon helicity distribution in Eq. (3):

$$\langle S_g \rangle(Q^2) = \int_0^1 \Delta g(x, Q^2) dx . \quad (9)$$

Equation (8) motivates a substantial part not only of RHIC spin physics, but of virtually all major current activities in the field of high-energy spin physics. More specifically, the compelling questions are:

How do gluons contribute to the proton spin? There are good reasons to be interested in $\Delta g(x, Q^2)$. First of all, its integral could well be a major contributor to the proton spin. In fact, it is a remarkable feature of QCD that at momentum scales relevant to RHIC physics $\langle S_g \rangle(Q^2)$ may well *be* significant, perhaps even large compared to the “1/2” on the right-hand-side of Eq. (8). The reason is that the integral of $\Delta g(x, Q^2)$ evolves as $1/\alpha_s(Q^2)$ [41], that is, rises logarithmically with Q . This peculiar evolution pattern is a very deep prediction of QCD, related to its so-called axial anomaly. It has inspired ideas that a reason for the smallness of the quark spin contribution should be sought in a “shielding” of the quark spins due to a particular perturbative part of the DIS process $\gamma^* g \rightarrow q\bar{q}$ [41]. The associated contributions arise only at order $\alpha_s(Q^2)$; however, the peculiar evolution of $\langle S_g \rangle(Q^2)$ would compensate this suppression. To be of any practical relevance, such models would require a large positive gluon spin contribution, $\langle S_g \rangle > 1$, even at low “hadronic” scales of a GeV or so. A very large polarization of the confining fields inside a nucleon, even though suggested by some nucleon models [42], would be a very puzzling phenomenon and would once again challenge our picture of the nucleon. Subsection 2.5 will discuss in detail the efforts being made at RHIC to address the questions related to Δg , and the prospects for the planned measurements.

What are the patterns of up, down, and strange quark and antiquark polarizations? As is evident from Eq. (1), polarized DIS has given us access to the combinations $\Delta q + \Delta \bar{q}$. We have already discussed one particularly interesting combination of these, $\Delta \Sigma$. To really understand the proton helicity structure in detail, one needs to learn about the various quark and antiquark densities, $\Delta u, \Delta \bar{u}, \Delta d, \Delta \bar{d}, \Delta s, \Delta \bar{s}$, *individually*. This also provides an important additional test of the smallness of the quark spin contribution, independent of the additional input from baryon β -decays necessary so far. It is also important for models of nucleon structure which generally make clear qualitative predictions about, for example, the flavor asymmetry $\Delta \bar{u} - \Delta \bar{d}$ in the proton sea [43, 44]. These predictions are often related to fundamental concepts such as the Pauli principle: since the proton has two valence- u quarks which primarily spin along with the proton spin direction, $u\bar{u}$ pairs in the sea will tend to have the u quark polarized opposite to the proton. Hence, if such pairs are in a spin singlet, one expects $\Delta \bar{u} > 0$ and, by the same reasoning, $\Delta \bar{d} < 0$. Such questions become all the more exciting due to the fact that rather large *unpolarized* asymmetries $\bar{u} - \bar{d} \neq 0$ have been observed in DIS and Drell-Yan measurements [45, 46, 47]. Further fundamental questions concern the strange quark polarization. The polarized DIS measurements point to a sizable negative polarization of strange quarks, in line with other observations of significant strange quark effects in nucleon structure. Recently, in the unpolarized case the asymmetry between strange and antistrange distributions has attracted much attention [48], due to its interest for nucleon models, but also due to its possible implications for an explanation of the $\sim 3\sigma$ “anomaly” in the NuTeV measurement [49] of the Weinberg angle. A measurement of the difference between strange and antistrange polarizations, while probably lying in the future, might give further insights. In subsection 2.7 we present the possibilities RHIC offers for disentangling the various flavor polarizations in the nucleon.

What orbital angular momenta do partons carry? Equation (8) shows that quark and gluon orbital angular momenta are the other candidates for the carriers of the proton spin. Consequently, theoretical work focused also on these in the years following the discovery of the “spin

crisis”. A conceptual breakthrough was made in the mid 1990s when it was realized [39] that a particular class of “off-forward” nucleon matrix elements, in which the nucleon has different momentum in the initial and final states, measure total parton angular momentum. Put simply, orbital angular momentum is $\vec{r} \times \vec{p}$, with \vec{r} a derivative with respect to momentum transfer in Quantum Mechanics. Thus, in analogy with the measurement of the Pauli form factor it takes a finite momentum transfer on the nucleon to access matrix elements with operators containing a factor \vec{r} . It was also shown how these “off-forward” distributions, really generalizations of the ordinary parton distributions, may be experimentally determined from certain rare exclusive processes in lepton-nucleon scattering, the prime example being “Deeply-Virtual Compton Scattering (DVCS)” $\gamma^*p \rightarrow \gamma p$ [39]. A major emphasis in current and future experimental activities in lepton scattering is on the DVCS and related reactions. There are other observables that are related to orbital angular momentum of nucleon constituents [50]. The Pauli form factor is one of them. Another, accessible in proton-proton scattering, may contribute to spin asymmetries measured with a single transversely polarized proton and an unpolarized one. This brings us to the next compelling question.

What is the role of transverse spin in QCD? So far, we have only considered the helicity structure of the nucleon, that is, the partonic structure we find when we probe the nucleon when its spin is aligned with its momentum. High-energy protons may also be studied when *transversely* polarized, and it has been known for a long time now that very interesting spin effects are associated with this in QCD. Partly this is known from theoretical studies which revealed that besides the helicity distributions Δf discussed above, for transverse polarization there is a new set of parton densities, called “transversity” [51, 52]. They are defined analogously to Eq. (2), but now for transversely polarized partons polarized along or opposite to the transversely polarized proton. Nothing is known so far experimentally about the transversity densities. Their measurement is highly desirable, for a number of reasons. Not only does transversity complete the set of nucleon parton distributions. Differences between the helicity and transversity densities give information about relativistic effects in the nucleon [52]. The transversity densities also give the nucleon tensor charge [52, 53], which is equally fundamental as its axial charge mentioned earlier. Finally, transversity also plays a role in predictions for the neutron electric dipole moment. We will discuss transversity and the prospects for its measurement at RHIC in more detail in Sec. 2.8.

The other reason why transverse spin has captured the attention of researchers in QCD for a long time is related to experimental observations of very large single-transverse spin asymmetries in pp scattering [29, 30, 31], where really none were expected. Related azimuthal asymmetries were seen in lepton scattering [54, 55]. Often, when simple expectations are refuted experimentally, new insights emerge, and this has been no different in this case. With time it was realized that single-spin asymmetries may tell us many more things about QCD and the nucleon than anticipated. Particularly interesting examples are parton orbital angular momenta [56] and the color Lorentz force inside a polarized nucleon [57]. We are, however, still far from a complete understanding of all mechanisms that may be involved in single-spin asymmetries. We will show in more detail in section 2.8 that RHIC is poised to provide answers.

We now turn in more detail to the various physics topics relevant at RHIC. We start by a brief description of the underpinnings for the theoretical description of “deeply inelastic” hadronic reactions, considering unpolarized scattering for simplicity. We then discuss how polarized pp scattering at RHIC addresses the compelling questions in spin physics raised above. We will also describe other exciting physics opportunities the RHIC spin program offers.

2.3 Unpolarized pp scattering

The basic concept that underlies most of RHIC spin physics is the factorization theorem [24]. It states that large momentum-transfer reactions may be factorized into long and short-distance contributions. The long-distance pieces contain information on the structure of the nucleon in terms of its distributions of constituents, “partons”. The short-distance parts describe the hard interactions of these partons and can be calculated from first principles in QCD perturbation theory. While the parton distributions describe universal properties of the nucleon, that is, are the same in each reaction, the short-distance parts carry the process-dependence and have to be calculated for each reaction considered.

As an explicit example, we consider the cross section for the reaction $pp \rightarrow \pi(p_T)X$, where the pion is at high transverse momentum p_T , ensuring large momentum transfer. X denotes an arbitrary hadronic final state. The statement of the factorization theorem is then:

$$d\sigma = \sum_{a,b,c} \int dx_a \int dx_b \int dz_c f_a(x_a, \mu) f_b(x_b, \mu) D_c^\pi(z_c, \mu) \times d\hat{\sigma}_{ab}^c(x_a P_A, x_b P_B, P_\pi/z_c, \mu) , \quad (10)$$

where the sum is over all contributing partonic channels $a + b \rightarrow c + X$, with $d\hat{\sigma}_{ab}^c$ the associated partonic cross section. The $f_{a,b}$ describe the distributions of partons in the nucleon*. Any factorization of a physical quantity into contributions associated with different length scales will rely on a “factorization” scale that defines the boundary between what is referred to as “short-distance” and “long-distance”. In the present case this scale is represented by μ in Eq. (10). μ is essentially arbitrary, so the dependence of the calculated cross section on μ represents an uncertainty in the theoretical predictions. However, the actual dependence on the value of μ decreases order by order in perturbation theory. This is a reason why knowledge of higher orders in the perturbative expansion of the partonic cross sections is important. We also note that Eq. (10) is of course not an exact statement. There are corrections to Eq. (10) that are down by inverse powers of the momentum transfer, the so-called “power corrections”. These corrections may become relevant towards lower p_T . As we shall see in Figs. 6 and 8 below, comparisons of RHIC data for unpolarized cross sections with theoretical calculations based on Eq. (10) do not suggest that power corrections play a very significant role in the RHIC kinematic regime, even down to fairly low p_T .

Figure 5 offers a graphic illustration of QCD factorization. Thanks to factorization, one can study nucleon structure, represented by the parton densities $f_{a,b}(x, \mu)$, through a measurement of $d\sigma$, hand in hand with a theoretical calculation of $d\hat{\sigma}$. The partonic cross sections may be evaluated in perturbation theory. Schematically, they can be expanded as

$$d\hat{\sigma}_{ab}^c = d\hat{\sigma}_{ab}^{c,(0)} + \frac{\alpha_s}{\pi} d\hat{\sigma}_{ab}^{c,(1)} + \dots . \quad (11)$$

$d\hat{\sigma}_{ab}^{c,(0)}$ is the leading-order (LO) approximation to the partonic cross section. The lowest order can generally only serve to give a rough description of the reaction under study. It merely captures the

*In this particular example, the fact that we are observing a specific hadron in the reaction requires the introduction of additional long-distance functions, the parton-to-pion fragmentation functions D_c^π . These functions have been determined with some accuracy by observing leading pions in e^+e^- collisions and in DIS [58].

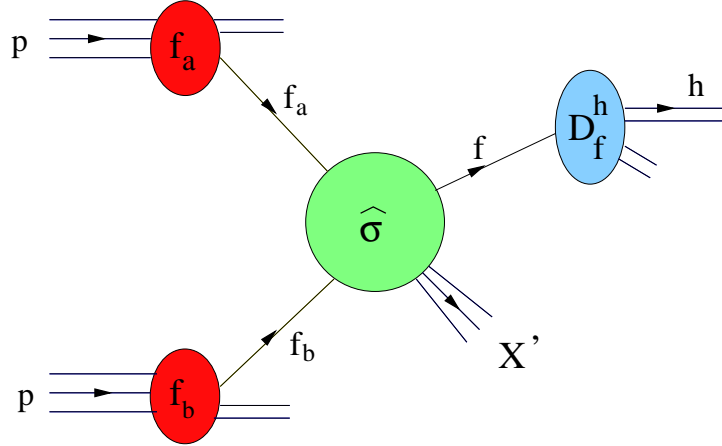


Figure 5: Factorization of $pp \rightarrow \pi^0 X$ in terms of parton densities, partonic hard-scattering cross sections, and fragmentation functions.

main features, but does not usually provide a quantitative understanding. The first-order (“next-to-leading order” (NLO)) corrections are generally indispensable in order to arrive at a firmer theoretical prediction for hadronic cross sections.

There have already been results from RHIC that demonstrate that the NLO framework outlined above is very successful. Figure 6 shows comparisons of data from PHENIX [59] and STAR [60] for inclusive-pion production $pp \rightarrow \pi^0 X$ with NLO calculations [61, 62, 63]. As can be seen, the agreement is excellent at central and forward rapidities, and down even to p_T values as low as $p_T \gtrsim 1$ GeV. In Fig. 7 we decompose the π^0 cross sections of Fig. 6 into the contributions from the various two-parton initial states [65]. It is evident that in both cases, central and forward, processes with initial gluons dominate by far for the pion transverse momenta accessed so far. This implies that $pp \rightarrow \pi^0 X$ provides an excellent probe of gluons in the nucleon.

A similar comparison is shown for prompt-photon production $pp \rightarrow \gamma X$ in Fig. 8. The left part presents the recent result of a measurement by PHENIX [66], along with the NLO calculation [67, 68]. Again, very good agreement is found. On the right, we show the decomposition of the NLO prompt-photon cross section into the contributions from the initial partonic states. The quark-gluon “Compton process” dominates at a level of 75%.

We note that an agreement between data and NLO calculations like the one seen in Figs. 6 and 8 was not found in previous comparisons made in the fixed-target regime [69]. The good agreement of the pion and photon spectra with NLO QCD at RHIC’s \sqrt{s} , and the good precision of the RHIC data provide a solid basis to extend this type of analysis to polarized reactions. The clear sensitivity to gluons in the initial state further makes the reactions very promising probes of gluon polarization.

We have so far only discussed single-inclusive reactions. There are also data from unpolarized proton-proton collisions at RHIC that mark the beginning of promising studies of two-particle correlations in the final state. Figure 9 shows results from STAR for azimuthal correlations of two produced charged hadrons in coincidence [70]. Correlations of the type shown in Fig. 9 are interesting as they are sensitive probes of QCD dynamics. For instance, at lowest order and for initial partons collinear with their parent hadrons, the distribution in Fig. 9 would only have

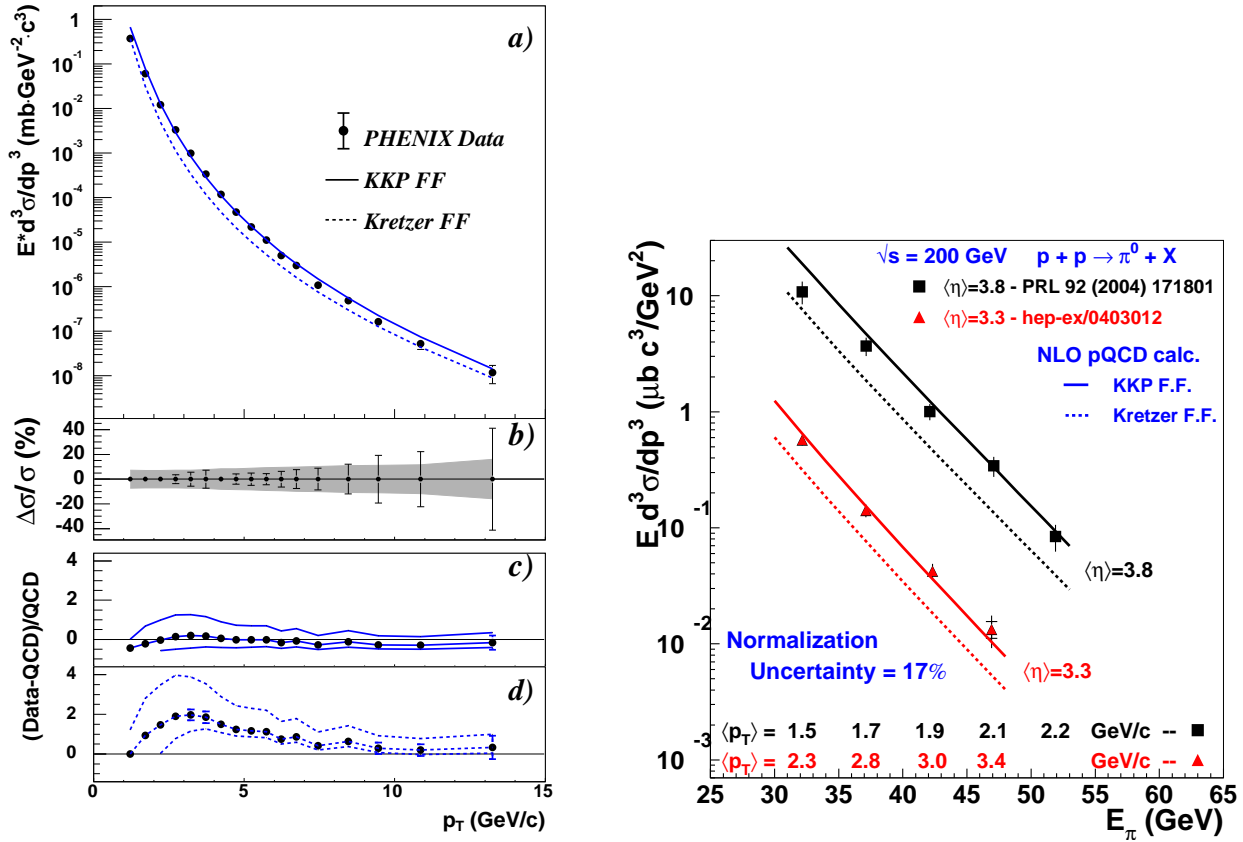


Figure 6: Data from PHENIX (left, [59]) and STAR (right, [60]) for the cross section for inclusive π^0 production $pp \rightarrow \pi^0 X$ at $\sqrt{s} = 200$ GeV. The lines show the results of the next-to-leading order calculation [61, 62, 63] for the set of proton parton distributions of [64], and for two different sets of pion fragmentation functions [58].

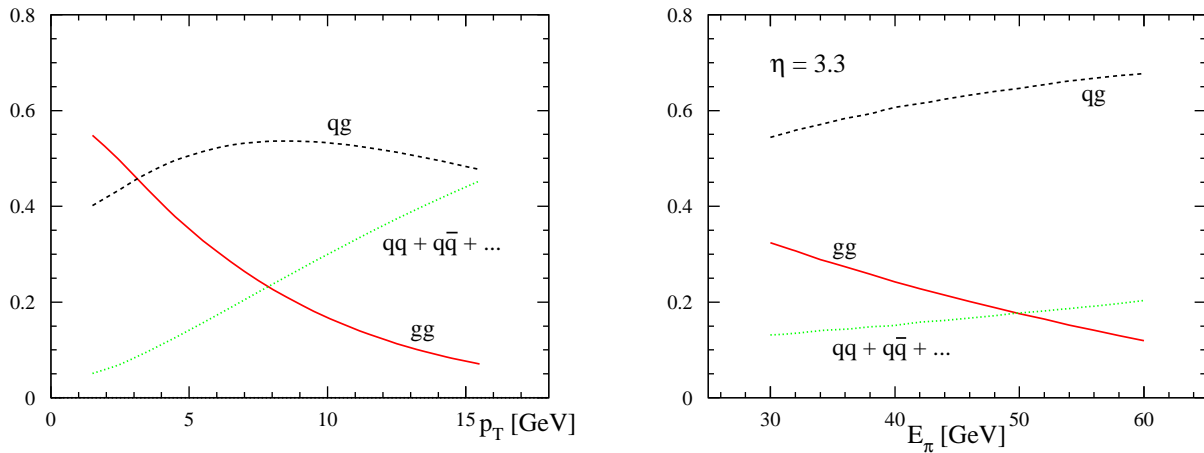


Figure 7: Decomposition of the NLO cross sections for $pp \rightarrow \pi^0 X$ collisions shown in Fig. 6 into the contributions from initial gg , qq , and qq states [65].

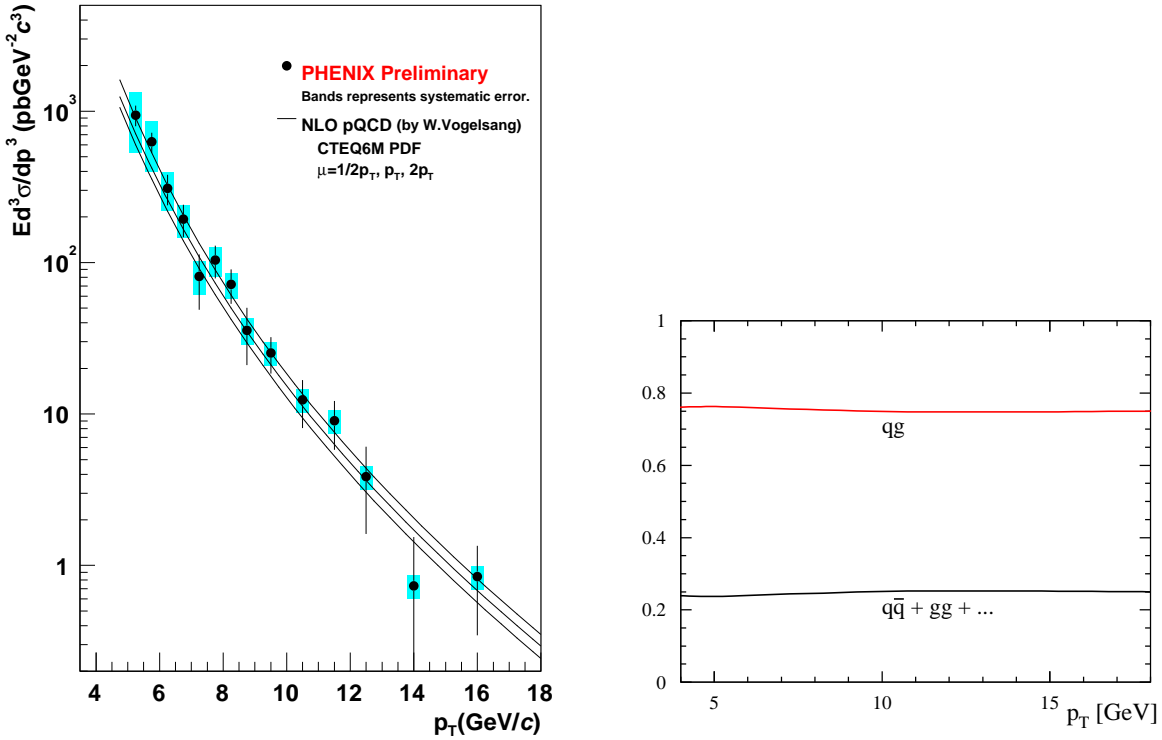


Figure 8: *Left: PHENIX data [66] for inclusive prompt-photon production, $pp \rightarrow \gamma X$, compared to the NLO calculation [67, 68]. Right: Decomposition of the NLO cross section into the contributions from initial qg and $q\bar{q} + \text{other states}$.*

support at $\Delta\phi = \pi$, corresponding to exact back-to-back kinematics. A broad distribution around $\Delta\phi = \pi$ as seen in the figure may result in QCD from gluon radiation, and from “intrinsic” parton transverse momenta. The theoretical analysis of these effects involves *all-order* summations of certain perturbative corrections and is relatively well understood. As we will see in Sec. 2.8, for transversely polarized initial protons there may be interesting spin effects associated with distributions such as the one shown in Fig. 9, that possibly probe parton orbital angular momenta in the proton. We note that also rapidity correlations between two particles in the final state are investigated at RHIC. With improving detector capabilities, these, too, will play an important role in spin physics at RHIC since they allow to pin down the subprocess kinematics to a good degree and hence may contribute to precise mappings of the spin-dependent parton densities of the proton.

We will now turn to polarized pp collisions at RHIC.

2.4 Probing the spin structure of the nucleon in polarized pp collisions

The measured quantities in spin physics experiments at RHIC are *spin asymmetries*. As an example, for collisions of longitudinally polarized proton beams, one defines a double-spin asymmetry

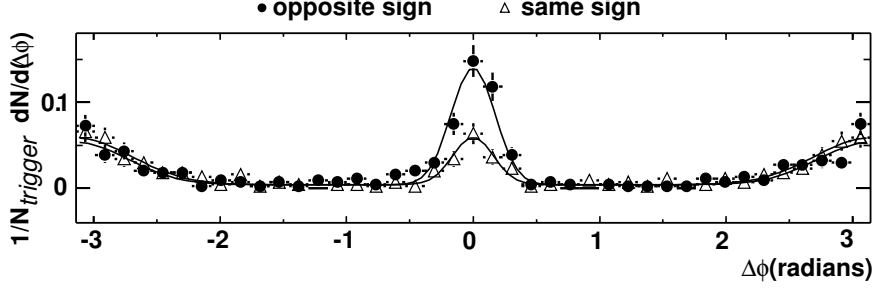


Figure 9: Azimuthal correlations of two charged hadrons produced in coincidence, as seen by STAR [70]. The correlation function is normalized by the number of trigger charged particles having $4 < p_T^{trig} < 6 \text{ GeV}/c$ in the pseudorapidity interval $|\eta| < 0.7$. The associated charged particle has $2 \text{ GeV}/c < p_T < p_T^{trig}$ in the same η interval. Same-sign and opposite-sign charged particles are discriminated. The data are fit by the sum of two Gaussian distributions to represent near-side ($|\Delta\phi| \sim 0$) correlations from di-hadron fragments of the same jet, and opposite-side ($|\Delta\phi| \sim \pi$) hadron fragments from nearly back-to-back jet pairs.

for a given process by

$$A_{LL} = \frac{d\sigma(++) - d\sigma(+-)}{d\sigma(++) + d\sigma(+-)} \equiv \frac{d\Delta\sigma}{d\sigma}, \quad (12)$$

where the signs indicate the helicities of the incident protons. The basic concepts laid out so far for unpolarized inelastic pp scattering carry over to the case of polarized collisions: spin-dependent inelastic pp cross sections factorize into “products” of polarized parton distribution functions of the proton and hard-scattering cross sections describing spin-dependent interactions of partons. As in the unpolarized case, the latter are calculable in QCD perturbation theory since they are characterized by large momentum transfer. Schematically, one has for the numerator of the spin asymmetry:

$$d\Delta\sigma = \sum_{a,b=q,\bar{q},g} \Delta f_a \otimes \Delta f_b \otimes d\Delta\hat{\sigma}_{ab}, \quad (13)$$

where \otimes denotes a convolution and where the sum is over all contributing partonic channels $a + b \rightarrow c + X$ producing the desired high- p_T or large-invariant mass final state. $d\Delta\hat{\sigma}_{ab}$ is the associated perturbative spin-dependent partonic cross section, defined as

$$d\Delta\hat{\sigma}_{ab} = \frac{1}{2} [d\hat{\sigma}_{ab}(++) - d\hat{\sigma}_{ab}(+-)] , \quad (14)$$

the signs denoting the helicities of the initial partons a, b . The sensitivity with which one can probe the polarized parton densities will foremost depend on the weights with which they enter the cross section. Good measures for this are the so-called partonic “analyzing powers”. The latter are just the spin asymmetries

$$\hat{a}_{LL} = \frac{d\hat{\sigma}_{ab}(++) - d\hat{\sigma}_{ab}(+-)}{d\hat{\sigma}_{ab}(++) + d\hat{\sigma}_{ab}(+-)} \quad (15)$$

for the individual partonic subprocesses. Figure 10 shows these analyzing powers at LO for all partonic reactions. One can see that they are usually very substantial. For future reference, we also give the subprocess asymmetries for *transverse* polarization. Here, Eq. (13) applies as well. The parton densities are then the transversity distributions, to be discussed in more detail below,

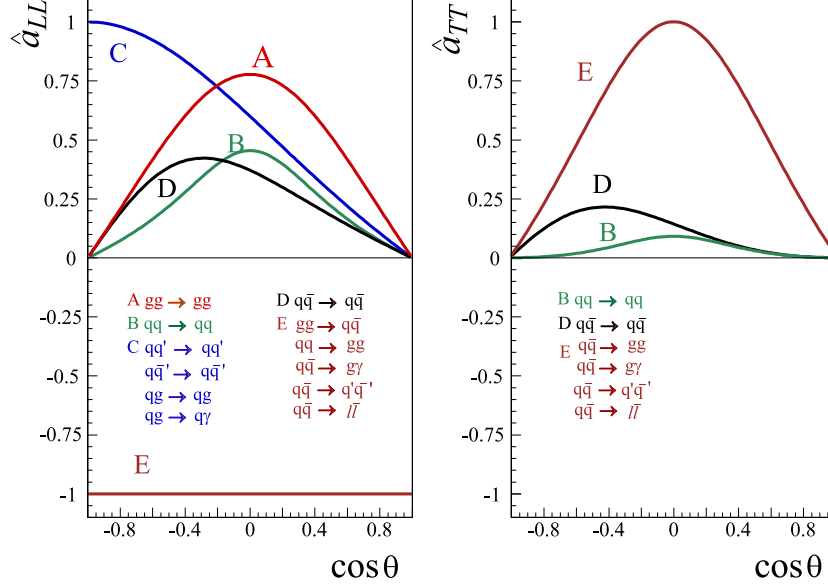


Figure 10: *Spin asymmetries for the most important partonic reactions at RHIC at lowest order in QCD. Left: helicity dependence, right: transverse polarization.*

and the partonic cross sections are defined as in Eq.(14), but for transverse initial polarization. One customarily uses a small δ to designate transversely polarized quantities. In this section, we will focus on the longitudinal case; we will return to transverse polarization in Sec. 2.8.

Since the partonic cross sections are calculable from first principles in QCD, Eq. (13) may be used to determine the polarized parton distribution functions from measurements of the spin-dependent pp cross section on the left-hand side. The crucial point here is, as discussed in the previous section, that the parton distributions are universal. They are the same in all inelastic processes, not only in pp scattering, but also for example in deeply-inelastic lepton nucleon scattering which up to now has mostly been used to learn about nucleon spin structure. This means that inelastic processes with polarization have the very attractive feature that they probe fundamental and universal spin structure of the nucleon. In effect, we are using the asymptotically free regime of QCD to probe the deep structure of the nucleon.

At RHIC, there are a number of sensitive and measurable processes at our disposal. The key ones, some of which will be discussed in detail in the following, are listed in Table 1, where we also give the dominant underlying partonic reactions and the aspect of nucleon spin structure they probe. We emphasize that, even though we have only shown LO results in Fig. 10, the NLO corrections are available for each process relevant for RHIC-Spin, thanks to considerable efforts made over the past decade or so. We give reference to the corresponding work in the first column of Table 1. These calculations bring the theoretical calculations for RHIC-Spin to the same level that has been so successful in the unpolarized case, as demonstrated by Figs. 6 and 8. For each of the processes in Table 1 the parton densities enter with different weights, so that each has its own role in helping to determine the polarized parton distributions. Some will allow a clean determination of gluon polarizations, others are more sensitive to quarks and antiquarks. Eventually, when data from RHIC will become available for most or all processes, a “global” analysis of the data, along with information from lepton scattering, will be performed which then determines the Δq , $\Delta \bar{q}$, Δg . For further details, see Sec. 2.6.

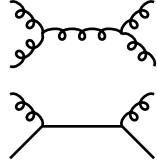
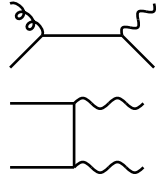
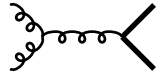
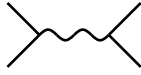
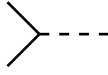
Reaction	Dom. partonic process	probes	LO Feynman diagram
$\vec{p}\vec{p} \rightarrow \pi + X$ [61, 62]	$\vec{g}\vec{g} \rightarrow gg$ $\vec{q}\vec{g} \rightarrow qg$	Δg	
$\vec{p}\vec{p} \rightarrow \text{jet}(s) + X$ [71, 72]	$\vec{g}\vec{g} \rightarrow gg$ $\vec{q}\vec{g} \rightarrow qg$	Δg	(as above)
$\vec{p}\vec{p} \rightarrow \gamma + X$ $\vec{p}\vec{p} \rightarrow \gamma + \text{jet} + X$ $\vec{p}\vec{p} \rightarrow \gamma\gamma + X$ [67, 73, 74, 75, 76]	$\vec{q}\vec{g} \rightarrow \gamma q$ $\vec{q}\vec{g} \rightarrow \gamma q$ $\vec{q}\vec{q} \rightarrow \gamma\gamma$	Δg Δg $\Delta q, \Delta\bar{q}$	
$\vec{p}\vec{p} \rightarrow DX, BX$ [77]	$\vec{g}\vec{g} \rightarrow c\bar{c}, b\bar{b}$	Δg	
$\vec{p}\vec{p} \rightarrow \mu^+\mu^- X$ (Drell-Yan) [78, 79, 80]	$\vec{q}\vec{q} \rightarrow \gamma^* \rightarrow \mu^+\mu^-$	$\Delta q, \Delta\bar{q}$	
$\vec{p}\vec{p} \rightarrow (Z^0, W^\pm)X$ $p\vec{p} \rightarrow (Z^0, W^\pm)X$ [78]	$\vec{q}\vec{q} \rightarrow Z^0, \vec{q}'\vec{q} \rightarrow W^\pm$ $\vec{q}'\vec{q} \rightarrow W^\pm, q'\vec{q} \rightarrow W^\pm$	$\Delta q, \Delta\bar{q}$	

Table 1: Key processes at RHIC for the determination of the parton distributions of the longitudinally polarized proton, along with the dominant contributing subprocesses, the parton distribution predominantly probed, and representative leading-order Feynman diagrams. The references given in the left column are for the corresponding next-to-leading order calculations.

We will now address some of the most important processes in more detail, summarizing theoretical predictions and experimental plans and prospects at RHIC. We will start with those that are sensitive to gluon polarization in the proton, and then discuss W production which will give information about the quark and antiquark polarizations.

2.5 Exploring the gluon contribution to the proton spin

To learn about the contribution of gluons to the proton spin is the most compelling motivation for doing experiments with polarized protons at RHIC. The importance of measuring the polarized gluon distribution $\Delta g(x, Q^2)$ has been universally recognized ever since the ‘‘spin crisis’’ was discovered. In fact, besides RHIC, there are – and have been in the past – several other efforts in the world to access Δg . In the early 1990s, the E704 experiment at Fermilab measured [81] the double-spin asymmetry $A_{LL}^{\pi^0}$ in $pp \rightarrow \pi^0 X$ with a polarized proton beam and polarized target at $\sqrt{s} \approx 20$ GeV, accessing pion transverse momenta of $1 \lesssim p_T \lesssim 4$ GeV. As we described in

Sec. 2.1, fixed-target inclusive DIS, so far the main tool in QCD spin physics, is not well suited for measuring the gluon density of the probed nucleon, since the photon primarily “sees” the quarks and antiquarks. Constraints on $\Delta g(x, Q^2)$ may be derived from the Q^2 -evolution of the structure function $g_1(x, Q^2)$. Certain more exclusive final states such as pairs of heavy flavors or high-transverse momentum hadrons select the photon-gluon fusion process $\gamma^* g \rightarrow q\bar{q}$, resulting in sensitivity to Δg . This is the strategy adopted by the lepton-nucleon scattering experiments SMC [4], HERMES [5] and COMPASS [6]. The ongoing experiments are briefly described in Sec. 2.9, and their sensitivities to Δg are included in Fig. 15 below.

RHIC unites several features that make it unique to explore the gluon polarization. Its first asset is the high energy, where the all-important theoretical concept of factorization (see Sec. 2.3) is expected to work best. Indeed, several unpolarized pp cross sections for reactions sensitive to gluons have already been measured at RHIC and are described well by perturbative QCD predictions, see Figs. 6 and 8. At collider energies, a range of kinematics opens up, allowing transverse momenta of an observed final state well into the region described by perturbative QCD, for mid and forward rapidities. The span in p_T allows probes of $\Delta g(x)$ over a wide range of x , thus helping to significantly constrain its x -integral. In addition, quark polarization measurements at RHIC will be compared to those from DIS.

The next crucial feature of RHIC is that two different energies, $\sqrt{s} = 200$ and 500 GeV, will be available. It is conceivable that gluons are still rather strongly polarized towards low momentum fractions x , so that a significant contribution to the integral of Δg could come from that region. This becomes evident from the left part of Fig. 11, which shows again results for $\Delta g(x, Q^2 = 5 \text{ GeV}^2)$ from several recent analyses [1, 2, 36] of scaling violations in polarized DIS, along with ranges in Δg that were found in these analyses to be presently not ruled out by the data. We plot $x\Delta g(x, Q^2)$ as a function of $\log(x)$, so that any part of the area underneath the curve directly gives the contribution to the integral $\int_0^1 \Delta g(x, Q^2) dx$. The current uncertainties do not rule out sizable contributions from $x \lesssim 0.01$. It is therefore important to have information on Δg at as small momentum fractions as possible. Roughly, at mid rapidity at RHIC, the lowest momentum fraction probed by a high- p_T final state is $x \sim p_T/\sqrt{s}$. Since p_T needs to be high enough for the process to remain amenable to QCD perturbation theory, a key to access smaller x is to *increase* energy. This makes collisions at 500 GeV indispensable. At the same time, measurements at $\sqrt{s} = 200$ GeV better probe larger x , which may also contribute significantly to the integral of Δg . In addition, there is a large overlap between the x regions covered at $\sqrt{s} = 200$ and 500 GeV, respectively. The importance of this is easily overlooked, but hard to overrate. Perturbative QCD makes definite predictions for the energy dependence of the cross section, so the consistency of the $\sqrt{s} = 200$ vs 500 GeV results with the predicted changes will provide an important test of the theoretical framework. QCD spin interactions at such high energies are uncharted territory, becoming only now accessible at RHIC, and their test is of fundamental importance.

What we have described so far would already give RHIC good possibilities to access Δg even if there were only one physics channel to study. The experiments at RHIC will measure a variety of channels, each of them highly sensitive to gluon polarization, and each with its individual strengths. We have listed the key processes in Table 1. PHENIX and STAR differ in their capabilities to detect the various channels. With major upgrades in preparation, coverage will be increased with time, allowing ever more detailed studies of the key physics processes, for instance also in terms of coincidences of two particles in the final state. Again, this will

be instrumental in precisely mapping the x -dependence of Δg . The main power of RHIC in telling us about $\Delta g(x, Q^2)$ lies in the *combination* of all these planned measurements, which will determine $\Delta g(x, Q^2)$ over a wide range of x and Q^2 as well as test the robustness of the overall approach. We will now address each of the key processes individually. In what follows, we will select the GRSV “ Δg -band” [2] shown in Fig. 11 (and for the quark distributions in Fig. 4) as a guide. Within the framework of the NLO calculation available for each of the key processes, we will translate this band into a band for the double-spin asymmetries A_{LL} for the various key processes. This band, which we will refer to as “NLO theory band” indicates a current range in theoretical model predictions for A_{LL} . We will then confront the result with the expected sensitivities at RHIC. Note that the right part of Fig. 11 displays the corresponding band for $\Delta g/g$. The measured spin asymmetries A_{LL} are effectively proportional to $\Delta g/g$ in linear or quadratic form. The “target” luminosities used for experimental sensitivities aim to improve the statistical precision for Δg over current DIS analyses by at least a factor ≈ 3 , even for the pp channel with the smallest cross section (but cleanest) used to probe Δg .

The abundant probes: high- p_T pions and jets. To match the expected improvements in machine and detector capabilities, STAR and PHENIX will address the gluon polarization with a progression of probes. At the moment, as RHIC is still developing higher luminosity and polarization, measurements exploit the abundant channels for inclusive pion and jet production. Indeed, PHENIX has already published [83] first A_{LL} data for $pp \rightarrow \pi^0 X$ from the 2003 RHIC run, shown in Fig. 12. Even with an integrated luminosity of only a few hundred nb^{-1} and a beam polarization of $\approx 30\%$ the data are already at the verge of constraining Δg at a level comparable to the information extracted from the polarized-DIS database. This is only the beginning, of course. The improved luminosity and beam polarization anticipated for the 2005 run should

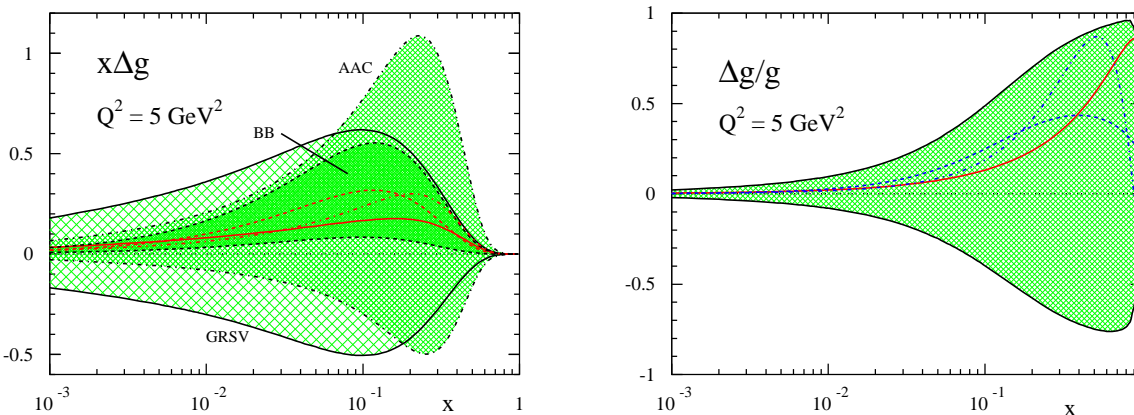


Figure 11: *Left: results for $\Delta g(x, Q^2 = 5 \text{ GeV}^2)$ from recent NLO analyses [1, 2, 36] of polarized DIS. The various bands indicate ranges in Δg that were deemed consistent with the scaling violations in polarized DIS in these analyses. The rather large differences among these bands partly result from differing theoretical assumptions in the extraction, for example, regarding the shape of $\Delta g(x)$ at the initial scale. Note that we show $x\Delta g$ as a function of $\log(x)$, in order to display the contributions from various x -regions to the integral of Δg . Right: the “net gluon polarization” $\Delta g(x, Q^2)/g(x, Q^2)$ at $Q^2 = 5 \text{ GeV}^2$, using Δg of [2] and its associated band, and the unpolarized gluon distribution of [82].*

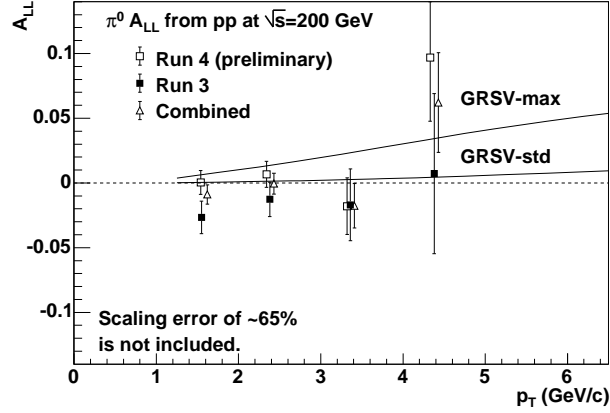


Figure 12: PHENIX measurements [83] for the double-spin asymmetry $A_{LL}^{\pi^0}$ at central rapidities. The curves are NLO calculations [61] based on the parton densities of [2]. “GRSV-std” refers to the central fit to polarized DIS data, “GRSV-max” to the upper end of the bands shown in Fig. 11.

already provide an order of magnitude decrease in statistical uncertainties. With time, this channel will become a high-precision probe. Figure 13 shows the “NLO theory band” for $A_{LL}^{\pi^0}$ at $\sqrt{s} = 200$ GeV, along with expected sensitivities for the PHENIX experiment to be achieved for integrated luminosity of 65/pb and polarization 70%. We emphasize that these sensitivities are based on measurements already made [59], and hence incorporate realistic π^0 triggering and reconstruction efficiencies (40% at high p_T for the PHENIX π^0 measurement). Note that we have chosen the kinematic regime in Fig. 13 corresponding to Figs. 6 and 7, that is, where measurements have already been made in the unpolarized case and comparisons to NLO theory have been successful.

Figure 14 shows projections for the spin asymmetry for inclusive-jet production $pp \rightarrow \text{jet} + X$ at STAR, in the rapidity region $-1 \leq \eta^{\text{jet}} \leq 2$. On the left we show calculations for $\sqrt{s} = 200$ GeV. We also show projected uncertainties for the 2005 run. Again, these are based on measurements already made, and hence incorporate realistic jet triggering and reconstruction efficiencies (at least one jet successfully reconstructed in $\approx 50\%$ of events triggered by the mix of triggers anticipated for the 2005 pp RHIC run with STAR). Evidently, the data anticipated from the 2005 run alone will significantly reduce the current $\Delta g(x)$ uncertainties. On the right of Fig. 14 we show the prospects for the longer-term future, when collisions at $\sqrt{s} = 500$ GeV will be available. With luminosity 309/pb and polarization of 70%, very precise measurements should emerge. Experimental efficiencies and bandwidth limits are assumed. A systematic uncertainty on the raw asymmetry measurement is assumed at 10^{-3} .

Figure 15 shows sensitivities for the gluon polarization for RHIC and the DIS experiments. Projections in the left panel are for RHIC-PHENIX future measurements for π^0 at 200 GeV center of mass energy and the right panel shows projections for jets for RHIC-STAR for 500 GeV energy. These are for the RHIC target luminosities. It is important to recognize that the experiments measure the beam helicity asymmetry A_{LL} . Its conversion to $\Delta g/g$ requires a global analysis, to be discussed in the next section. This plot represents an *example* of the sensitivity to $\Delta g/g$ of the different experiments.

Pion and jet production are very powerful probes of gluon polarization at the single-inclusive

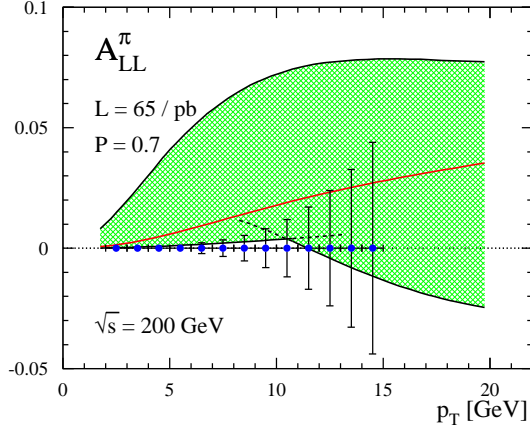


Figure 13: The current uncertainty in $A_{LL}^{\pi^0}$ due to Δg (see Fig. 11), and projected sensitivities for measurements by PHENIX at mid rapidities and $\sqrt{s} = 200$ GeV for integrated luminosity of 65/pb and polarization 70%. Note the “cusp” in the theory band near $p_T = 10$ GeV which results from use of a gluon distribution with strong negative polarization. The cusp occurs when the process $qg \rightarrow qg$ (which contributes negatively to the spin asymmetry for $\Delta g < 0$) starts to dominate over $gg \rightarrow gg$ (which is always positive). This is emphasized by the dashed lines.

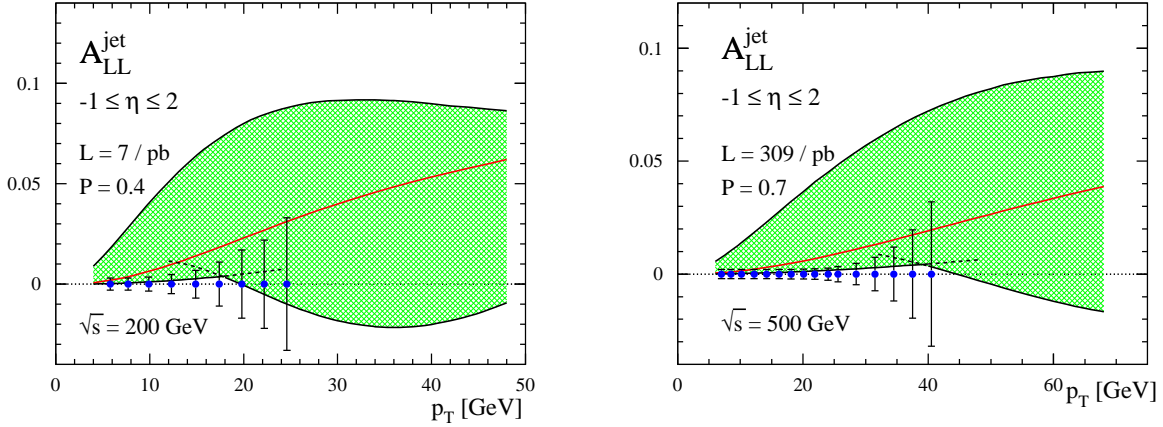


Figure 14: “NLO theory bands” for inclusive-jet production at $\sqrt{s} = 200$ and 500 GeV, for rapidities $-1 \leq \eta \leq 2$. As before, the bands illustrate the current uncertainty due to Δg . The errors are projections as described in the text. The left panel shows expected uncertainties for the 2005 run only.

level ($pp \rightarrow \pi^0 X$, or $pp \rightarrow \text{jet} X$, respectively). Further important measurements will be A_{LL} for the production of *pairs* of hadrons or jets detected in coincidence, as a function both of transverse momenta $p_{T1,2}$ and pseudorapidities $\eta_{1,2}$ of the detected particles. For example, in the case of dijet production, if LO $2 \rightarrow 2$ processes and kinematics dominate, one can unambiguously reconstruct the partonic momentum fractions in the incident protons as $x_1 = p_T(e^{-\eta_1} + e^{-\eta_2})/\sqrt{s}$,

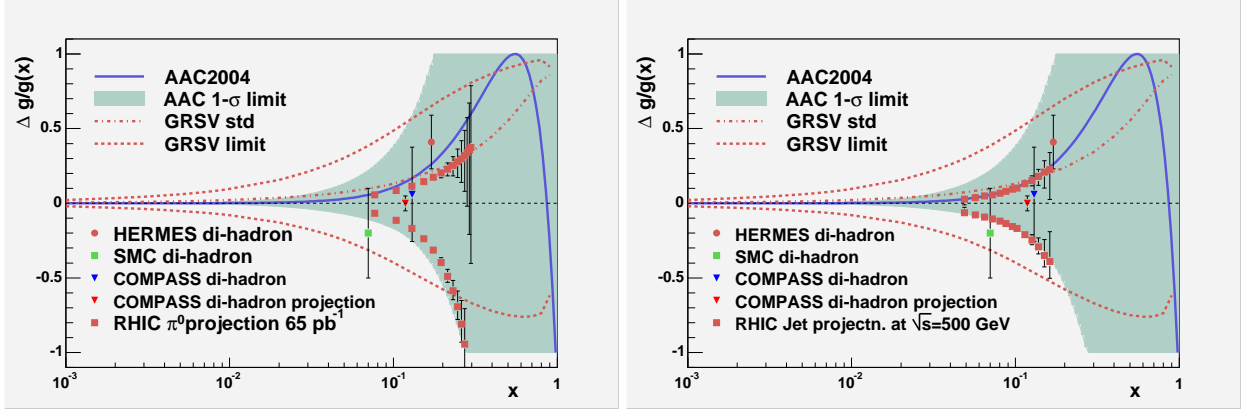


Figure 15: Plot of the gluon polarization, $\Delta g/g$, vs. x , the fraction of the proton momentum carried by the gluon. The curves in both panels show the gluon polarizations from two analyses [1, 2] of polarized deeply-inelastic scattering data [3]. Projections in the left panel are for RHIC-PHENIX future measurements for π^0 at 200 GeV center of mass energy and the right panel shows projections for jets for RHIC-STAR for 500 GeV energy. These are for the RHIC target luminosities. Results and projections from existing fixed target deep inelastic scattering experiment di-hadron data [4, 5, 6] are also shown. Experiments measure the beam helicity asymmetry A_{LL} . Its conversion to $\Delta g/g$ requires a global analysis. This plot represents an example of sensitivity to $\Delta g/g$ of the different experiments.

$x_2 = p_T(e^{\eta_1} + e^{\eta_2})/\sqrt{s}$, where p_T is the transverse momentum of each of the jets. Likewise, strong correlations between measured kinematic variables and partonic momentum fractions are found when the jets are replaced by π^0 's as surrogates. We give an example from a Monte-Carlo simulation in Fig. 16. A neutral “trigger” pion is detected at forward rapidities, $3 \leq \eta_{\pi,1} \leq 4$ and with $p_{T,\pi_1} \geq 2.5$ GeV. Because $\eta_{\pi,1}$ is so large, partonic collisions tend to become very asymmetric, with the momentum fraction x_1 associated with the proton moving in forward direction large, and x_2 small. More precisely, selecting a second pion within $1.5 \leq p_{T,\pi_2} \leq p_{T,\pi_1}$, one can now virtually “dial” x_2 , as shown by the correlation in Fig. 16. In particular, choosing $\eta_{\pi,1}$ fairly large as well, the smallest x_2 become accessible. Selective information obtained in this way may be more powerful in providing information on $\Delta g(x, Q^2)$ at lower x than single-inclusive production, and hence be vital in constraining the integral of Δg . As an additional benefit, in this kinematic regime $A_{LL}^{\pi^0}$ is mainly driven by quark-gluon scattering (see the right part of Fig. 7) and hence is mostly sensitive to $\Delta q(x_1)\Delta g(x_2)$. At high x_1 , quark polarization is known to be large from the polarized-DIS measurements. A region of phase space with sizeable p_T and large $\Delta\eta$, where qq scattering is important, can also be exploited to provide quark polarization results that can be compared to DIS.

Direct-photon production. Another important process at RHIC for measuring $\Delta g(x, Q^2)$ is direct-photon production $pp \rightarrow \gamma X$. For RHIC kinematics, this channel is dominated at the $\sim 75\%$ level by quark-gluon scattering, starting with the LO QCD Compton process $qg \rightarrow q\gamma$ (see the right part of Fig. 8). The simple pointlike coupling of the photon in this process is well-understood in Quantum Electrodynamics, and the analyzing power is large (see Fig. 10). Thus direct-photon production provides strong and nearly undiluted sensitivity to $\Delta g(x, Q^2)$. In particular, its spin asymmetry is *linear* in Δg , unlike the case of pion and jet production discussed

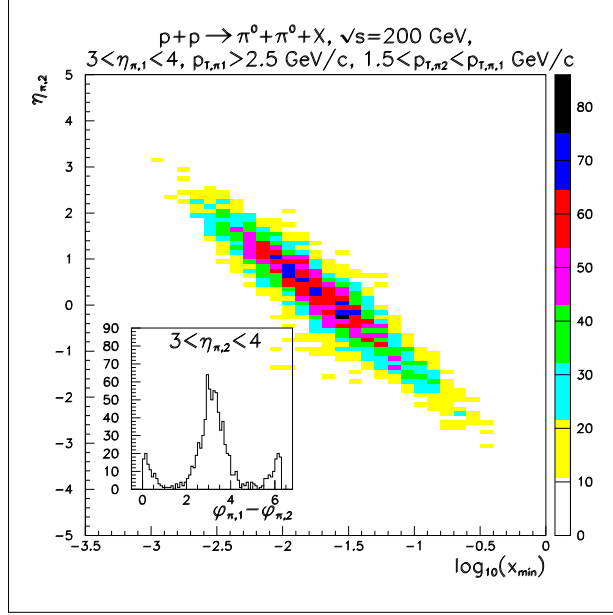


Figure 16: *PYTHIA* study of $\pi^0\pi^0$ pair production in pp collisions at $\sqrt{s} = 200$ GeV. A trigger pion is detected at forward rapidities. The plot shows correlations between the rapidity of an associated pion and the softer momentum fraction probed in the proton (see text). For the conditions used for this figure, the expected uncertainty for A_{LL} measurements will be at the half-per cent level over the whole range of $\eta_{\pi,2}$.

above where at lower p_T terms quadratic in Δg may dominate. An important role of direct-photon production will therefore be to determine the *sign* of gluon polarization. This becomes evident in Fig. 17 which shows the “NLO theory band” for A_{LL}^γ for inclusive photon production at RHIC, for both $\sqrt{s}=200$ and 500 GeV. The calculations include an isolation cut on the photon [74], as will be imposed experimentally to suppress contributions from jets. The projected experimental error bars in Fig. 17 represent statistical and background subtraction errors with realistic p_T cuts, achievable at RHIC with beam polarizations of 0.7 and integrated luminosities recorded at PHENIX of 65 pb^{-1} at 200 GeV and 309 pb^{-1} at 500 GeV. Comparison of these error bars with the present theoretical band shows that from prompt photon production alone, despite its small cross section, one can substantially improve upon present uncertainties in the gluon polarization. In particular, the sign of $\Delta g(x, Q^2)$ readily translates into the sign of A_{LL}^γ . We emphasize again that there are already measurements of the unpolarized cross section for $pp \rightarrow \gamma X$ at $\sqrt{s} = 200$ GeV from PHENIX [66] which are in good agreement with the NLO theoretical calculations (see Fig. 8).

As for pions and jets, studies of coincidences in the final state, in this case of a photon and a recoiling jet or leading hadron, will prove very useful for providing an experimental map of the so far unconstrained shape of $\Delta g(x, Q^2)$. This again allows event-by-event constraints on the colliding parton kinematics. Measurements of $pp \rightarrow \gamma + \text{jet} + X$ will be a particular emphasis in the STAR experiment. The possibilities are illustrated by STAR simulations in Fig. 18. Here, a LO analysis of the parton kinematics from the detected photon and jet properties has been used to determine the quark and gluon x -values event by event. Conservative cuts requiring $p_T \geq 10$ GeV and the larger of the two momentum fractions to be bigger than 0.2 (the latter to select the quarks with highest polarization) have been imposed on the events included in Fig. 18. The simulations

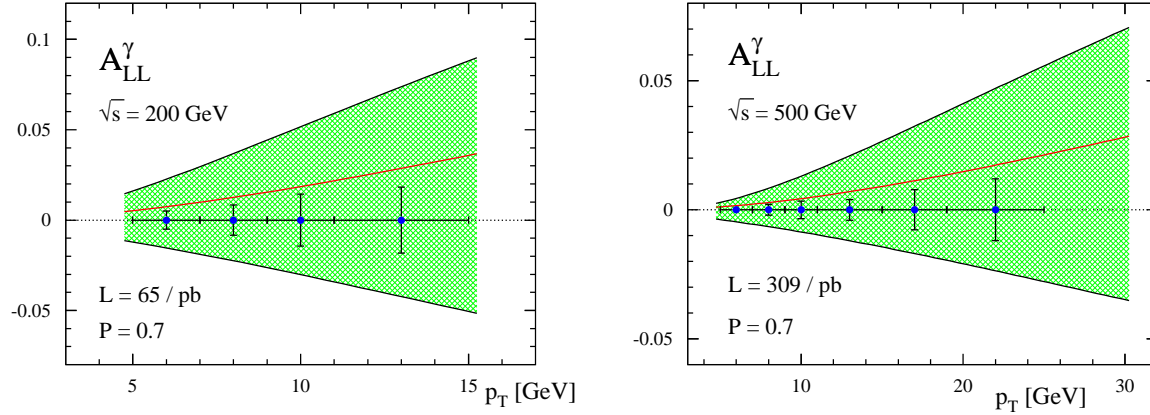


Figure 17: “NLO theory bands” for single-inclusive direct-photon production $pp \rightarrow \gamma X$ at $\sqrt{s} = 200$ and 500 GeV, for central rapidities. As before, the bands illustrate the current uncertainty due to Δg . The errors are projections for the PHENIX experiment for the RHIC target luminosities. Comparable precision on A_{LL}^γ will be attained for inclusive direct-photon production in STAR at both 200 and 500 GeV.

illustrate the statistical uncertainties achievable in $\Delta g(x)$ for three different parameterizations of [8] consistent with the DIS database. The sensitivity to gluon polarization is evident.

Heavy-flavor production. One final set of channels for probing gluon polarization at RHIC that we will discuss here involves the production of hadrons carrying “open” charm or bottom quarks. Planned vertex detectors for both STAR and PHENIX are necessary to select these events based on displaced vertices. The heavy-flavor final states are produced predominantly by gluon-gluon fusion, $g + g \rightarrow Q + \bar{Q}$ (see Table 1), so that the spin asymmetry provides quadratic sensitivity to Δg . The decay of heavy-flavor mesons dominates the inclusive production of leptons in the $\sim 2 - 10$ GeV/c range, so that the highest statistics measurements of heavy flavor production will be made via inclusive electron or muon spectra. Forward lepton detection would provide access to gluons at low x . Figure 19 shows PHENIX projections of A_{LL} uncertainties attainable via inclusive electron detection at mid-rapidity. RHIC measurements of heavy flavor production, including hidden flavor in J/ψ production, will also help to test the quantitative level of understanding of these channels and the assumption of gluon fusion dominance.

2.6 Global Analysis

Global analysis of hard reaction data with longitudinally polarized beams will provide an optimal framework to combine the various production channels of the previous section into a systematically controlled extraction of $\Delta g(x)$. The technique is to optimize the agreement between measured cross sections σ^{exp} , relative to the data accuracy $\delta\sigma^{\text{exp}}$, and the theoretical σ^{th} by min-

$\vec{p} + \vec{p} \rightarrow \gamma + \text{jet} + X$ with STAR + EEMC at
 $\sqrt{s} = 200 \text{ GeV} (320 \text{ pb}^{-1}) + \sqrt{s} = 500 \text{ GeV} (800 \text{ pb}^{-1})$

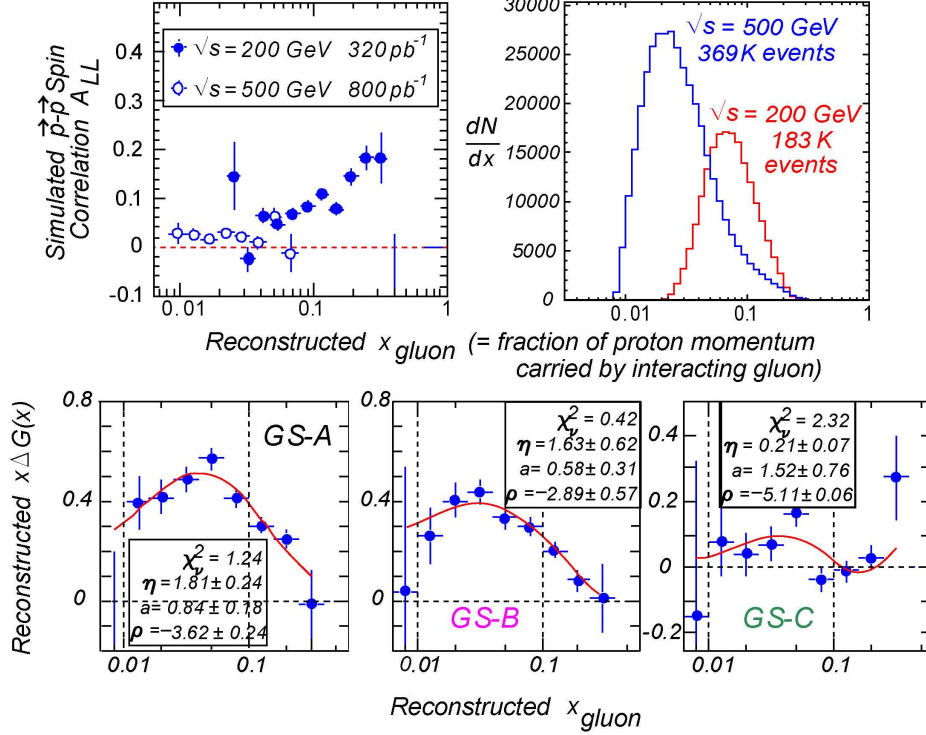


Figure 18: Simulated gluon polarization effects for a measurement and analysis of A_{LL} for γ -jet coincidences with the STAR detector at $\sqrt{s}=200 \text{ GeV}$ and 500 GeV . In order to illustrate the sensitivities, results are plotted vs. the x_{gluon} values reconstructed event-by-event from the coincidence kinematics, under the simplifying assumption of a collinear quark-gluon collision. Upper panels show the distribution of events and the projected pp A_{LL} values based on a particular parameterization (set A in [8]) of $\Delta g(x)$, with statistical errors only. The lower panels show gluon helicity preferences reconstructed from a LO analysis for three different input gluon distributions [8], plus fits demonstrating consistency of the extracted and input gluon polarizations. 200 (500) GeV data are needed to constrain the shape of $x\Delta g(x)$ above (below) its anticipated maximum. The net gluon contribution to the proton spin is represented by the area under the $x\Delta g(x)$ curve, from $x = 0$ to $x = 1$. With the integrated recorded luminosities assumed in this document, updated analysis cuts, and inclusion of updated γ reconstruction efficiencies and subtraction of residual π^0 background, the measurement uncertainties would be a factor ~ 2 larger than those shown, while the peaks of the x -range probed would shift downward by $\sim 25\%$.

imizing the χ^2 function

$$\chi^2 = \sum_{\text{measurements}} \left(\frac{\sigma^{\text{th}}(\Delta g, \dots) - \sigma^{\text{exp}}}{\delta\sigma^{\text{exp}}} \right)^2, \quad (16)$$

through variation of the shapes of the polarized parton distributions. As demonstrated, RHIC will add to the above sum over “global” measurements new reactions that are mostly sensitive to the gluon polarization $\Delta g(x)$. The advantages of a full-fledged global analysis program are manifold:

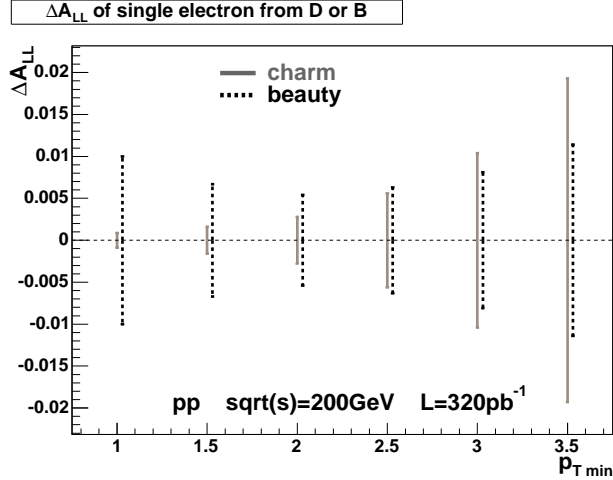


Figure 19: *Projected uncertainties in the spin asymmetry for heavy flavor production for PHENIX measurements at $\sqrt{s} = 200$ GeV with a proposed vertex detector.*

- The information from the various reaction channels, outlined above, is all combined into a single result for $\Delta g(x)$.
- The global analysis effectively deconvolutes the experimental information, which in its raw form is smeared over the fractional gluon momentum x , and fixes the gluon polarization at definite values of x .
- State-of-the-art (NLO) theoretical calculations can be used without approximations.
- It provides a framework to determine an error on the gluon polarization.
- Correlations with other experiments, to be included in χ^2 in Eq. (16) and sensitive to degrees of freedom different from Δg , are automatically respected.

The above items have been developed very successfully over many years for unpolarized parton densities [64, 84, 85]. The extraction of Δg will benefit from the fact that these techniques can be adapted to the analysis of polarized data [1, 2, 8, 35, 36, 86]. To constrain the polarized quark and antiquark distributions, the global analysis will include also the results from polarized DIS, and eventually from W production at RHIC, to which we will turn now.

2.7 W production at RHIC

2.7.1 Introduction

Measurements in polarized DIS [3], when combined with information from baryon octet β -decays [87], show that the total quark-plus-antiquark contribution to the proton's spin, summed over all flavors, is surprisingly small. In the standard interpretation of the β -decays [87], this finding is equivalent to evidence for a large negative polarization of strange quarks in the proton, which makes it likely that also the SU(2) (u, d) sea is strongly negatively polarized. This view is corroborated by the fact that in this analysis the spin carried, for example, by u quarks comes

out much smaller than generally expected in quark models [87], implying that a sizeable negative u -sea polarization partly compensates that of the valence u quarks. Alternative treatments of the information from β -decays [88, 89], when combined with the DIS results, also directly yield large negative \bar{u} and \bar{d} polarizations. Inclusive DIS (through γ^* exchange) itself is sensitive to the combined contributions of quarks and antiquarks of each flavor but cannot provide information on the polarized quark and antiquark densities separately. Directly measuring the individual polarized antiquark distributions is therefore an exciting task and will also help to clarify the overall picture concerning DIS and the β -decays.

Further motivation for dedicated measurements of antiquark densities comes from unpolarized physics. Experiments in recent years have shown [45, 46, 47] a strong breaking of $SU(2)$ symmetry in the antiquark sea, with the ratio $\bar{d}(x)/\bar{u}(x)$ rising to 1.6 or higher. It is very attractive to learn whether the polarization of \bar{u} and \bar{d} is large and asymmetric as well. Within the chiral quark soliton model based on a $1/N_c$ expansion, it is expected that the polarized flavor asymmetry, $\Delta\bar{u} - \Delta\bar{d}$, is larger than the experimentally established flavor asymmetry in the unpolarized sector [43]. A measurement of the polarized flavor asymmetry will shed light into the underlying mechanism responsible for the expected polarized flavor asymmetry. RHIC experiments will measure the \bar{d}/\bar{u} unpolarized ratio and the \bar{u} and \bar{d} polarizations separately.

Semi-inclusive DIS measurements [90] are one approach to achieving a separation of quark and antiquark densities. This method combines information from proton and neutron (or deuteron) targets and uses correlations in the fragmentation process between the type of leading hadron and the flavor of its parton progenitor, expressed by fragmentation functions. The dependence on the details of the fragmentation process limits the accuracy of this method. At RHIC the polarization of the $u, \bar{u}, d,$ and \bar{d} quarks in the proton will be measured directly and precisely using maximal parity violation for production of W bosons in $u\bar{d} \rightarrow W^+$ and $d\bar{u} \rightarrow W^-$ [78, 91, 92, 7].

2.7.2 Basic concepts of W production

Within the standard model, W bosons are produced through pure V - A interaction. Thus, the helicity of the participating quark and antiquark are fixed in the reaction. In addition, the W couples to a weak charge that correlates directly to flavors, if we concentrate on one generation. Indeed the production of W s in pp collisions is dominated by $u, d, \bar{u},$ and \bar{d} , with some contamination from $s, c, \bar{s},$ and \bar{c} , mostly through quark mixing. Therefore W production is an ideal tool to study the spin-flavor structure of the nucleon.

The leading-order production of W s, $u\bar{d} \rightarrow W^+$, is illustrated in Fig. 20. The longitudinally polarized proton at the top of each diagram collides with an unpolarized proton, producing a W^+ . At RHIC the polarized protons will be in bunches, alternately right- (+) and left- (−) handed. The parity-violating single-longitudinal spin asymmetry is the difference of left-handed and right-handed production of W s, divided by the sum and normalized by the beam polarization:

$$A_L^W = \frac{1}{P} \times \frac{N_-(W) - N_+(W)}{N_-(W) + N_+(W)} . \quad (17)$$

We can construct this asymmetry from either polarized beam, and by summing over the helicity states of the other beam. The production of the left-handed weak bosons violates parity maximally. Therefore, if for example the production of the W^+ proceeded only through the diagram

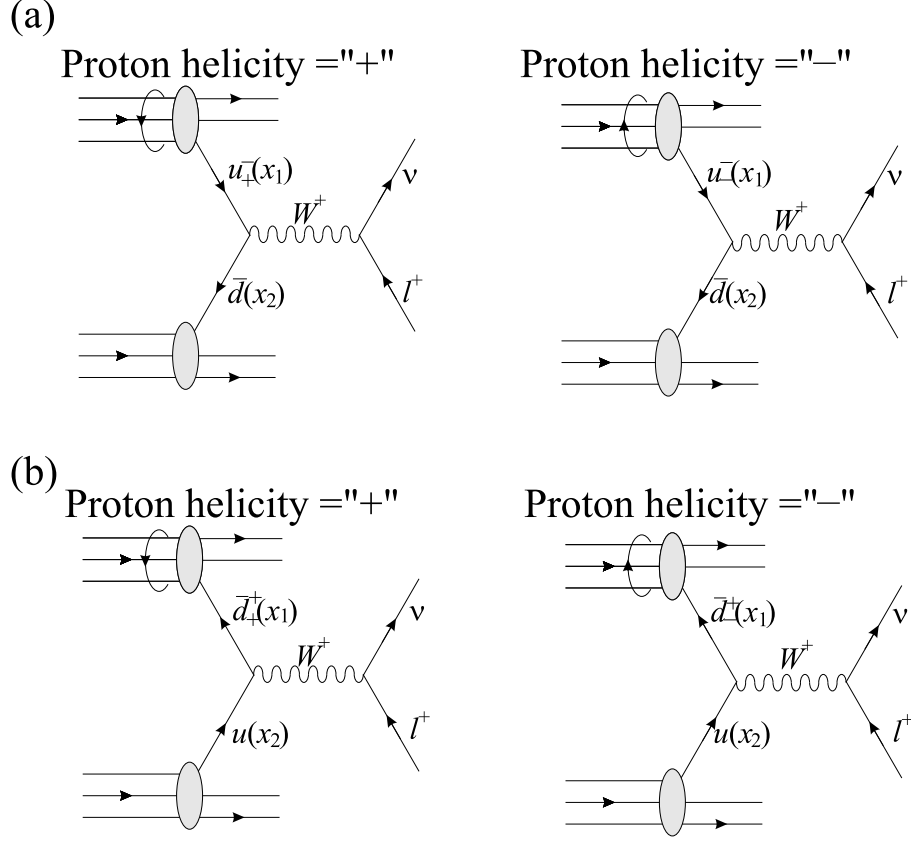


Figure 20: Production of a W^+ in a $\bar{p}p$ collision, at lowest order. (a) Δu is probed in the polarized proton. (b) $\Delta \bar{d}$ is probed.

in Fig. 20a, the parity-violating asymmetry would directly equal the longitudinal polarization asymmetry of the u quark in the proton:

$$A_L^{W^+} = \frac{u_-(x_1)\bar{d}(x_2) - u_+(x_1)\bar{d}(x_2)}{u_-(x_1)\bar{d}(x_2) + u_+(x_1)\bar{d}(x_2)} = \frac{\Delta u(x_1)}{u(x_1)}. \quad (18)$$

Similarly, for Fig. 20b alone,

$$A_L^{W^+} = \frac{\bar{d}_-(x_1)u(x_2) - \bar{d}_+(x_1)u(x_2)}{\bar{d}_-(x_1)u(x_2) + \bar{d}_+(x_1)u(x_2)} = -\frac{\Delta \bar{d}(x_1)}{\bar{d}(x_1)}. \quad (19)$$

In general, the asymmetry is a superposition of the two cases:

$$A_L^{W^+} = \frac{\Delta u(x_1)\bar{d}(x_2) - \Delta \bar{d}(x_1)u(x_2)}{u(x_1)\bar{d}(x_2) + \bar{d}(x_1)u(x_2)}. \quad (20)$$

To obtain the asymmetry for W^- , one interchanges u and d .

For the pp collisions at RHIC with $\sqrt{s} = 500$ GeV, the quark will be predominantly a valence quark. By identifying the rapidity of the W , y_W , relative to the *polarized* proton, we can obtain direct measures of the quark and antiquark polarizations, separated by quark flavor: $A_L^{W^+}$ approaches $\Delta u/u$ in the limit of $y_W \gg 0$, whereas for $y_W \ll 0$ the asymmetry becomes $-\Delta \bar{d}/\bar{d}$. Higher-order corrections change the asymmetries only a little [78].

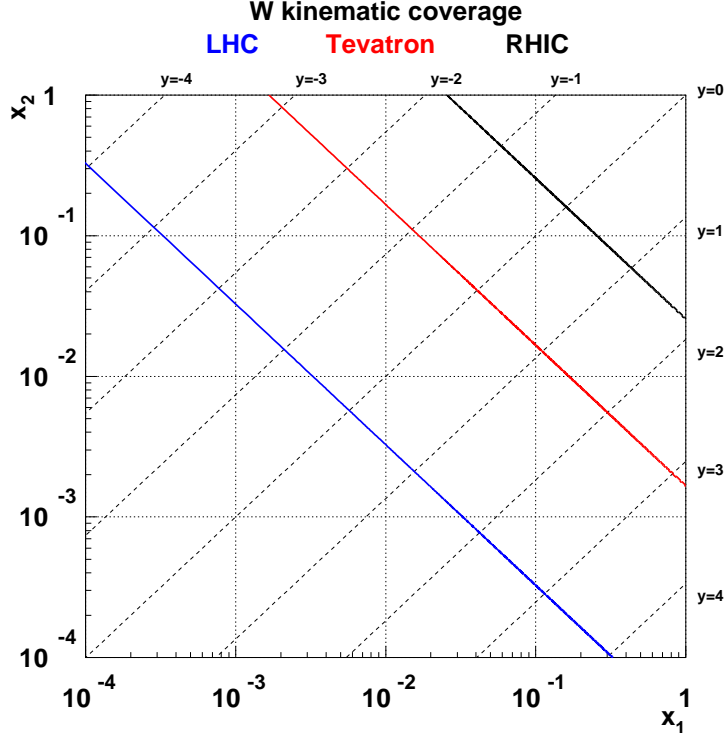


Figure 21: W kinematic coverage of x_1 and x_2 for different values of y , $-4 < y < 4$, comparing RHIC at $\sqrt{s} = 500 \text{ GeV}$ to the Tevatron kinematic region at $\sqrt{s} = 1.96 \text{ TeV}$ and LHC at $\sqrt{s} = 14 \text{ TeV}$.

The kinematics of W production and Drell-Yan production of lepton pairs is the same. The momentum fraction carried by the quarks and antiquarks, x_1 and x_2 (without yet assigning which is which), can be determined from y_W ,

$$x_1 = \frac{M_W}{\sqrt{s}} e^{y_W}, \quad x_2 = \frac{M_W}{\sqrt{s}} e^{-y_W}. \quad (21)$$

Note that this picture is valid for the predominant production of W s at $p_T \sim 0$. The experimental difficulty is that the W is observed through its leptonic decay $W \rightarrow l\nu$, and only the charged lepton is observed. We therefore need to relate the lepton kinematics to y_W , so that we can assign the probability that the polarized proton provided the quark or antiquark. Only then will we be able to translate the measured parity-violating asymmetry into a determination of the quark or antiquark polarization in the proton.

Figure 21 shows the W kinematic coverage of x_1 and x_2 for different values of y , $-4 < y < 4$, comparing RHIC at $\sqrt{s} = 500 \text{ GeV}$ to the Tevatron kinematic region at $\sqrt{s} = 1.96 \text{ TeV}$ and LHC at $\sqrt{s} = 14 \text{ TeV}$. RHIC is in a unique position to constrain quark distribution functions, both unpolarized and polarized, at high Bjorken- x where quark distribution functions exhibit larger uncertainties compared to lower values in Bjorken- x .

The rapidity of the W is related to the lepton rapidity in the W rest frame (y_l^*) and in the lab



Figure 22: Helicity configuration of W^- (left) and W^+ (right) production showing on top the helicity configuration of the incoming quark and antiquark. The middle panel shows the direction of the W spin. The lower panel displays the preferred direction of e^-/e^+ quoting the scattering angle θ^* in the W centre-of-mass system measured with respect to the positive z axis.

frame (y_i^{lab}) by

$$y_i^{\text{lab}} = y_i^* + y_W, \quad \text{where } y_i^* = \frac{1}{2} \ln \left[\frac{1 + \cos \theta^*}{1 - \cos \theta^*} \right]. \quad (22)$$

Here θ^* is the decay angle of the lepton in the W rest frame, and $\cos \theta^*$ can be determined from the transverse momentum (p_T) of the lepton with an irreducible uncertainty of the sign [93], since

$$p_T^{\text{lepton}} = p_T^* = \frac{M_W}{2} \sin \theta^*. \quad (23)$$

In this reconstruction, the p_T of the W is neglected. In reality, it has a p_T , resulting for example from higher-order contributions such as $gu \rightarrow W^+d$ and $u\bar{d} \rightarrow W^+g$, or from primordial p_T of the initial partons.

The Standard Model W boson is a purely left-handed current. The helicities of the respective quarks (negative helicity) and antiquarks (positive helicity) are therefore fixed. The cross sections for W^+ and W^- differential in y_W and the scattering angle θ^* of the decay lepton in the W centre-of-mass system is given as follows:

$$\left(\frac{d^2 \sigma}{dy_W d \cos \theta^*} \right)_{W^+} \sim u(x_1) \bar{d}(x_2) (1 - \cos \theta^*)^2 + \bar{d}(x_1) u(x_2) (1 + \cos \theta^*)^2 \quad (24)$$

and

$$\left(\frac{d^2 \sigma}{dy_W d \cos \theta^*} \right)_{W^-} \sim d(x_1) \bar{u}(x_2) (1 + \cos \theta^*)^2 + \bar{u}(x_1) d(x_2) (1 - \cos \theta^*)^2 \quad (25)$$

The characteristic dependence on the θ^* is shown graphically for the helicity configuration of W^- (left) and W^+ (right) production. The top panel shows the helicity configuration of the incoming quark and antiquark. The middle panel shows the direction of the W spin. The lower panel displays the preferred direction of e^-/e^+ quoting the scattering angle θ^* in the W centre-of-mass system measured with respect to the positive z axis.

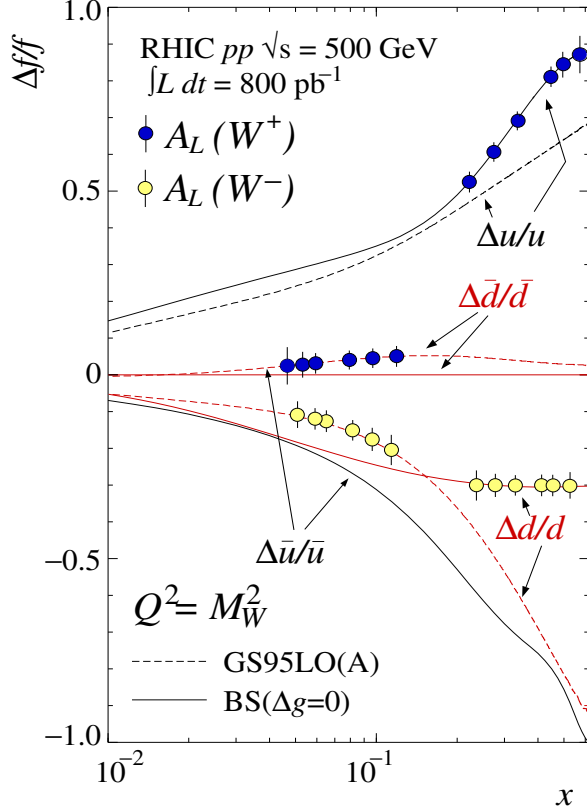


Figure 23: Expected sensitivity for the flavor-decomposed quark and antiquark polarization overlaid on the parton densities of Reference [7] (BS) and of Reference [8] [GS95LO(A)]. Darker points and error bars refer to the sensitivity from $A_L(W_+)$ measurements, and lighter ones correspond to $A_L(W_-)$.

2.7.3 Experimental aspects on W production at RHIC

Usually W production is identified by requiring charged leptons with large p_T and large missing transverse energy, due to the undetected neutrino. Since none of the detectors at RHIC is hermetic, measurement of missing p_T is not available, which leads to some background. Possible sources of leptons with high p_T include charm, bottom, and vector boson production. Above $p_T \geq 20$ GeV/c, leptons from W decay dominate, with a smaller contribution from Z^0 production. Both PHENIX and STAR can estimate the single-lepton Z^0 background from measured Z^0 production. The additional background from misidentified hadrons is expected to be small at high p_T .

Expected yields were estimated with PYTHIA [94] and RESBOS [95]. The cross section at RHIC for W^+ (W^-) production is about 1.3 nb (0.4 nb). These estimates vary by 5–10% according to the choice of the parton distribution set. For 800 pb^{-1} and $p_T \geq 20$ GeV/c, PHENIX expects about 8000 W^+ s and 8000 W^- s in the muon arms (that the numbers are equal is due to the decay angle distribution and acceptance), as well as 15,000 W^+ and 2500 W^- electron decays in the central arms. Using Eq. (21) to reconstruct x , Figure 23 shows the expected sensitivity for $\Delta f(x)/f(x)$, with $f = u, d, \bar{u}, \bar{d}$, for the PHENIX muon data.

RHICBOS W simulation at 500GeV CME

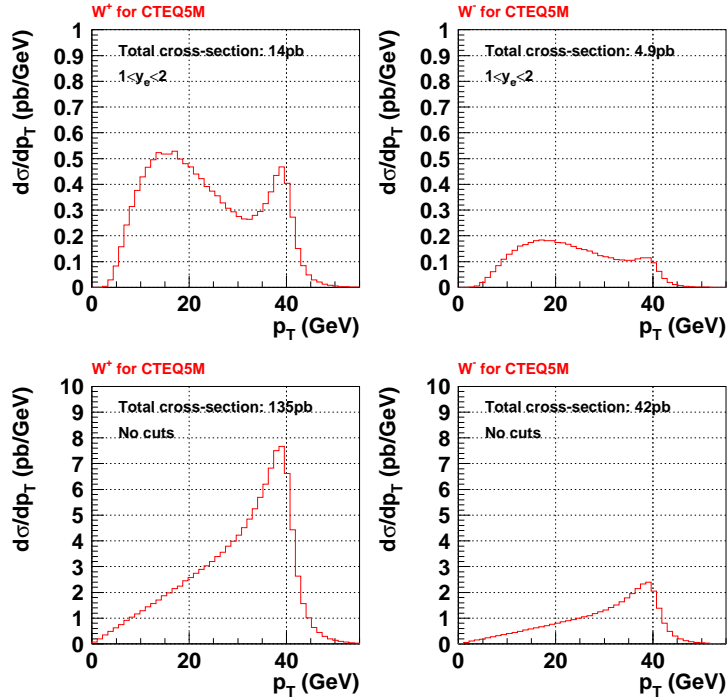


Figure 24: Leptonic p_T cross section for the W^+ and W^- case with and without a cut on the electron rapidity of $1 < y_e < 2$.

The sensitivity for STAR has been estimated using the RHICBOS MC program [96] based on a calculation for resummation of large logarithmic contributions originating from multiple soft gluon contribution. This framework allows the prediction of the leptonic longitudinal single-spin asymmetry for various distribution functions taking into account the impact of leptonic cuts such as p_T . The STAR Electromagnetic Endcap Calorimeter spans the region of $1 < y_e < 2$ which is foreseen to be upgraded by a new tracking system to allow charge discrimination of e^- and e^+ and therefore the identification of W^- and W^+ events.

Figure 24 shows the leptonic p_T cross section for the W^+ and W^- case with and without a cut on the electron rapidity of $1 < y_e < 2$. RHICBOS predicts for 800 pb^{-1} based on CTEQ5M [84] 11200 W^+ s and 3920 W^- s in comparison to 80800 W^+ s and 24000 W^- s for the central rapidity region of $-1 < y_e < 1$.

The sensitivity to different distribution functions of the underlying quark and antiquark distributions based on GRSV-STD, GRSV-VAL [2] and GS-A [8] is shown in Fig. 25. GRSV-VAL considers a flavor asymmetry scenario of Δu and Δd whereas GRSV-STD is based on a flavor symmetric description. The projections in Fig. 25 are shown for a beam polarization of 70% and an integrated luminosity of 400 pb^{-1} . Clear discrimination power to the choice of the underlying distribution function is seen in the forward direction in case of W^- production. For W^+ production, the sensitivity is similar in the forward and barrel region.

RHIC will also significantly contribute to our knowledge about the unpolarized parton densities of the proton, since it will have the highest-energy pp collisions. $\bar{p}p$ production of W s has a much stronger valence component in the determined [97] $u(x)/d(x)$ ratio. Isospin dependence

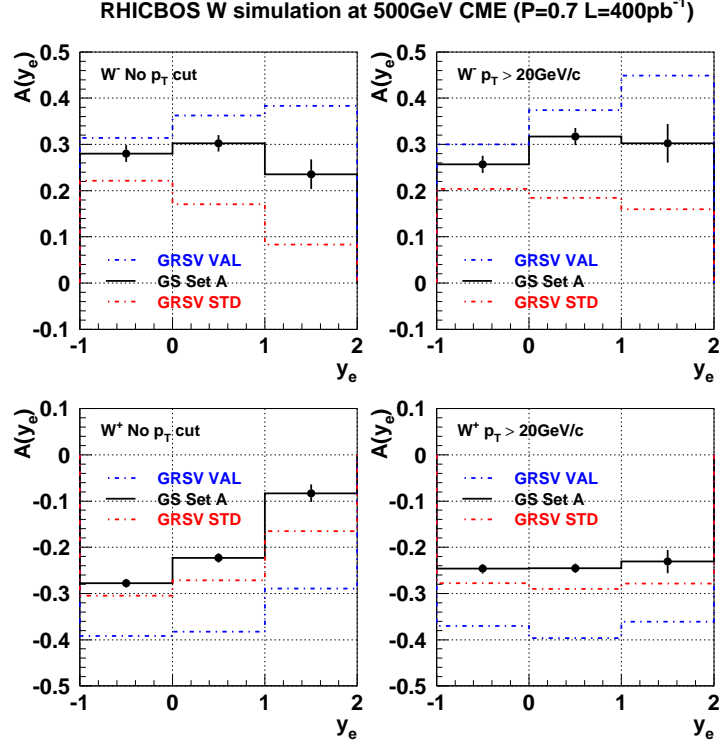


Figure 25: The sensitivity to different underlying quark and antiquark distributions based on GRSV-STD, GRSV-VAL [2] and GS-A [8]. GRSV-VAL considers a flavor asymmetry scenario of Δu and Δd whereas GRSV-STD is based on a flavor symmetry description.

in Drell-Yan production of muon pairs in pp, pd scattering [46], violation of the Gottfried sum rule [45, 98], and recent semi-inclusive DIS measurements [47] have shown that the unpolarized sea is not SU(2) symmetric. At RHIC, the ratio of unpolarized W^+ and W^- cross sections will directly probe the \bar{d}/\bar{u} ratio, as shown in Figure 26.

2.8 Transverse spin structure

With the proton spin transversely polarized with respect to its momentum or the collision axis, a novel helicity-flip *chiral-odd* twist-2 quark distribution, known as the transversity distribution $\delta q(x)$, appears [51, 52, 101]. In a (double) density matrix notation [102], the leading-twist quark distribution function $\mathcal{F}(x)$ of a nucleon may be written in terms of the unpolarized quark distribution $q(x)$, the helicity distribution $\Delta q(x)$, and the transversity distribution $\delta q(x)$, as

$$\mathcal{F}(x) = \frac{1}{2}q(x) I \otimes I + \frac{1}{2}\Delta q(x) \sigma_3 \otimes \sigma_3 + \frac{1}{2}\delta q(x) (\sigma_+ \otimes \sigma_- + \sigma_- \otimes \sigma_+) . \quad (26)$$

In Eq. (26), the first matrix in the direct product is in the nucleon helicity space and the second in the quark helicity space. The transversity distribution $\delta q(x)$ is as fundamental as $q(x)$ and $\Delta q(x)$ in QCD, and has its unique factorization scale dependence [103, 104, 105] and transverse spin sum rule [40]

$$\frac{1}{2} = \frac{1}{2} \sum_{a=q, \bar{q}} \int dx \delta q_a(x, Q^2) + \sum_{a=q, \bar{q}, G} \langle L_{\mathcal{S}_T} \rangle_a(Q^2) , \quad (27)$$

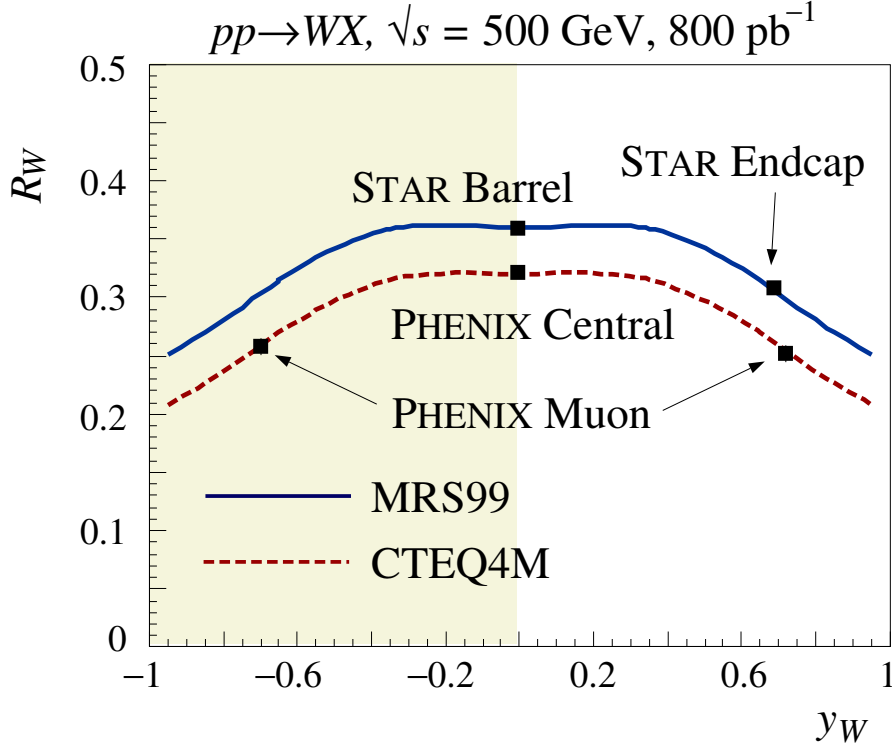


Figure 26: The ratio $R_W = (d\sigma(W^-)/dy)/(d\sigma(W^+)/dy)$ for unpolarized pp collisions at RHIC. The shaded region indicates that unpolarized pp collisions are symmetric in y_W . To illustrate the sensitivity of the measurement, we show an earlier set of parton densities (CTEQ4M [99]) and a set (MRS99 [100]) that includes the latest information from Drell-Yan data [46]. Both curves include an asymmetric sea with \bar{d}/\bar{u} rising to 1.6 for increasing antiquark momentum fraction $x_{\bar{q}}$, but the latter also includes a drop-off in the ratio for higher $x_{\bar{q}}$.

where L_{S_T} is the component of orbital angular momentum along the transverse spin s_T of the nucleon.

We note that $\delta q(x)$ and $\Delta q(x)$ are not identical because boosts and rotations do not commute in a relativistic theory. The difference between these two distributions thus carries important information about the nonperturbative structure of the proton. The three distributions, $q(x)$, $\Delta q(x)$, $\delta q(x)$ are, however, connected through an inequality first derived by Soffer [106]:

$$|2\delta q(x)| \leq q(x) + \Delta q(x), \quad (28)$$

which is valid for each quark flavor q . Independent measurements of $q(x)$, $\Delta q(x)$, and $\delta q(x)$ and their factorization scale dependence provide a direct test of QCD dynamics. Determinations of $\delta q(x)$ over a large x -range will allow to extract the contribution to the nucleon tensor charge, $\int_0^1 dx(\delta q(x) - \delta \bar{q}(x))$, which may be compared to evaluations in lattice QCD [107].

It is also important to note that gluon transversity distributions for nucleons do not exist at leading twist. This is unlike the case for longitudinal spin where both quark and gluon polarizations can make contributions to the spin of the proton. For transverse polarization, gluon transversity would require two units of helicity-flip, which the nucleon density matrix cannot provide.

Unlike $q(x)$ and $\Delta q(x)$, in the helicity basis the transversity distribution does not reveal its probabilistic interpretation because the operator defining $\delta q(x)$ represents an interference between two different quark helicity amplitudes. In a basis of transverse polarization states, however, $\delta q(x)$ has a probabilistic interpretation analogous to the interpretation of $\Delta q(x)$ in the helicity basis. This implies that transversity can be measured by transverse-spin asymmetries. Since perturbative hard processes conserve helicity, chiral-odd distributions must appear in pairs. Although the transversity distributions can be in principle extracted from the measurements of *double* transverse spin asymmetries, $A_{TT} \propto \delta q(x) \otimes \delta q'(x')$, the asymmetries often turn out to be too small to be useful because of the dominance of the gluonic contribution to the unpolarized cross sections. Therefore, $\delta q(x)$ is better determined from observables dominated by quark-initiated partonic processes, like A_{TT} of Drell-Yan [51, 52], or *single* transverse spin asymmetries (SSA), $A_N \propto \delta q(x)$. The latter requires also the aid of another chiral-odd unpolarized nonperturbative function, like the Collins function [108] described below.

Single longitudinal-spin asymmetries for single particle inclusive production vanish due to parity and time-reversal invariance of QCD. Transverse single-spin asymmetries are not forbidden by these basic symmetries. Because of Lorentz invariance of QCD, we need at least four vectors including the spin vector to construct a physically observed SSA. With a proton spin vector S not parallel to its momentum, a hadron level SSA can be constructed to be proportional to $\epsilon_{\mu\nu\alpha\beta} S^\mu P_A^\nu P_B^\alpha p^\beta$ with beam momenta, P_A and P_B , and observed particle momentum p in single hadron inclusive production, $P_A(\mathbf{S}) + P_B \rightarrow h(p_T) + X$.

Significant single transverse-spin asymmetries, A_N , of ten or more percent of the unpolarized cross sections, were recorded by Fermilab E704 experiment in the beam fragmentation region of hadronic π production at p_T as large as 3 GeV [29, 109]. Since then, nonvanishing single transverse-spin asymmetries have been observed in lower energy hadronic collisions [30, 110] and semi-inclusive lepton-hadron deeply inelastic scattering (SIDIS) [54, 111], as well as in much higher energy pp collisions at RHIC [60].

However, theoretically, it was pointed out a long time ago [112] that perturbative QCD at leading power in the collinear factorization formalism predicts nearly-vanishing single transverse-spin asymmetries, $A_N \propto \alpha_s m_q/p_T$, in inclusive single hadron production at large p_T . This is because the SSA requires a hadron-level helicity-flip and is proportional to a T-odd combination of the vectors, $A_N \propto \mathbf{S} \cdot (\mathbf{P}_A(\text{or } \mathbf{P}_B) \times \mathbf{p}_T)$. Within the leading-twist collinear factorization formalism, the hadron helicity-flip requires a quark helicity-flip, which leads to the m_q dependence, while the suppression of a power of α_s is due to the T-odd combination which requires a phase (or an imaginary part) from one of the two amplitudes.

Major theoretical progress has been made in the last decade in understanding the “unexpected”, but observed, large SSA. It is believed that SSA is a unique and excellent probe for studying parton’s transverse motion and the strength of the color Lorentz force inside a bound nucleon.

Within the collinear factorization formalism, the parton-level helicity-flip can be achieved from the interference between an amplitude of a spin (1/2) quark state and a spin (-1/2) quark-gluon composite state without requiring a quark helicity-flip and quark mass [57, 113, 114]. The required phase for the SSA can be generated from a partonic pole, which corresponds to the non-local feature of the composite quark-gluon state and leads to a natural growth of the SSA into

the fragmentation region [57, 113, 115]. Because of the coherent interference of a single parton state and a two-parton composite state, corresponding nonperturbative matrix elements, known as higher-twist matrix elements, do not have probability interpretations. Since the parton's transverse momentum k_T is integrated over in defining the matrix elements, quark-gluon correlation functions in the collinear factorization formalism provide *averaged* (or integrated) information on partons' transverse motion, related to the averaged color Lorentz force experienced by the quarks [57]. These correlation functions are new physical observables for probing nonperturbative QCD dynamics.

If we go beyond the collinear factorization formalism, the necessary hadron-level helicity-flip for SSA can be achieved by parton transverse motion or orbital angular momentum without requiring a parton-level helicity-flip. A k_T -dependent (or un-integrated) parton distribution provides direct information on both longitudinal and transverse motion of a parton inside a bound nucleon. As pointed out by Sivers [56], a k_T -dependent quark distribution of a transversely polarized nucleon, could have both symmetric and antisymmetric terms when the nucleon spin $\mathbf{S} \rightarrow -\mathbf{S}$. The antisymmetric term, known as the Sivers function, could be a source of nonvanishing single transverse spin asymmetries. It represents an initial state correlation between the transverse spin of the nucleon \mathbf{S}_T and the parton transverse momentum in the nucleon \mathbf{k}_T of the form $\mathbf{S}_T \cdot (\mathbf{P} \times \mathbf{k}_T)$, where \mathbf{P} is the nucleon momentum. Similarly, the Sivers mechanism can apply to the un-integrated gluon distribution to define a gluonic Sivers function [116]. The Sivers functions should be directly related to parton's transverse motion and orbital angular momentum. Understanding this connection is an active area of theoretical research [117].

It is also possible to generate a SSA by combining a non-zero quark transversity distribution together with the Collins-Heppelmann effect [118]. Since transversity is a chiral-odd function, measurements of transversity require another chiral-odd function. This can be a polarized chiral-odd fragmentation function (FF) which acts as an analyzer of the transversely polarized quark. The single-hadron Collins FF $H_1^\perp(z, k_T)$ [108] displays itself as a correlation of the form $\mathbf{S}_T \cdot (\mathbf{P}_{jet} \times \mathbf{k}_T)$ where \mathbf{S}_T is the transverse spin vector, \mathbf{P}_{jet} is the jet momentum and \mathbf{k}_T is the transverse momentum of the hadron with respect to the fragmenting quark. This FF depends not only on the momentum fraction of the hadron with respect to the parton $z = E_h/E_{parton}$, but also on k_T . Early on it was realized that the measurement of two hadrons (h_1 and h_2) within a jet would also be sensitive to the Collins-Heppelmann effect via the correlation $\mathbf{S}_T \cdot (\mathbf{P}_{h_1} \times \mathbf{P}_{h_2})$ [118]. However, a recent theoretical study [119] suggests that the Collins-Heppelmann effect may be suppressed for inclusive pion production in p+p collisions due to cancellations induced by quantum phases. It was also pointed out that interference between s-wave and p-wave mesons can analyze the transverse polarization of a quark [120]. This so-called di-hadron interference FF $\delta\hat{q}_T$ has an advantage in that the theory can work within a collinear approximation, free from gluon radiation effects which can modify the asymmetry. The Interference FF depends on the invariant mass of the two hadrons and the total momentum fraction $z = z_{h1} + z_{h2}$. A model calculation [120] suggests that there will be a sign change around the ρ mass for fragmentation into $\pi^+ + \pi^-$. Recent data from the HERMES collaboration provide some indication of the existence of this change in sign [121].

Much of the predictive power of QCD is provided by the universality of nonperturbative parton distributions and/or fragmentation functions in factorization theorems for hadronic processes. In order to quantify and measure the parton transverse motion inside a polarized nucleon, it is necessary to have gauge invariant definitions of k_T -dependent parton distributions and/or frag-

mentation functions [122, 123, 124, 125]. To extract the k_T -dependent distributions, such as the Sivers and Collins functions, from physical observables, a factorization formalism in terms of these universal distributions is required. Since the Sivers and Collins functions are sensitive to the transverse motion of partons at relatively low parton transverse momentum k_T , which is nonperturbative, another large physical scale, $Q \gg k_T$, is needed to ensure the k_T -dependent factorization [126]. For example, a Drell-Yan pair of invariant mass Q at low transverse momentum $q_T \sim k_T$ is a good probe of k_T -dependent quark and antiquark distributions because the large Q ensures the factorization [126]. Sivers functions could also be measured in terms of asymmetric di-jet correlations at RHIC [127].

The k_T -factorization formalism was used to calculate the SSA in hadronic inclusive-pion production, A_N , in terms of contributions of Sivers functions [128] and/or a combination of transversity and Collins functions [129]. Although there presently exists no formal proof for k_T -factorization for inclusive pion production in hadronic collisions, the calculated A_N , with x_F dependence mainly determined by the extracted Sivers and/or Collins functions from fitting low energy data, are consistent with new RHIC data at $\sqrt{s} = 200$ GeV [60]. When the pion p_T is much larger than the typical k_T of the parton transverse motion in a nucleon, $p_T \gg \langle k_T \rangle$, the k_T factorization formalism used in these calculations is not expected to be valid. On the other hand, the proven collinear factorization formalism at twist-3 for hadronic A_N should be a good approximation then [57, 113]. Measurements of the SSA in its transition from the low p_T region where $A_N \propto p_T/\langle k_T \rangle \sim k_T/\langle k_T \rangle$, sensitive to the parton transverse motion k_T , to the high p_T region where $A_N \propto \langle k_T \rangle/p_T$, probing the *averaged* transverse momentum or *averaged* color Lorentz force [57], would provide unique insights into nucleon structure.

With the ability to measure correlations of two hadrons (or jets) at RHIC, it is possible to separate the Sivers effect, parton transverse motion in initial-state hadron wave functions, from the Collins-Heppelmann effect, a parton spin effect in final-state hadronization. Sivers functions, Collins functions, transversity distribution and quark-gluon correlations all provide information on nucleon's spin structure that cannot be reached by measurements of longitudinal spin asymmetries.

There have been several measurements of transverse single spin asymmetries for pion production in collisions of polarized protons. The E704 collaboration observed [29, 109] that the analyzing power (A_N) for pions produced in polarized proton collisions at $\sqrt{s}=20$ GeV at large Feynman- x_F had magnitudes up to $\sim 30\%$ that increased with increasing x_F . A_N was found to be positive for π^+ production, negative for π^- production and positive for π^0 production, although smaller in magnitude than for π^+ production. Similar trends for the x_F dependence of A_N for pion production are also observed for pion production at lower \sqrt{s} [130]. More recently, new polarized p+p experiments [30, 110] as well as semi-inclusive deep-inelastic lepton scattering (SIDIS) experiments [54, 111] have reported measurements of transverse single-spin asymmetries (SSA) which are significantly different from zero. The excitement from these results has motivated a number of experiments to further explore the unexpectedly large signals. For example, the HERMES collaboration has devoted several years of data taking to measuring SIDIS with a transversely polarized target [55]. At RHIC, A_N for pion production has been measured at $\sqrt{s} = 200$ GeV over a large rapidity range [60, 131] as shown in Figs. 27 and 28. At forward rapidity, a large value of A_N was found for positive x_F at collision energies a factor of 10 larger than in earlier experiments. The STAR experiment has more recently reported preliminary A_N results at $x_F < 0$ which are consistent with zero within the experimental accuracy [131]. Ac-

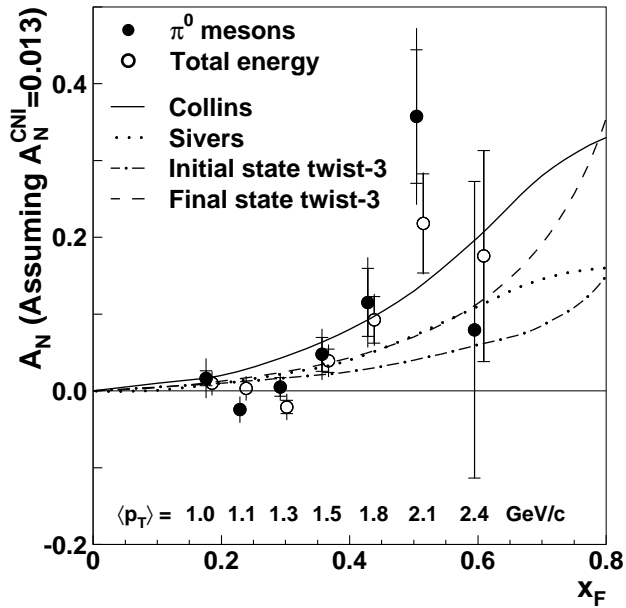


Figure 27: The A_N for π^0 meson produced in the interval $3.3 < \eta < 4.1$ with polarized proton collisions at $\sqrt{s}=200$ GeV from STAR [60]. The solid points are for identified π^0 mesons. The open points are measurements of the total electromagnetic energy shifted by 0.01 in x_F . The curves are predictions from pQCD models evaluated at $p_T=1.5$ GeV/c.

According to a recent study [119], the large negative x_F region is dominated by gluon Siverson effects. While the preliminary STAR data may already exclude a saturated gluon Siverson function, more data are required to establish its size.

There has been tremendous theoretical progress towards understanding of transverse spin effects within QCD, as reviewed at the most recent International Symposium on Spin Physics [133]. In part, the significant theoretical progress has been stimulated by new experimental results for transverse SSA results from SIDIS experiments and from polarized proton collisions at RHIC. There is promise that this progress can be sustained since we also know that the unpolarized yield for large x_F π^0 production in p+p collisions at $\sqrt{s} = 200$ GeV is well described with fixed order pQCD calculations, unlike at lower \sqrt{s} [69].

Higher precision measurements of A_N over a wide range of x_F and p_T at $\sqrt{s} \geq 200$ GeV will provide the opportunity to understand the physics behind these large spin effects. With a data sample 3 pb^{-1} and $P = 0.5$, the statistical precision for the negative x_F analyzing power for π^0 production [131] will be improved by a factor of 5. Measuring the p_T dependence of A_N can also be accomplished with such a data sample and will provide a crucial test of these pQCD based models, as they all predict A_N to decrease as p_T increases. Figure 29 shows the statistical error projection for A_N as function of p_T at fixed $x_F = 0.5$ for π^0 production at STAR. Obtaining precise data for very large x_F is interesting in order to test the expectation of A_N to decrease [135], rather than continuing to increase with increasing x_F , due to the upper bound (28) on transversity. It is also expected that comparable precision will be achieved for similar sized data samples for π^\pm production at $\sqrt{s}=200$ GeV by the BRAHMS collaboration.

To disentangle the different mechanisms behind A_N , it is required to go beyond inclusive measurements and measure either two final state particles or jets. There is a class of observables

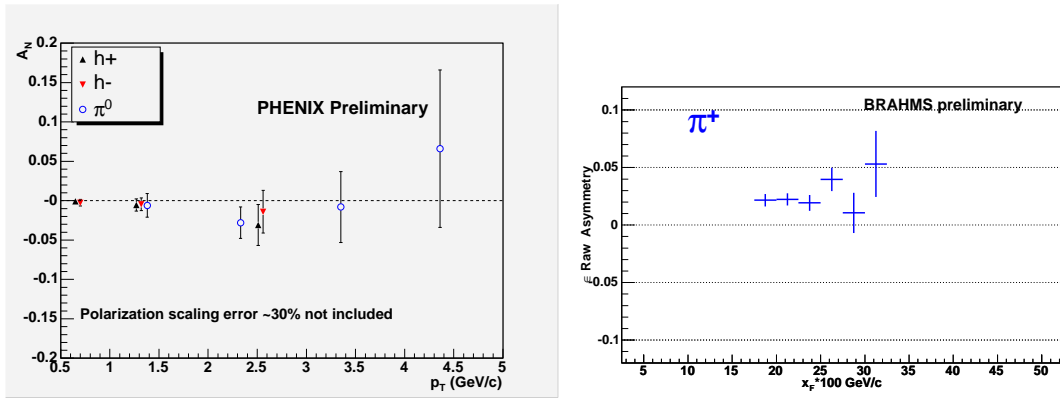


Figure 28: *Left: preliminary results of A_N for $\pi^{0,\pm}$ produced at mid-rapidity ($-0.35 < \eta < 0.35$) with polarized proton collisions at $\sqrt{s}=200$ GeV as a function of p_T from PHENIX [132]. Right: preliminary results of the asymmetry $P_{beam} \cdot A_N$ for π^+ meson production in the interval $2.3^\circ < \theta < 3.5^\circ$ as function of x_F from BRAHMS.*

for which the k_T -dependent distributions or fragmentation functions appear at leading-power, and are directly sensitive to a small measured transverse momentum [108, 118, 127]. A goal of the transverse spin program at RHIC is to disentangle the potential contributions to A_N by directly measuring the intrinsic k_T of partons in nucleon or transverse momentum in fragmentation process.

Back-to-back di-jet production in $p^\uparrow p$ collisions can be used to measure the Sivers function [127]. The deviation of the azimuthal angle difference $\delta\phi = \phi_{jet1} - \phi_{jet2} + \pi$ from zero directly measures the k_T of the partons. When the jet production plane is close to the spin of the nucleon, the k_T imbalance of the parton will affect the $\delta\phi$ distribution and will give a spin asymmetry $A_N(\delta\phi) = (\sigma^\uparrow(\delta\phi) - \sigma^\downarrow(\delta\phi))/(\sigma^\uparrow(\delta\phi) + \sigma^\downarrow(\delta\phi))$. At mid rapidity, this asymmetry may reach a few percent or more and could provide access to the gluon Sivers function, as shown in Fig. 30. The error bars are estimated statistical uncertainties for di-jet measurement at STAR with two luminosity and polarization assumptions based on existing data [136] and an expected increase in the acceptance, but possible improvements of the trigger to enrich di-jet events are not taken into account.

Measurements at RHIC are planned to study the Collins FF and the Interference FF for two particles within a jet with unpolarized and transversely polarized pp collisions. In case of single hadron fragmentation the Collins asymmetry A_T , will be observed as azimuthal modulation of single hadron distributions around the jet-axis and with respect to the transverse proton spin: $S \cdot (P_{jet} \times k_T)$, where k_T is the transverse hadron momentum with respect to the jet axis. At the present time the STAR detector is capable of reconstructing the jet-axis required for this measurement. In PHENIX single hadron Collins measurements will become feasible only after the addition of a large acceptance inner silicon vertex- and tracking-detector.

For di-hadron fragmentation the Collins asymmetry A_T will manifest itself in the modulation of the angular distribution of the di-hadron plane with respect to the transverse proton spin; $S \cdot (P_{h1} \times P_{h2})$. Figure 31 contains projections for A_T observed in the production of charged pion pairs with the PHENIX experiment. The projections are based on a model for the interference fragmentation function by Tang and Jaffe [120]. For the simulations leading to the projected asymmetries in Fig. 31 it was assumed that transversity distributions saturate the Soffer limit. On

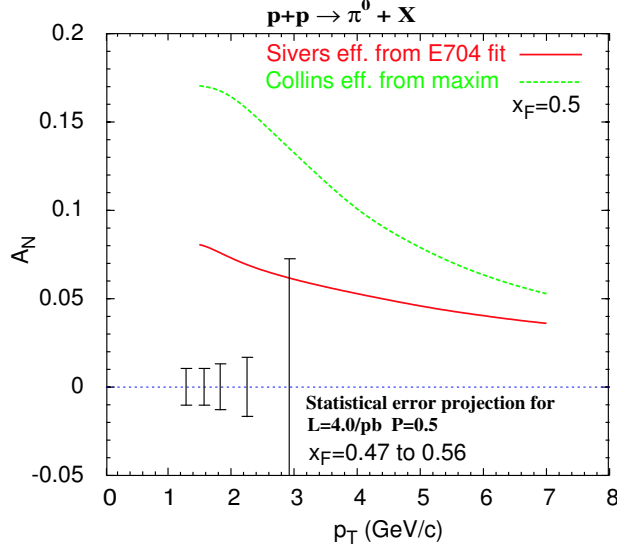


Figure 29: Statistical error projection for A_N at $\sqrt{s} = 200$ GeV as function of p_T at fixed x_F for π^0 production at STAR for anticipated luminosity and polarization for the 2005 run. The red curve is a theory prediction based on the Sivers effect fitted to E704 data and extrapolated, and the green curve is the maximized A_N based on the Collins effect with saturated transversity and Collins functions [119, 134].

the experimental side it was required that one or more pions in the event have momentum above the Cherenkov threshold and can be triggered as a coincidence between RICH and a low threshold cluster in the electromagnetic calorimeter. Projections for A_T are shown for the invariant mass of the pion pair in the interval between $800 < m_{\pi_1, \pi_2} < 950$ MeV. Tang and Jaffe predict a specific dependence of the analyzing power of the interference fragmentation function on the invariant mass of the two pion system. Specifically, it is predicted that the interference fragmentation function changes sign at the ρ -mass and is positive below and negative above the ρ -mass. The statistical errors in the projections are based on an assumed integrated luminosity of 30 pb^{-1} and a polarization of 50%. It is demonstrated that the sign change in the invariant mass dependence of the interference fragmentation function can be studied with good statistical resolution. This will provide an excellent tool to control systematic uncertainties in the measurement.

By increasing the coverage of electromagnetic calorimetry in the forward direction in STAR, spin-dependent particle correlation studies are enabled in the rapidity range where large transverse single spin effects have already been observed. With calorimetry that spans $2.5 < \eta < 4.0$, coincident $\pi^0 - \pi^0$ pairs can be observed at large rapidity. Near-side correlations ($|\Delta\phi| = |\phi_{\pi,1} - \phi_{\pi,2} + \pi| \approx 0$) can be used to identify di-hadron fragments from a jet produced at large rapidity. In general, di-hadron fragmentation functions are not well constrained. Nonetheless, their rate can be estimated by the Lund string model, as implemented in PYTHIA 6.222 [94]. There are two interesting scenarios to consider, each involving azimuthally correlated $\pi^0 - \pi^0$ pairs indicative of di-hadron fragmentation of a forward jet.

In the Sivers picture A_N should be associated with the forward jet. We should therefore expect that the large A_N observed for a single π^0 with $x_{F1} > 0.4$ produced at $\eta_1 \approx 3.8$ would also be present for forward jets that fragment into forward $\pi^0 - \pi^0$ pairs having $x_{F1} + x_{F2} > 0.4$. From PYTHIA, we expect $\approx 1.5 \times 10^4$ $\pi^0 - \pi^0$ events with $x_{F1} > 0.25$ and $x_{F2} > 0.15$ in the near-

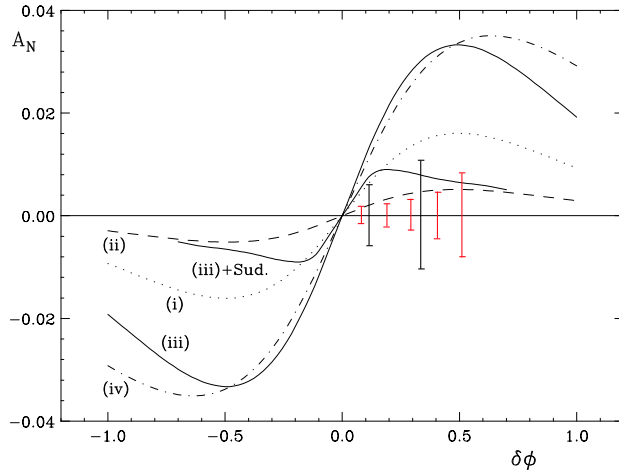


Figure 30: Predictions [127] for the spin asymmetry A_N for back-to-back di-jet production at $\sqrt{s} = 200$ GeV, for various different models for the gluon Sivers function. The solid line marked as “(iii)+Sud” shows the impact of leading logarithmic Sudakov effects on the asymmetry for model (iii). The error bars are estimated statistical uncertainties for di-jet measurement at STAR with 4 pb^{-1} , beam polarization of 50% (black) which is anticipated in 2005 run, and with 30 pb^{-1} , 70% (red).

side jet-like peak in $\Delta\phi$ for 1 pb^{-1} of integrated luminosity for p+p collisions at $\sqrt{s}=200$ GeV. PYTHIA predicts the near-side $\Delta\phi$ peak sits atop a uniform background. The signal to background ratio is approximately 1 : 1. With corrections for background, an accuracy of $\delta A_N \approx 0.01$ could be achieved with 3 pb^{-1} of integrated luminosity and 70% beam polarization.

The Collins mechanism attributes A_N to the correlation $\mathbf{S}_T \cdot (\mathbf{P}_{h_1} \times \mathbf{P}_{h_2})$ involving the momenta of two hadronic fragments of a jet and the proton spin vector. The transverse momentum associated with jet fragmentation that produces a π^0 with $x_{F1} > 0.4$ and $3 < \eta_1 < 4$ can be determined by detecting a second forward π^0 with $x_{F2} > 0.15$ and by requiring the $\pi^0 - \pi^0$ pair have $|\eta_1 - \eta_2| < 0.5$. Again, PYTHIA predicts the $\Delta\phi$ correlation has a jet-like near-side correlation peak sitting atop a uniform background. For these kinematics, we expect 2×10^3 $\pi^0 - \pi^0$ pairs in the near-side correlation peak for 1 pb^{-1} of integrated luminosity. If a non-zero Collins-Heppelmann effect is observed, then larger integrated luminosity samples would be required to map out the x dependence of the transversity structure function.

In addition, Collins and Interference FF's are being measured at $e^+ + e^-$ colliders [137] such as Belle, where analysis is currently ongoing [138]. Once these FF's are available, measurements at RHIC can be used to access the transversity distribution function. For a given partonic sub-process, eg. $qg \rightarrow qg$ the observed asymmetries are proportional to $A_T \sim \delta q(x_1) \cdot G(x_2) \cdot H_1^\perp(z)$. Experimental asymmetries contain contributions from many sub-processes, including processes without Collins-type analyzing power for transverse spin. The extraction of transversity distributions from the observed single spin asymmetries A_T will be obtained from a QCD-analysis using the experimental information available for parton distribution functions and fragmentation functions.

As stated earlier, transversity asymmetries require two chiral-odd functions, and both can be transversity. Transverse double-spin asymmetries A_{TT} for jet or high- p_T particle production will be sensitive to the product of two transversity functions. The advantage of this method

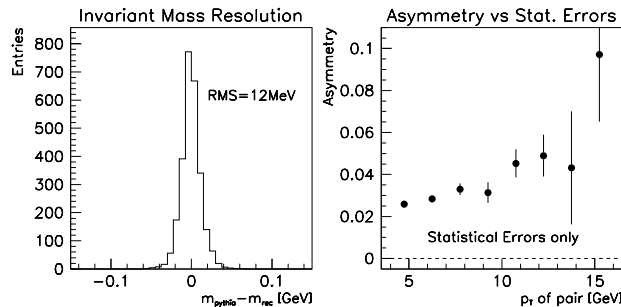


Figure 31: A statistical error projection for the Collins asymmetry, A_T in di-hadron interference fragmentation at PHENIX. The Soffer bound is assumed to be saturated. The interference fragmentation functions were taken from the model in reference [120]. The simulation assumes an integrated luminosity of 30 pb^{-1} and a beam polarization of $P = 0.5$

is that it does not require any knowledge of polarized fragmentation functions. On the other hand, as we discussed earlier, this asymmetry is highly suppressed because there is no gluon transversity and also because double chirality-flip process are color suppressed. It is important that A_{TT} measurements are done in a kinematical region where gluon contributions are small. Such measurements require the full luminosity and polarization of RHIC. There are other ideas to access transversity via the production of J/ψ [139] and D mesons [140]. Perhaps the cleanest way to measure transversity is through the Drell-Yan process [143], but this likely requires a RHIC luminosity upgrade to have sufficient sensitivity.

Table 2: Physics cases with transverse spin and its luminosity and polarization requirements

Channel	Luminosity [pb^{-1}]	Polarization
Inclusive A_N	0.4	0.2
Mapping A_N in x_F and p_T space	3	0.5
Sivers from di-jet	10	0.5
Transversity from di-hadron correlations within a jet	30	0.5
A_{TT} of jet or high- p_T particle	100	0.7
DY	1000	0.7

Table 2 is a summary of physics channels with transverse spin and its luminosity and polarization requirement. The first polarized proton collisions at RHIC have already produced exciting transverse spin asymmetry results. As the luminosity and polarization increase, more channels will become accessible. It is reasonable to expect that measurements of both the Sivers function and transversity can be achieved with $\sim 20 \text{ pb}^{-1}$ of integrated luminosity with polarization of 0.7. To achieve this goal, and minimize the impact on the longitudinal spin physics cases, we expect to use 20 – 30% of beam time for transverse spin physics. It is important to note that PHENIX and STAR have separate spin rotators; the two experiments can choose longitudinal and transverse spin independently. In general, most of the transverse spin physics is better done at $\sqrt{s}=200 \text{ GeV}$ rather than $\sqrt{s}=500 \text{ GeV}$.

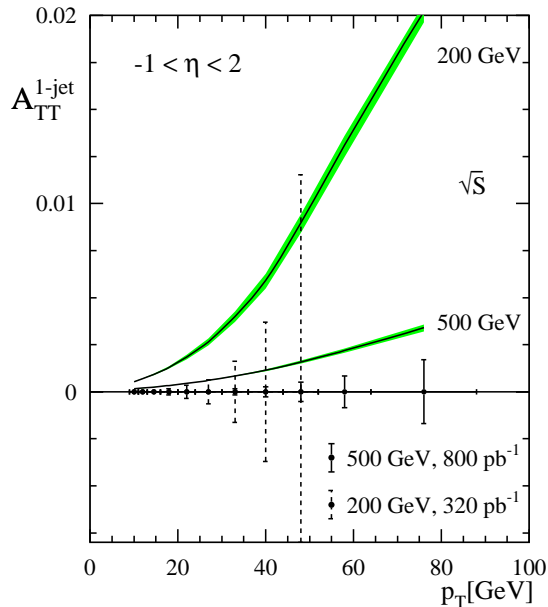


Figure 32: Maximally possible A_{TT} for single-inclusive jet production at $\sqrt{s} = 200$ and 500 GeV as a function of p_T . Jet rapidities are integrated over $-1 < \eta < 2$. The shaded bands represent the theoretical uncertainty in A_{TT} estimated by varying scale by factor 2. Also indicated as error bars is the expected statistical accuracy with design luminosity of the RHIC [144].

2.9 What else is going on around the world?

The fundamental nature of the nucleon spin puzzle and the high interest in understanding its spin structure as has lead to experimental programs around the world, to study this problem. In addition to RHIC spin at BNL, they are the COMPASS experiment at CERN in Geneva Switzerland, the HERMES experiment at DESY and the Jefferson Laboratory's Continuous Electron Beam Accelerator Facility (CEBAF) in Newport News, VI in the US. In this section we emphasize the essential features of their physics program.

2.9.1 COMPASS experiment at CERN

The COMPASS (Common Muon and Proton Apparatus for Structure and Spectroscopy) collaboration at CERN has built a dual purpose experiment, aiming to study hadron spectroscopy and hadron structure. The main spin objectives are to measure: 1) the polarization of gluons within polarized nucleons, 2) light quark helicity distributions by flavor, 3) lambda and anti-lambda polarization, 4) transverse spin distributions. Leptoproduction of open charm and of hadron pairs with large transverse momenta are considered to be the most promising options to measure $\Delta g/g$.

The experiment is located in the CERN-SPS M2 beamline of longitudinally polarized 160 GeV muons, which was used also by the former EMC and SMC experiments. The kinematic coverage is thus similar. A solid polarized target filled with ^6LiD provides both longitudinal and transverse target polarizations. A newly designed large-angle spectrometer is used to reconstruct

the scattered muons and the produced hadrons in wide momentum and angular ranges. Muon, pion, kaon, and proton identification are among its distinctive features.

The first data, collected in 2002 and 2003 using predominantly longitudinal configurations of the beam and target spins, correspond to integrated luminosities of about 600 and 900 inverse picobarn, respectively. A much smaller sample with transverse target polarizations has been collected. The recently released results on the inclusive structure function g_1^d are in agreement with those from previous experiments and provide a factor two improvement in statistical uncertainty in the region $0.004 < x < 0.03$ [145]. Similar improvements in the semi-inclusive measurements of quark helicities by flavor may be anticipated.

While the improved measurements of the inclusive structure function may lead to some refinement in the indirect extraction of gluon polarization via NLO pQCD analysis, the main COMPASS objective is of course in the direct determination of $\Delta g/g$ via the production of open charm and of high p_T hadron pairs. A first preliminary result on $\Delta g/g$ from high p_T hadron pairs [146] has a precision similar to those from the preceding HERMES and SMC analyses. The first open charm measurements are statistics limited.

The COMPASS detector will not take data in 2005 but the spin program is expected to resume in 2006, sharing its beam time with the spectroscopy program. The spectrometer acceptance will benefit greatly from an upgrade to the target magnet planned to be installed in 2005.

2.9.2 HERMES experiment at DESY

The HERMES experiment at DESY studies the spin structure of the nucleon by scattering the lepton beam in HERA off pure internal targets that can be polarized longitudinally and transversely. The large acceptance of the detector allows for inclusive and semi-inclusive measurements and, like the COMPASS spectrometer, has particle identification. The longitudinal program has delivered measurements of: 1) the inclusive structure function g_1 of the proton and neutron with similar precision and kinematic coverage as preceding measurements at SLAC, 2) detailed semi-inclusive measurements which allow the extraction of quark helicity distributions functions with different model assumptions than preceding work [90], and 3) the first analysis of spin effects in lepton production of high p_T hadron pairs, a process which is sensitive to Δg .

The present focus is on transverse and nuclear spin effects. HERMES has made the first measurement of the single-spin asymmetries for semi-inclusive electroproduction of charged pions in deep-inelastic scattering of positrons with a transversely polarized hydrogen target [90]. The asymmetry depends on the azimuthal angles of the pion and the target spin axis about the virtual photon direction and relative to the positron scattering plane. Transverse quark polarization in the target nucleon and a correlation between the intrinsic transverse quark momentum and the transverse target polarization give rise to signal of this nature, and can be distinguished in experiment with this technique. The latter might provide an indication for non-zero orbital momentum of quarks in the polarized nucleon. The HERMES program is foreseen to continue to the summer of 2007.

2.9.3 Nucleon Spin related experiments at Jefferson Laboratory

Unlike the above two experimental detectors, the CEBAF accelerator at Jefferson laboratory is a superconducting radio frequency electron accelerator facility that was commissioned during early 1990s. The accelerator uses state of the art photocathode gun that is capable of delivering beams of high polarization and high currents ($\sim 200 \mu\text{A}$) to two of its three experimental halls while maintaining high polarizations but low current ($\sim \text{few nA}$) beam to the third. Polarizations of the order of 85% are routinely achieved, and maximum beam energies are 5.5 GeV. The main machine consists of a "racetrack" layout of circulating beam line with two linear accelerators joined by two 180° arcs. The accelerator design also allows experiments with bremsstrahlung photons off of the continuous electron beams in experimental areas with fluxes ranging from $10^{7-8}/\text{sec}$.

The relatively low beam energies (compared to COMPASS, HERMES and in general RHIC) available at CEBAF and the fixed target experimental halls A, B, and C [147] makes the facility ideally suited to study the nucleon structure (including spin) in the transition region from non-perturbative to perturbative QCD. This is also the region where higher twist effects play an important role and hence can be studied at JLab. The high intensity electron beams coupled with solid or gaseous targets allows exclusive measurements using the high acceptance detectors in the halls [147]. With these characteristics of the experimental conditions, Jlab experiments explore regions of $Q^2 \rightarrow 0$ with high statistical accuracies. To date some of the most accurate tests of the GDH sum rule [148], high precision high x spin structure functions of the nucleon, azimuthal single spin asymmetries relating to transverse dynamics of the partonic spin structure and measurements of a class of reactions such as DVCS (Deeply-Virtual Compton Scattering) which are proposed to lead us to the measurement of the total angular momentum of the quarks [39], are results of experiments performed at Jefferson Lab [149]. It is the proposed measurement of the orbital angular moment of the partons inside the nucleon, those of transversity related structure functions, and their role in understanding the overall spin structure of the nucleon makes Jlab measurements complementary to those of Δg and transversity with RHIC Spin.

2.10 Elastic Scattering of polarized high energy protons

The previous sections discuss the physics of hard scattering at RHIC with polarized protons, which can be understood as collisions of polarized quarks and gluons. The scattering is so energetic that we can use perturbative QCD to describe the interactions of the quarks and gluons, and, thus, probe the spin structure of the proton at very small distances. For example, scattering at $Q^2=(80 \text{ GeV})^2$ probes wave lengths of 0.003 fermi. Small-angle scattering, from total cross section to $t = -1 (\text{GeV}/c)^2$, probes the static proton properties and constituent quark structure of the proton, covering distances from 4 fermi [$-t = 0.003 (\text{GeV}/c)^2$ in the Coulomb nuclear interference (CNI) region] to a distance of ≈ 0.2 fermi. Unpolarized scattering shows striking behavior in this region, from the surprise that total cross sections rise at high energy, to observed dips in elastic cross sections around $-t = 1 (\text{GeV}/c)^2$. Both polarimetry at RHIC and the PP2PP experiment explore this region for spin-dependent cross sections, for $\sqrt{s}=7\text{-}500 \text{ GeV}$, for the first time.

In the very forward region, the nuclear and electromagnetic amplitudes are of comparable

magnitude, and the interference between them results in a small but significant maximum in the single transverse spin asymmetry A_N making elastic scattering in the CNI region useful for polarimetry [150]. Important results have already been obtained in the RHIC spin program in this region. There have been measurements made near RHIC injection energy (24 GeV/c) using a carbon micro-ribbon target both at the AGS (E950) and in RHIC; there have been measurements made with a 100 GeV/c beam on a carbon target and independently on a gas jet target. In addition, a measurement in the colliding beam mode has been carried out (pp2pp).

CNI scattering produces an asymmetry from the scattering of an unpolarized particle, a proton in one RHIC beam or a carbon nucleus in a fixed target, from the anomalous magnetic moment of a polarized proton, with a maximum of $A_N = 0.04$ at $-t = 0.003$ (GeV/c)². However, a hadronic spin-flip term can also contribute to the maximum, and this term is sensitive to the static constituent quark structure of the proton. The authors of Reference [151] remark that the helicity flip probes the shortest interquark distance in the proton, and that the helicity nonflip is sensitive to the largest quark separation in the proton due to color screening. The helicity-flip term, if present, can indicate an isoscalar anomalous magnetic moment of the nucleons [152], an anomalous color-magnetic moment causing helicity nonconservation at the constituent quark-gluon vertex [153], and/or a compact quark pair in the proton [154, 155].

The results from scattering 100 GeV/c polarized protons on carbon [156] are shown on the left side of Fig. 33. An asymmetry reaching 0.02 is observed, with a t -dependence quite different from pure electro-magnetic spin flip (the top curve in the figure). The curves use a standard CNI form [157], with the lower curve including hadronic spin flip. Results from scattering 100 GeV/c protons on a highly polarized hydrogen jet target [158] are shown on the right side of Fig. 33. In this figure, the solid line is the prediction with only electromagnetic spin flip. For pp scattering at this energy ($\sqrt{s}=14$ GeV), no hadronic spin flip is observed. Further, the preliminary measurement from the pp2pp experiment with colliding beams at RHIC is also shown on the right side of the figure. For $\sqrt{s}=200$ GeV, the asymmetry is somewhat larger than the CNI curve without hadronic spin flip, but, including present uncertainty on the beam polarization (the measurement was made in 2003 before the jet provided more precise polarization results), the result is consistent also with no hadronic spin flip for pp scattering.

Small-angle scattering at high energy is presently understood in a Regge picture as being dominated by Pomeron exchange [161]. The Pomeron, which has the vacuum quantum numbers with charge-conjugation $C = +1$, can be interpreted as a two-gluon exchange. These results for A_N for carbon and proton targets imply that the isospin 0 Reggeons (which include the Pomeron) have a significant spin flip coupling for the carbon target. The $I = 1$ Regge poles for the proton target scattering must be sufficiently strong to nearly cancel the $I = 0$ contribution at this energy. The couplings required have been determined and indicate that asymptotically the Pomeron will contribute about 10% spin-flip; i.e. the cancellation leading to no spin-flip in pp at 100 GeV/c will go away as the energy increases [162].

Many other measurements can be made at RHIC, for elastic scattering and also for diffractive scattering with rapidity gap measurements. The two-spin transverse asymmetry in the CNI region, for example, is sensitive to a C-parity odd exchange, referred to as the Odderon [163]. For larger t , a steep exponential fall with momentum transfer, characteristic of pomeron exchange matches on to an approximate t^{-8} dependence at larger $-t$ in the unpolarized cross sections. The latter has a natural interpretation in terms of three vector exchanges between pairs of valence

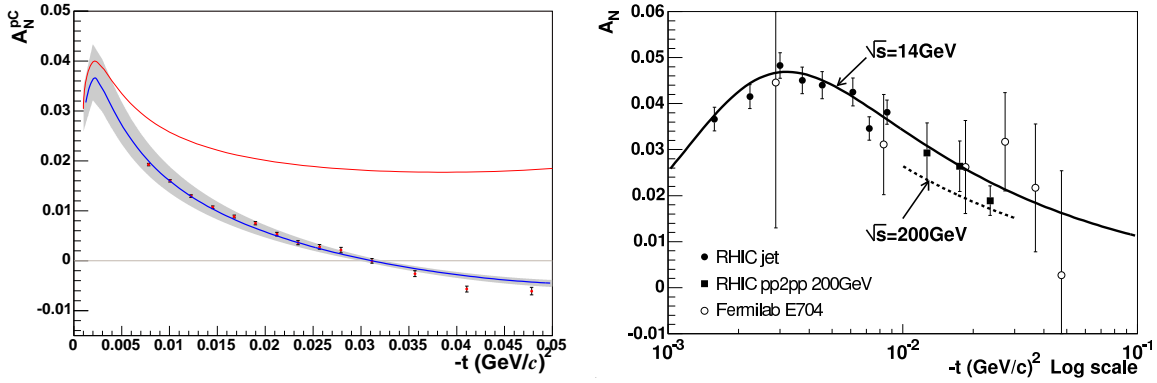


Figure 33: $A_N(t)$ for pC elastic scattering at 100 GeV, left side [156]. The shaded band represents the systematic uncertainties of the measurement. The solid line in the band is a fit to the data including a significant hadronic spin-flip contribution (see text). The result is significantly different from the no hadronic spin-flip prediction (top curve). The right side shows preliminary measurements (solid points) of proton-proton elastic scattering with 100 GeV protons incident on a highly polarized atomic hydrogen jet target [158]. The open squares are data from E704 at Fermilab [159]. In this case, the curve with no hadronic spin flip describes the data well. The closed box is the preliminary result from the colliding beam experiment $pp2pp$, $\sqrt{s}=200$ GeV [160]. A 20% systematic uncertainty for the beam polarization is not shown. The dashed curve is the pure CNI prediction for this energy.

quarks. Whether these individual scatterings should be thought of as single gluons, or as (at least in part) perturbative exchanges in color-singlet configurations remains to be seen. This profile is fairly stable with energy, even as the details of its shape change. The observation of a stable profile in polarized elastic scattering at RHIC would surely initiate a new class of theoretical investigations. Lastly, the dramatic spin dependence of proton-proton elastic scattering at moderate $-t$ observed in the Argonne and BNL experiments of twenty years ago remains an outstanding puzzle [164]. This could also be explored at RHIC.

2.11 Search for Physics beyond the Standard Model

Single beam helicity asymmetries violate parity and give access to searches for potential physics beyond the Standard Model (SM), for example for quark substructure, new neutral gauge bosons present in some supersymmetric models, and supersymmetric particle production. In general, parity violation searches can compete with the sensitivity of much higher energy unpolarized colliders, and a parity violation signal beyond known electro-weak effects would be a decisive signal for new physics. Furthermore, if a new interaction is discovered for example at the LHC, and lower-lying masses are accessible at RHIC, RHIC will be able to explore the chiral structure of the new interaction. We discuss the potential new particles and mass ranges where RHIC can contribute in this section. For sensitivities we generally consider the target luminosity for $\sqrt{s}=500$ GeV of $\sim 1 \text{ fb}^{-1}$ and a large acceptance detector, for example STAR with high luminosity capability. However, a suggested new detector [165] and an order of magnitude higher luminosity

from a RHIC II can also be considered. Fig. 34 shows the single beam helicity asymmetry A_L

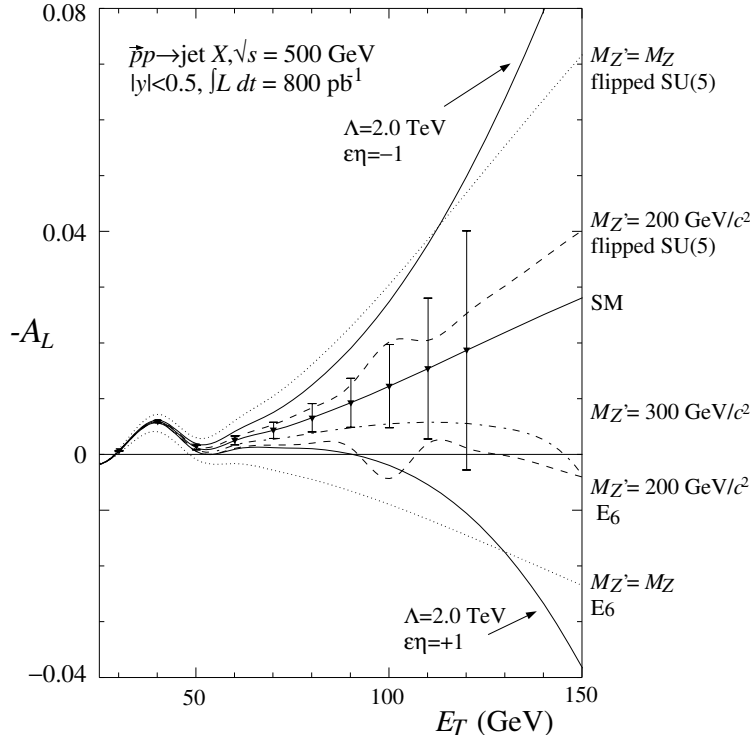


Figure 34: A_L , for one-jet inclusive production in $\vec{p}p$ collisions versus transverse energy, for $\sqrt{s} = 500$ GeV. The solid curve with error bars represents the SM expectations. The error bars show the sensitivity at RHIC for 800 pb^{-1} , for the STAR detector. The other solid curves, labeled by the product of $\epsilon\eta$, correspond to the contact interaction at $\Lambda = 2$ TeV [166]. The dashed and dotted curves correspond to different leptophobic Z' models. The calculations are at leading order.

for single jet production versus the transverse energy of the jet, for the SM and its extensions. The SM predicts a parity violating asymmetry, around $E_T = M_W/2$ for $W \rightarrow 2 \text{ jet}$ production, and from QCD-electroweak interference. Indeed, the data in the peak provides a calibration for the SM effects. The figure uses the top RHIC energy, our target luminosity for this energy, and the acceptance of the STAR detector [166]. The sensitivities shown do not include detector efficiency. Two extensions of the SM are considered: quark compositeness, and new neutral gauge bosons that appear in several string-derived models [167] (non-supersymmetric models may be also constructed [168]).

The quark compositeness curves in the figure use a compositeness scale $\Lambda=2$ TeV and maximal parity violation $\eta = \pm 1$. Composite models of quarks and leptons [169] generally violate parity, since the scale of compositeness $\Lambda_c \gg M_W$. The present limit from unpolarized collisions, at the Tevatron, is [170] $\Lambda \cong 1.6$ TeV. Due to the direct sensitivity to parity violation, RHIC can compete with the much higher energy Tevatron. Further, if an anomalous parity violation signal is observed, it would be a definitive observation of new physics. The limits of sensitivity for Λ in the contact model of quark compositeness [166] are tabulated in Table 3 for RHIC, the Tevatron and the LHC, with $L \sim 1 \text{ fb}^{-1}$ integrated luminosity the RHIC spin target for $\sqrt{s}=500$ GeV, and $L \sim 10 \text{ fb}^{-1}$ a potential target for RHIC II.

Collider	\sqrt{s} (TeV)	L (fb $^{-1}$)	Λ (TeV)
RHIC $p^\uparrow p$	0.5	1	3.3
	0.5	10	5.5
Tevatron limit	1.8	0.5	1.6
Tevatron $p\bar{p}$	2.0	30	5
LHC pp	12	100	30

Table 3: *Limits on quark compositeness (Λ) at 95% CL for different colliders. RHIC uses $P=0.7$, STAR detector acceptance, single jet production, parity violation signal with maximal parity violation for compositeness. The Tevatron and LHC use the deviation from the SM for the inclusive-jet cross section versus p_T . 10 % systematic errors in asymmetry are assumed [166].*

Also shown in Fig. 34 are Z' curves. In the framework of supersymmetric models with an additional Abelian $U(1)'$ gauge, it has been shown [171] that the Z' boson could appear with a relatively low mass ($M_Z \leq M_{Z'} \leq 1$ TeV) and a mixing angle with the standard Z close to zero. The effects of different representative models are also shown in Fig. 34 (see Ref. [172] for details). RHIC covers some regions of parameters space of the different models that are unconstrained by present and forthcoming experiments, and RHIC would also uniquely obtain information on the chiral structure of the new interaction.

There are also a number of other examples. Using a RHIC luminosity of 1 fb^{-1} at $\sqrt{s}=500$ GeV, parity violating asymmetry in the production of supersymmetric sparticles (multijets plus large missing E_T ; trileptons, etc.) of mass up to 75 GeV would be observable [173]. Another example is to search for a transverse asymmetry for W or Z boson production, where the SM prediction is very small [92, 175, 176]). W^\pm and Z^0 production in $p^\uparrow p$ collisions at RHIC is expected to have good sensitivity to $\mathcal{L}_{SM}-\mathcal{L}_{nonSM}$ interference at the parton level due to strong correlation between the proton spin and the polarization of high- x valence quarks, that participate in the gauge boson production [174]. This asymmetry could arise from anomalous electroweak dipole moments of quarks [176, 177, 178]. The RHIC sensitivity can improve present experimental limits [179] by a factor $\sim 5-10$ [178]. These limits do not approach the SM expectations, and a signal would be direct indication of new physics.

2.12 Connection to eRHIC

The addition of a high energy, high polarization lepton (electron/positron) beam facility to the existing RHIC Complex, able to collide with its hadron beam, would dramatically increase RHIC's capability to do precision QCD physics. Such a facility with 10 GeV/c polarized electrons/positrons has been proposed and is called eRHIC. There are many connections between the RHIC spin program and eRHIC. We categorize them in two groups:

- *Direct connections to RHIC Spin:* In these, the physics observables measured by the existing RHIC spin physics program will be measured in complementary kinematic regions, or in some cases augmented to complete the understanding of nucleon spin.

- *Indirect Connections to RHIC Spin:* These include measurements not possible with RHIC Spin, but of significance to understanding QCD with spin in general or nucleon spin in particular.

2.12.1 Direct Connections

Direct connections between RHIC Spin and eRHIC are made on three principal topics : the measurement of the polarized gluon distribution, the measurement of polarized quark-anti-quark distributions, and on transverse physics measurements.

For polarized gluon distribution measurements, eRHIC enables an increase in the kinematic range and precision, particularly at low x . At eRHIC the polarized gluon distribution will be measured using a) the scaling violations of spin structure functions $g_1^{p/n}$ and b) di-jet and high p_T di-hadron production in the photon gluon fusion process [180]. The RHIC spin measurements discussed earlier in this document will be most significant in the medium-high x range, $x > 10^{-2}$, while eRHIC will complement them with precision on low x , ($x < 10^{-2}$) all the way to $x \sim 10^{-4}$.

RHIC Spin will be the first to measure in a model independent way the polarized quark and anti-quark distributions using single spin longitudinal asymmetry measurements in pp scattering at $\sqrt{s}=500$ GeV/ c via (W^\pm) production. Analysis of these asymmetries will give us $\Delta u, \Delta \bar{u}, \Delta d, \Delta \bar{d}$ (see Sec. 2.7). The quark-anti-quark separation in such a way is not possible in fixed target DIS where the virtual γ is the propagator of the force which cannot differentiate between quarks and anti-quarks. However, at high enough energy, in DIS at eRHIC, virtual W^\pm also get exchanged. If $\Delta q = u, \bar{u}, d, \bar{d}$ are known by early next decade from RHIC Spin, eRHIC will be able to continue this program by exploring the heavy quarks, i.e. identify the spin contributions from $\Delta c/\bar{c}$ and $\Delta s/\bar{s}$. Of course, traditional methods to get quark flavor distributions (quark-antiquark unseparated) using semi-inclusive DIS measurements of charged and neutral pions and kaons will also continue, with access to flavor separation at lower x than is possible in current fixed target DIS experiments.

Transversity is the last as yet unmeasured spin structure function, discussed in detail in 2.8. The measurements at RHIC with pp scattering will be made using measurements of Collins Fragmentation Function (CFF), Interference Fragmentation Functions (IFF) and if very large luminosities are achieved, also with Drell Yan (DY) processes (see Sec. 2.8). These measurements will be made in the center of mass energy range from 200 to 500 GeV. The eRHIC will make a complementary set of measurements, with high precision using CFF and IFF measurements, not unlike those made by the HERMES collaboration currently.

2.12.2 Indirect Spin Connections

In addition to the measurements eRHIC will do that will extend or complement the investigation of nucleon spin with RHIC Spin, there is another class of nucleon spin and other helicity related measurements that could also be made with eRHIC. A partial list includes:

- Measurement of spin structure functions g_1 of the proton and neutron and the difference between them that tests the Bjorken spin sum rule. eRHIC will do this with accuracies

that will for the first time start competing and challenging the experimental systematic uncertainties at the level of 1- 2%. Low x phenomena have been some of the most exciting aspects of the physics coming from unpolarized DIS measurements in the last decade, and eRHIC will probe low x kinematics for the first time with polarized beams

- eRHIC will be the only possible facility in the foreseeable future at which QCD spin structure of the quasi-real photon could be explored. The process employed for this investigation is that of photon-gluon fusion [181].
- Deeply virtual Compton scattering (DVCS) for final state photons as well as other vector mesons measured using almost complete acceptance (4π) detectors has been suggested as a preliminary requirement towards the measurement of the Generalized Parton Distributions (GPDs). A series of different GPD measurements may be required eventually to extract the orbital angular momentum of the partons. This is the last part of the nucleon spin puzzle which we may have to address after the spin of the gluon is understood. Although the theoretical formulation is not yet ready, it is expected that by the time eRHIC comes on line, there will be a formalism available to take the measured GPDs and determine the orbital angular momentum of partons. These measurements at eRHIC will be complementary, at much higher energy scales, to those being planned at Jefferson Laboratory after its 12 GeV upgrade plan.
- Drell Hearn Gerasimov spin rule [148] measurements presently underway at Jefferson laboratory [149] and at the Mainz Microtron (MAMI) are mostly at low values of ν [182]. While the significance of the contribution the spin sum rule from high ν is small, absolutely no measurements exist beyond the value of $\nu > \approx 1$ GeV. eRHIC will extend direct measurements of the high ν component up to 500 GeV.
- Precision measurements of spin structure functions in very high $x \sim 0.9$ region could be part of the eRHIC physics program with specially designed detectors as has been discussed in [183].

The physics programs with polarized proton beams at RHIC and eRHIC have much in the way of complementarity of physics measurements. It's also clear that success at eRHIC passes through a period of successful measurements and collider development by the RHIC spin program not only at $\sqrt{s}=200$ GeV/ c but also at $\sqrt{s}=500$ GeV/ c .

3 Accelerator performance

As of 2004, polarized proton beams have been accelerated, stored and collided in RHIC at a center of mass energy of 200 GeV. The average store luminosity reached $4 \times 10^{30} \text{cm}^{-2} \text{s}^{-1}$, and the average store polarization 45% (see Table 4). Over the next 4 years we aim to reach the Enhanced Luminosity goal for polarized protons, consisting of an average store luminosity of

- $60 \times 10^{30} \text{cm}^{-2} \text{s}^{-1}$ for 100 GeV proton energy, and
- $150 \times 10^{30} \text{cm}^{-2} \text{s}^{-1}$ for 250 GeV proton energy,

both with an **average store polarization of 70%**. Table 4 gives a projection of the luminosity and polarization evolution through FY2008. Luminosity numbers are given for 200 GeV center of mass energy and one of two interaction points. For operation with more than two experiments, the luminosity per interaction point is reduced due to an increased beam-beam interaction. For each year the maximum achievable luminosity and polarization is projected. Projections over several years are not very reliable and should only be seen as guidance for the average annual machine improvements needed to reach the goal. We assume that 10 weeks of physics running are scheduled every year to allow for commissioning of the improvements and development of the machine performance.

Table 4: *Maximum projected RHIC polarized proton luminosities through FY2008. Delivered luminosity numbers are given for 200 GeV center of mass energy and one of two interaction points. 10 weeks of physics operation per year are assumed. The designation 2002A refers to achieved, and 2005E refers to expected.*

Fiscal year		2002A	2003A	2004A	2005E	2006E	2007E	2008E
No of bunches	...	55	55	56	79	79	100	112
Protons/bunch, initial	10^{11}	0.7	0.7	0.7	1.0	1.4	2.0	2.0
β^*	m	3	1	1	1	1	1	1
Peak luminosity	$10^{30} \text{cm}^{-2} \text{s}^{-1}$	2	6	6	16	31	80	89
Average luminosity	$10^{30} \text{cm}^{-2} \text{s}^{-1}$	1.5	3	4	9	21	53	60
Time in store	%	30	41	41	50	53	56	60
Max luminosity/week	pb^{-1}	0.2	0.6	0.9	2.8	6.6	18.0	21.6
Max integrated luminosity	pb^{-1}	0.5	1.6	3	20	46	126	151
Average store polarization	%	15	30	45	49	65	70	70
Max LP ⁴ /week	nb^{-1}	0.1	5	37	160	1180	4330	5190

In Fig. 35 the integrated luminosity delivered to one experiment is shown through FY2012 for two scenarios: 10 weeks of physics operation per year, and 10 weeks of physics operation every other year. For every projected year shown in Fig. 35 the weekly luminosity starts at 25% of the final value, and increases linearly in time to the final value in 8 weeks. During the remaining weeks the weekly luminosity is assumed to be constant. For the maximum projection the values in Table 4 are used as final values until FY2008. For later years the FY2008 values are assumed with no further improvement. The minimum projection is one third of the maximum projection, based on past experience in projecting heavy ion luminosities [184].

For the scenario with 10 weeks of physics operation per year, the assumed center of mass energy is 200 GeV until mid-FY2009, and 500 GeV thereafter. For the scenario with 10 weeks

every other year, the assumed center of mass energy is 200 GeV throughout the entire period, reaching the target in 2012.

For the scenario with 10 weeks of physics operation every other year, the final values are not increased in years without proton operation, since no time is available to develop the machine performance. Thus in our projections we reach the Enhanced Luminosity goal in FY2009 with 10 week physics operation per year, but need until FY2012 with 10 weeks of physics operation every other year. For operation at 500 GeV center of mass energy, the luminosity projections in Table 4 need to be multiplied by 2.5. We expect no significant reduction in the average store polarization after full commissioning of polarized proton ramps to 250 GeV for the $\sqrt{s} = 500$ GeV running.

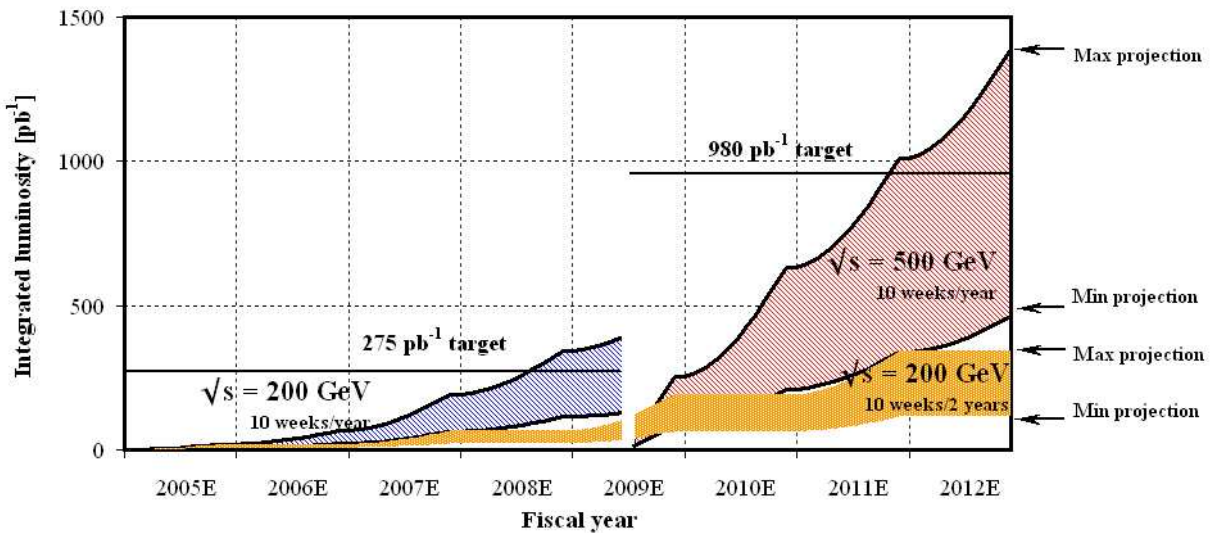


Figure 35: Minimum and Maximum projected integrated luminosity through FY2012. Delivered luminosity numbers are given for one of two interaction points. For the scenario with 10 weeks of physics operation per year, the assumed center of mass energy is 200 GeV to mid-FY2009, and 500 GeV thereafter. For the scenario with 10 weeks every other year, the assumed center of mass energy is 200 GeV throughout the entire period.

3.1 Polarization limitations

The RHIC beam polarization at the proton energy of 100 GeV is currently limited by the AGS beam polarization transmission efficiency of about 70%, and the source polarization. With the installation of a new solenoid in FY2005, the source polarization is expected to increase from 80% to 85%. The existing AGS polarized proton setup includes a 5% warm helical snake for overcoming imperfection spin depolarizing resonances and an RF dipole for overcoming 4 strong intrinsic spin resonances. This setup has two drawbacks:

1. All the weak intrinsic spin resonances are crossed with no correction and result in a total depolarization of about 16%.
2. Operation with the RF dipole still leads to about 15% depolarization.

In addition, the AGS has shown a dependence of the beam polarization on the bunch intensity. These shortcomings can be overcome with the installation of a new AGS cold snake, to be initially

commissioned in 2005. With a scheme that combines the AGS cold snake of 15%, and the AGS warm snake of 5%, depolarizations at all imperfection and all intrinsic spin resonances should be eliminated, making the AGS spin transparent with the exception of some mismatch at injection and extraction [185].

Obtaining 70% beam polarization in RHIC at 250 GeV proton energy is challenging because of strong intrinsic and imperfection resonances beyond 100 GeV. Betatron tunes and orbit distortions have to be controlled precisely to avoid depolarization due to snake resonances. Simulations show that orbit distortions have to be corrected to less than 0.3 mm rms. Orbit errors are introduced due to misalignments and remain if the orbit cannot be corrected completely. A realignment of the entire ring is scheduled for the 2005 summer shutdown. Efforts continue to improve the existing beam position monitor system, and the orbit correction techniques. A beam-based alignment technique is under development. With the existing hardware and software, orbit distortions of 1 mm rms were achieved, as measured by the beam position monitors. Acceleration of polarized proton beams beyond 100 GeV is planned in 2005. The result of this machine development effort will provide guidance for the tolerable levels of machine misalignments and orbit errors.

3.2 Luminosity limitations

A number of effects limit the achievable luminosity. Currently the bunch intensity is limited to about 1×10^{11} to maintain maximum polarization in the AGS. This restriction should be removed with the AGS cold snake. With intense bunches the beam-beam interaction will limit the luminosity lifetime. With bunches of 2×10^{11} protons and 2 interaction points, the total beam-beam induced tune spread will reach 0.015. Operation with more than two collision points will significantly reduce the luminosity lifetime. RHIC is also the first hadron collider to operate in a strong-strong beam-beam regime. High intensity beams also lead to a vacuum breakdown, caused by electron clouds. In the warm sections, NEG coated beam pipes are installed, that have a lower secondary electron yield, and provide linear pumping. In the cold regions, additional pumps are installed to improve the vacuum to an average value of 10^{-5} Torr before the cool-down starts. With the PHENIX and STAR detector upgrades, the vacuum system in the experimental regions will also be improved.

Time in store can be gained through faster machine set-up, a reduction in system failures, and the injection of multiple bunches in each AGS cycle. We project that the time in store can be increased to about 100 hours per week, or 60% of calendar time.

3.3 Polarimetry

Beam polarization measurements in RHIC provide immediate information for performance monitoring, and absolute polarization to normalize the experimental asymmetry results. Two types of polarimeters are used. Both are based on small angle elastic scattering, where the sensitivity to the proton beam polarization comes from the interference between the electromagnetic spin-flip amplitude that generates the proton anomalous magnetic moment and the hadronic spin non-flip amplitude, and possibly a hadronic spin-flip term.

One type of polarimeter uses a micro-ribbon carbon target, and provides fast relative polarization measurements. The other type uses a polarized atomic hydrogen gas target, and provides slow absolute polarization measurements. In addition, both PHENIX and STAR have developed local polarimeters that measure the residual transverse polarization at their interaction points. These polarimeters are used to tune and monitor the spin rotators that provide longitudinal polarization for the experiments. They polarimeters are discussed in the Experiments section.

The fast proton-carbon polarimeter was first developed at the AGS [186]. It measures the polarization in RHIC to $\Delta P = \pm 0.02$ in 30 seconds. Measurements taken during a typical store in 2004 are shown in Fig. 36. A carbon ribbon target is introduced into the beam, and the left-right scattering asymmetry of recoil carbon ions is observed with silicon detectors inside the vacuum. The silicon detectors observe the energy and time of flight of the recoil particles near 90° [187]. The detector selects carbon ions with a momentum transfer in the coulomb-nuclear interference (CNI) region, $-t = 0.005 - 0.02$ (GeV/c) 2 . In this region, the interference of the electromagnetic spin flip amplitude and the hadronic non-flip amplitude produces a calculable t -dependent asymmetry of 0.03 to 0.02. The cross section is large, so that the sensitivity to polarization is large. A term from a hadronic spin flip amplitude is also possible and is reported in Ref. [186]. This contribution is not calculable, so that this polarimeter must be calibrated using a beam of a known polarization.

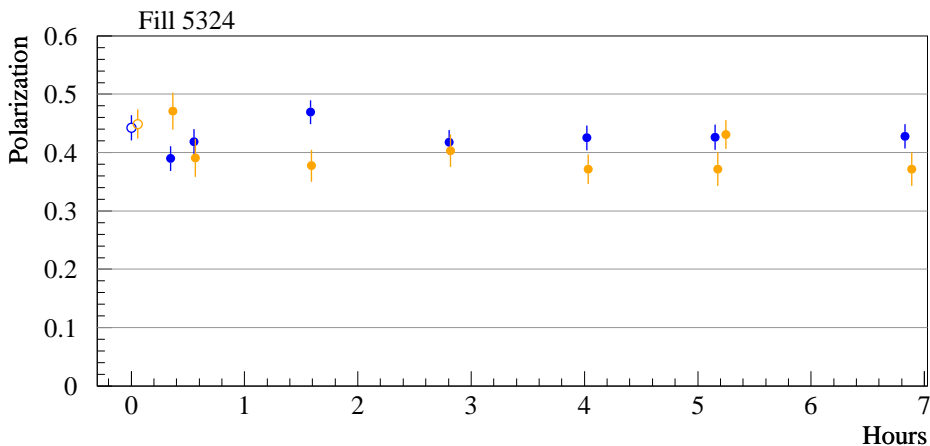


Figure 36: *Measured polarization during one store of RHIC in 2004.*

A polarized atomic hydrogen gas jet target was used for the first time in RHIC in 2004 [188]. The atoms are polarized with the Stern-Gehrlach process to select one electron polarization state, with rf transition to select proton polarization. The atoms are focused in the RHIC beam region to 6 mm FWHM using the atomic hydrogen magnetic moment. A Breit-Rabi polarimeter after the RHIC beam measures the polarization by cycling through rf transition states. The polarization was determined to be 0.92 ± 0.02 , including correction for the measured 2% molecular fraction (4% nuclear fraction) that is unpolarized. The online target polarization measurements are shown in Fig. 37. The target polarization was reversed roughly every 8 minutes by changing rf transitions. Silicon detectors measure a left-right asymmetry for proton-proton elastic scattering in the CNI region, similar to the p-carbon polarimeters. By measuring the asymmetry with respect to the target polarization sign, we measure the analyzing power for proton-proton elastic scattering, as shown in the elastic scattering subsection. By then measuring the left-right asymmetry with respect to the beam polarization sign, flipping each bunch (every 200 ns), we obtain the absolute beam polarization. The absolute beam polarization was measured to better than $\Delta P/P = 7\%$ in

2004 (preliminary).

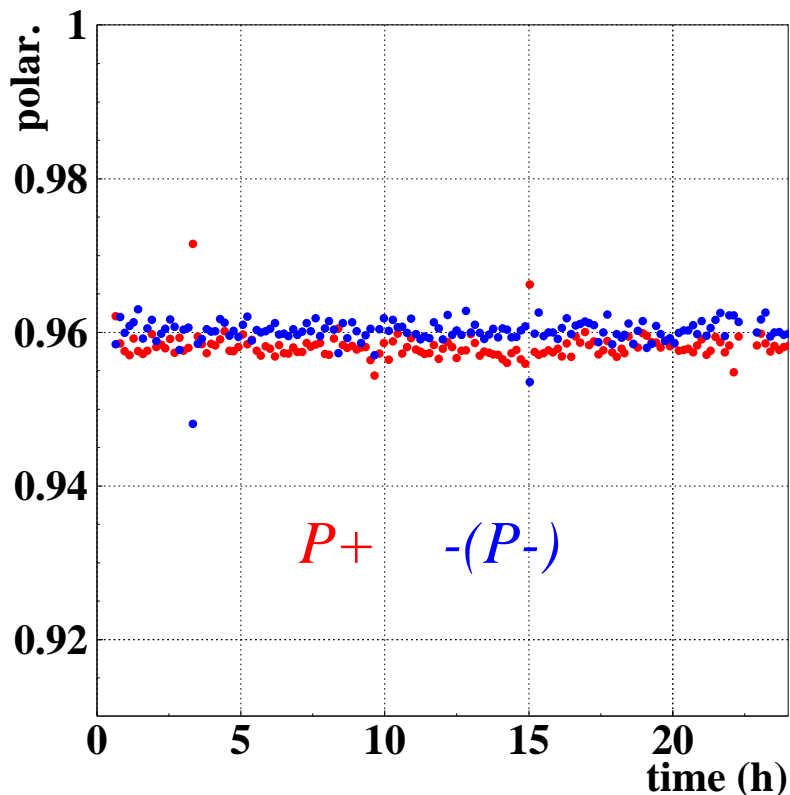


Figure 37: *Online polarization measurements for the polarized atomic hydrogen jet target in RHIC during the 2004 run. No correction is included for molecular hydrogen contamination (about 3%).*

A remaining issue is whether the carbon polarimeter calibration can be used for different detectors, from year to year, or whether it will be necessary to recalibrate each year using the jet target. We can also choose to use the jet target as the RHIC polarimeter, with the carbon polarimeter used for corrections, for example for different polarization of the bunches and for a polarization profile of the beams. It will also be necessary to improve the lifetime of the silicon detectors from radiation to avoid changing detectors mid-run, which worsens the RHIC vacuum and is not expected to be compatible with high luminosity running. A related issue is development to be able to bake out the polarimeter region.

3.4 Long-term perspective

A number of ideas are pursued for long-term improvements of the machine performance. RHIC II aims at increasing the heavy ion luminosity by an order of magnitude through electron cooling. For protons, cooling at store is not practical but pre-cooling at injection might be beneficial. A further reduction of β^* , especially at 250 GeV proton energy appears possible. Some benefits may

also come from stochastic cooling, currently developed for heavy ions. We expect a luminosity improvement of a factor 2-5 for polarized protons for RHIC II.

With a new interaction region design, the final focusing quadrupoles can be moved closer to the interaction point, thus allowing to squeeze β^* further. This, however, makes some space unavailable for the detectors. Additional increases in the luminosity may come from a further increase in the number of bunches, to close to 360, as is planned for eRHIC, or operation with very long bunches. The latter requires a substantial R&D effort, as well as a new timing system for the detectors.

4 Experiments

Beginning in FY 2003, DOE has funded a detector R&D program, as part of the RHIC operations budget, supporting the development of advanced detector techniques to meet specific needs for proposed upgrades to PHENIX and STAR. As a result, the upgrade proposals discussed below take advantage of extensive R&D effort within the RHIC community on the technologies of precision tracking with silicon detectors, multi-gap resistive plate chambers (RPC) for large-area time-of-flight measurements, and the GEM technology for electron multiplication in compact, high-resolution gaseous tracking detectors.

This section describes the three experiments capable of making spin measurements.

4.1 PHENIX

RHIC has made great strides toward providing high luminosity beams of highly polarized protons. To make statistically sensitive asymmetry measurements with low systematics requires well understood detectors; clean, highly selective triggers, reliable measurements of beam luminosity and polarization, and the ability to take and analyze data at high rates. In this section we discuss the current and proposed capabilities of the PHENIX detector in the context of meeting the challenges of the spin program.

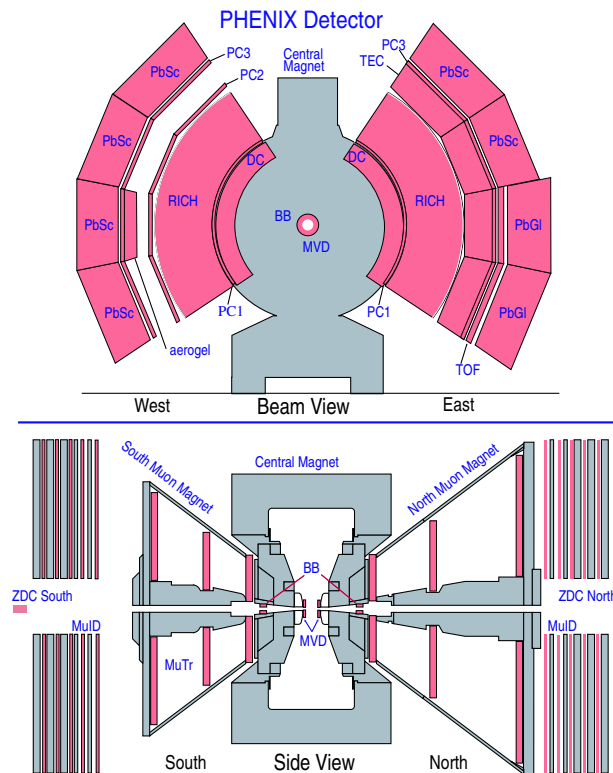


Figure 38: *Plan view and side views of the PHENIX detector.*

As shown in Fig. 38, the PHENIX detector comprises four instrumented spectrometers (arms)

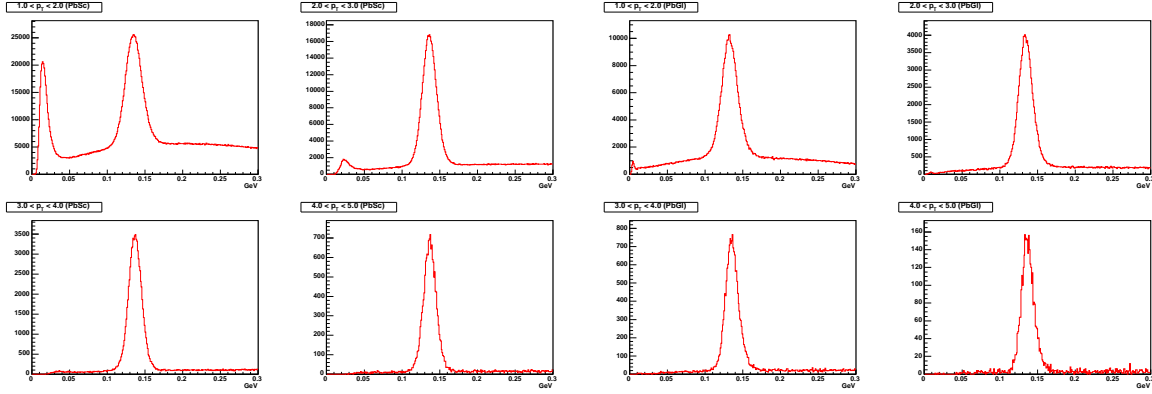


Figure 39: The π^0 mass spectrum in 1 GeV p_T bins 1-2 GeV/c, 2-3 GeV/c, 3-4 GeV/c and 4-5 GeV/c. The left four panels are for lead scintillator (PbSc), and the right four panels are for lead glass (PbGl) calorimeter sectors. Events are collected using the high p_T photon trigger of the EMCal. The combinatorial background is $\sim 30\%$ for a p_T range from 1 to 2 GeV/c, and $\sim 5\%$ for $p_T > 5$ GeV/c. The two-photon invariant mass resolution is 8.5% in the first p_T bin and 6.4% in the last p_T bin.

and two global detectors [189]. The east and west central arms are located at central rapidity and instrumented to detect electrons, photons, and charged hadrons. The north and south forward arms have full azimuthal coverage to detect muons. In addition, the zero degree calorimeters (ZDCs) and beam-beam counters (BBCs) measure the time and position of the collision vertex [190].

4.1.1 PHENIX Central Arms

The PHENIX central arms consist of tracking systems for charged particles and electromagnetic calorimetry. We require a calorimeter with the ability to distinguish isolated photons from those from π^0 decays over a large p_T range. A thorough understanding of the calorimeter and associated triggers is vital for these measurements.

The calorimeter (EMCal) [191] is the outermost subsystem of the central arms, located at a radial distance of ~ 5 m from the beam line. Each arm covers a pseudorapidity range of $|\eta| < 0.35$ and an azimuthal angle interval of $\Delta\phi \approx 90^\circ$, and is divided into sectors containing a lead scintillator (PbSc) calorimeter or lead glass (PbGl) calorimeter. Each calorimeter tower subtends a solid angle $\Delta\phi \times \Delta\eta \sim 0.01 \times 0.01$, ensuring the two photons from π^0 decay are resolved up to a p_T of 12 GeV/c. Shower profile analysis can extend this p_T range beyond 20 GeV/c. The energy calibration used the position of the two photon invariant mass peak from π^0 decay, the energy deposit from minimum ionizing charged particles traversing the EMCal (PbSc), and the momentum determined by the tracking detectors of electrons and positrons identified by the ring-imaging Čerenkov detector. It has been shown that the energy resolution was better than 1.5%. The effective energy resolution was deduced by comparing the measured energy and momentum for identified electrons and positrons and from the widths of the π^0 invariant mass peaks as shown in Fig.39.

The number of recorded high- p_T π^0 's is enhanced by a high- p_T trigger which uses threshold discrimination applied to sums of the analog signals from 4×4 groupings (tiles) of adjacent EMCAL towers. The efficiency reached a plateau of 0.9 at ~ 4 GeV, which is consistent with the geometrical acceptance of the active trigger tiles, and was reproduced by Monte Carlo calculations. Charged particle contamination in the photon sample was minimized by using information from the PHENIX ring-imaging Čerenkov and tracking detectors [192, 193].

The calorimeter and trigger performance have enabled PHENIX to make many significant measurements within the first few years of running. Measurements have been made of the cross-section [59] and double-helicity asymmetry [83] for π^0 production (see Figs. 6, 12). Figure 40 shows an experimental efficiency for π^0 detection at PHENIX including BBC and EMCAL trigger efficiencies, offline data selection, and reconstruction efficiencies. The prompt photon production cross-section in pp collisions has also been measured [66, 194] and the NLO pQCD calculation [67] is in good agreement with the data (see Fig.8). In Ref. [66], a photon isolation cut was applied as a first step toward a spin asymmetry measurement. The cut reduces the level of background photons diluting the analyzing power. With increased luminosity we expect improved precision on these measurements, and the first measurements of the double spin asymmetry $A_{LL}^{pp \rightarrow \gamma X}$.

The EMCAL will also be used for measurements of inclusive electron asymmetries from semi-leptonic decays of charm and beauty produced mainly by gluon-gluon fusion in pp scattering. Electrons in the central arms are identified by the RICH detector (Čerenkov threshold for $\pi^\pm \approx 4.9$ GeV/ c) and the EMCAL. The yield of electrons can be categorized into nonphotonic electrons mainly from semi-leptonic decays of charm and beauty, and photonic electrons mainly from gamma conversion and Dalitz decays of neutral mesons such as π^0 and η [195].

4.1.2 Muon Arms

The systematic study of J/ψ production at Relativistic Heavy Ion Collider (RHIC) energies with wide p_T and rapidity coverage should provide crucial tests of J/ψ production models. In addition, the RHIC proton-proton results provide a baseline for studying cold and hot nuclear matter in proton-nucleus and nucleus-nucleus collisions using J/ψ yields as a probe. PHENIX has two forward spectrometers devoted to the characterization of single and di-muon events in the forward rapidity regions [196]. The central magnet poles act as a hadron absorber in front of a radial field magnet with acceptance from $1.2 < \eta < 2.2$ (2.4) in the South (North) spectrometer. Inside the magnetic field, there are three high resolution cathode strip tracking chambers capable of determining space point position to < 100 microns. Downstream of each spectrometer magnet is a Muon Identifier (MuId) which covers the same rapidity region. They consist of five layers of steel absorber sandwiching both horizontal and vertical proportional tubes, with the total thickness of the absorber material of 60cm. The minimum muon momentum able to penetrate all 5 gaps is 2.7 GeV/ c , and the pion rejection factor at 3 GeV/ c is 400. The MuId is also used as trigger counter as well as identifying the muon. It uses full hit information of the detector, 9 cm in horizontal and vertical direction for each gap, and determines whether a muon candidate road exists for each beam crossing. Triggers on single and double tracks with sufficient depth in the MuId are passed to the global level-1 trigger of PHENIX. J/ψ yields in the muon arm were obtained by reconstructing $\mu^+ - \mu^-$ pairs. Muon tracks were reconstructed by finding a track seed in the

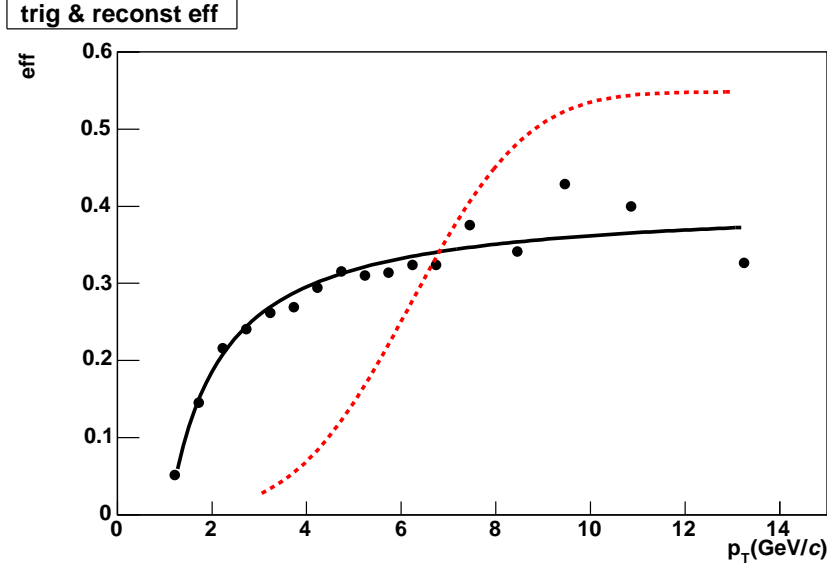


Figure 40: *Experimental efficiency for π^0 detection at PHENIX. It includes BBC and EMCal trigger efficiencies, offline data selection, and reconstruction efficiencies. Black points are efficiencies calculated from run2-pp data and the black line is a smoothed curve for eye guidance. It saturates around 35-40%. The dotted red line shows expected efficiency in the future. We can achieve this by removing the BBC coincidence from the trigger and setting the EMCal trigger threshold energy higher.*

MuID and matching it to clusters of hits in each of the three MuTr stations. The momentum was determined by fitting, with a correction for energy loss, the MuID and MuTr hit positions and the vertex position. J/ψ mass resolution of $160 \text{ MeV}/c^2$ in $p-p$ collisions has been achieved as shown in Fig.41. Together with the di-electron measurement in the central arm, PHENIX has published the p_T , rapidity and total cross-sections for J/ψ at $\sqrt{s} = 200 \text{ GeV}/c$ [197].

4.1.3 PHENIX Local Polarimetry and Relative Luminosity Detectors

Local polarimeters, sensitive to transverse polarization at collision, were used to set up the spin rotators and monitor the beam polarization direction at the PHENIX interaction point. The local polarimeters utilized a transverse single spin asymmetry in neutron production in pp collisions at $\sqrt{s} = 200 \text{ GeV}$ [198]. For vertically polarized beam a left-right asymmetry is observed for neutrons produced at very forward angles, with no asymmetry for production at very backward angles. A fully longitudinally polarized beam produces no asymmetry.

Neutrons with $E_n > 20 \text{ GeV}$ and production angle $0.3 < \theta_n < 2.5 \text{ mrad}$ were observed by two hadronic calorimeters, the Zero Degree Calorimeters (ZDC) [199], located ± 18 meters from the interaction point. Scintillator hodoscopes at 1.7 interaction length provided the neutron position at the ZDC, and thus the neutron production angle and azimuthal angle $\phi = \arctan(x/y)$ with \hat{y} vertically upward. The \hat{x} axis forms a right handed coordinate system with the \hat{z} axis defined by the beam direction for forward production. Figure 42 shows the observed asymmetry for the spin rotators off and on, for the blue and yellow beams. With the spin rotators off, a

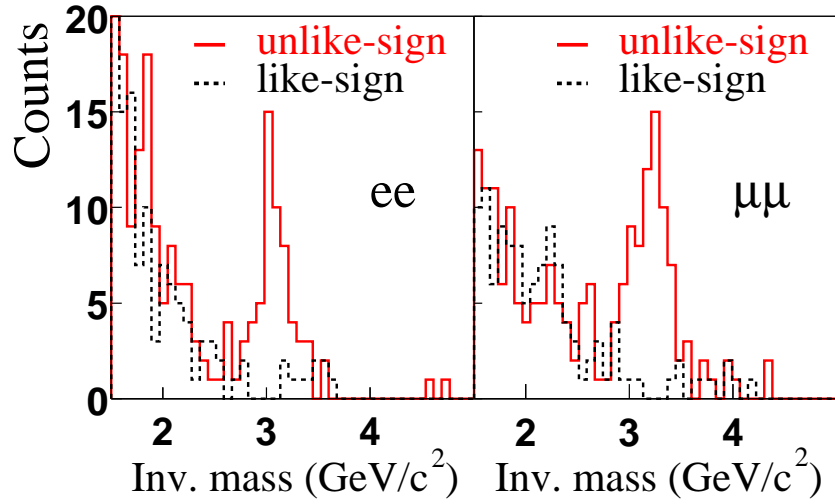


Figure 41: *The invariant mass spectra for dielectron and dimuon pairs. Unlike-sign pairs are shown as solid lines, the sum of like-sign pairs as dashed lines.*

left-right asymmetry is observed from the vertically polarized beam. With the spin rotators on, the transverse asymmetry is greatly reduced, indicating a high degree of longitudinal polarization (0.99 and 0.98 for the blue and yellow beams, respectively). A separate run with the spin rotators set to give radial polarization confirmed the direction of the polarization for each beam.

In addition to the polarization of the beams, we require information on the intensities and possibly the profiles of the colliding bunches. This knowledge is necessary because the spin structure information we seek appears in correlations between the rate or angular distribution of specific final states and the spin direction(s) of the colliding protons. However, spin correlated differences in the production rate of particular final states may appear even in the absence of a physics asymmetry simply because the luminosities of the colliding bunches are different. This necessitates measurements of the relative luminosities of the colliding bunches which are insensitive to the beam polarization and of greater precision than the smallest physics asymmetry to be measured. PHENIX is currently equipped with two forward detectors, the BBCs and ZDCs, which are primarily sensitive to the pp inelastic and double-diffractive cross-section respectively. They have demonstrated an insensitivity to the colliding bunch polarization at the level of 1.4×10^{-4} and have a high rejection of backgrounds. Scalars attached to these detectors counting a single event per crossing form the successful foundation of the relative luminosity measurements suitable for the current pp luminosity. As RHIC approaches its design luminosity, $2 \times 10^{32} \text{ cm}^{-2}\text{s}^{-1}$, there will be multiple pp interactions per bunch crossing, and ambiguities in determining whether the event vertices lay within the PHENIX acceptance. We believe these complications will be overcome by incorporating additional information from the detectors which is linear in the rate such as phototube charge and multiplicity. Bunch profile information from existing RHIC instrumentation, new analysis techniques and trigger logic will be used to minimize the effects of vertex ambiguities on the determination of relative luminosity. Also, a dedicated low cost, small acceptance detector is being considered to address these issues. Finally, we note that the uncertainty on the relative luminosity may be reduced through use of the spin flippers at RHIC, which will allow frequent reversals of the beam helicities.

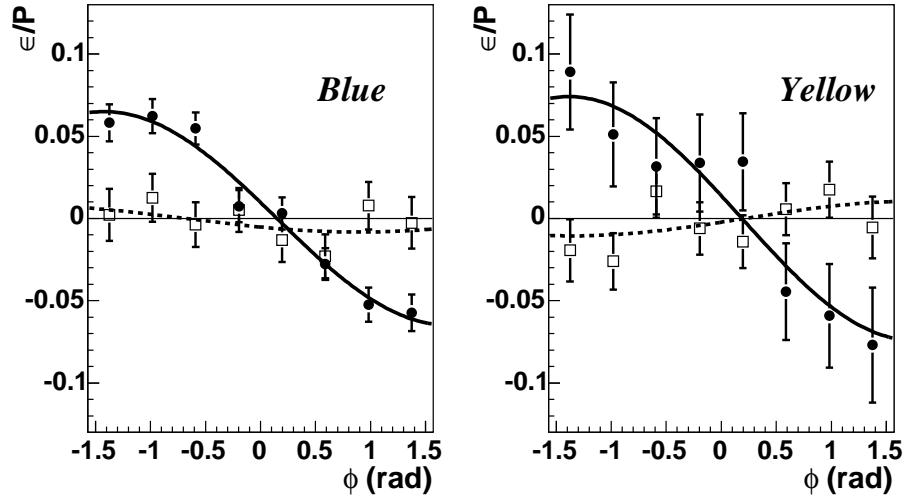


Figure 42: The raw asymmetry normalized by the beam polarization, ϵ/P , as a function of azimuthal angle ϕ , for forward neutron production. The solid points and curve correspond to the spin rotators off (transverse polarization) and the open points and dashed curve correspond to the spin rotators on (longitudinal polarization). Curves are sine function fits to the data, representing possible transverse polarization. The data are for special runs used to set up the spin rotators, where the blue (yellow) polarization was 0.24 and 0.33 (0.08 and 0.28), for spin rotators off and on, correspondingly.

4.1.4 PHENIX DAQ and Computing

The PHENIX DAQ has been designed from inception as a parallel pipelined buffered system capable of very high rates of nearly deadtime-less data-taking. In this kind of design, data is sent from each detector element in multiple parallel streams, buffered at each stage in the chain to smooth out fluctuations in rate, and then uses simultaneous read and write for the highest possible throughput with existing technology. At present, PHENIX has achieved data rates of over 4 kHz, and with improvements in noise reduction PHENIX should be able to approach the peak design interaction trigger rate of 12.5 kHz. Such high DAQ rates are crucial for providing the capability and flexibility to record the many different kinds of interesting rare events at RHIC.

In addition to the RHIC Computing Facility (RCF) at BNL, PHENIX has regional computing centers around the world. The biggest one is the RIKEN CC-J, Computing Center in Japan. The CC-J has comparable computing resources to the PHENIX part of the RCF, CPU power and data storage capability with the High Performance Storage System (HPSS). The main missions of the CC-J for the PHENIX experiment are the primary simulation center, an Asian regional computing center, and a computing center for the spin physics. In run5, it will be used for the reconstructed data production of all the polarized proton collision data. Raw data are sent from PHENIX to the CC-J as much as possible using a WAN connection in parallel to the RCF HPSS. A sustained transfer rate of the WAN connection between BNL and RIKEN of 10 MB/s has been routine and occasionally 60 MB/s has been sustained. The PHENIX DAQ rate is expected to be 60 - 100 MB/s in near future. The data which are not transferred in real time will be sent later through the WAN, and with tape transfer by air-shipments as a backup plan. A bottleneck of the WAN was upgraded very recently, so the transfer rate may reach 100 MB/s.

upgrade	channel	physics target	x coverage
muon trigger	$W^+ \rightarrow \mu^+$	$\Delta u(x), \Delta d(x)$	$0.2 < x_{u,d} < 0.6$
	$W^- \rightarrow \mu^-$	$\Delta \bar{u}(x), \Delta d(x)$	$0.04 < x_{\bar{u},\bar{d}} < 0.1$
silicon vertex tracker	$c \rightarrow e$		$0.01 < x_g < 0.1$
	$b \rightarrow e$		
	$D \rightarrow K\pi$	$\Delta g(x)$	$0.1 < x_g < 0.2$
	$B \rightarrow J/\psi$		$0.03 < x_g < 0.1$
	$\gamma + \text{jet}$		$0.02 < x_g < 0.1$
nose cone calorimeter	$\gamma + \text{jet}$	$\Delta g(x)$	$0.001 < x_g$

Table 5: *Physics goals of the PHENIX detector upgrades.*

4.1.5 PHENIX Detector upgrades

Three PHENIX detector upgrades related to spin are proposed to be completed around 2010. They will enhance the existing capabilities or make possible measurements of new spin observables. They are the 1) The muon trigger upgrade, 2) The Silicon Vertex Tracker 3) A Nose Cone Calorimeter. These upgrades will be described briefly in this section.

Muon Trigger Upgrade

The flavor separation of quark and anti-quark polarizations for up and down quarks, requires separate high statistics measurements of inclusive lepton counting rate asymmetries: $A_L^{W^+ \rightarrow \mu^+}(p_T)$ and $A_L^{W^- \rightarrow \mu^-}(p_T)$. These measurements translate into the following experimental requirements for the PHENIX muon arms: (a) superior event selection capability in order to reduce the 10MHz collision rate to the data archiving bandwidth available in PHENIX (b) the ability to assign the correct proton polarization (that is bunch crossing number) to a given W-event candidate, (c) tracking resolution to correctly determine the lepton charge sign and (d) good signal to background ratios in the off-line analysis.

Extensive Monte Carlo simulations including a full GEANT simulation of the muon arms show that the existing muon spectrometers are capable of defining a clean sample of W events for the off-line analysis: a requirement of $p_T > 25$ GeV on the transverse momentum of the final state decay muon will remove most of the collision and beam related backgrounds; we expect a signal to background ratio of about 2:1.

A new first level muon trigger is required to improve the online performance of the present first level muon trigger. Rejection factors achieved in the present PHENIX muon trigger, based on information from the existing muon identifier system are about $R=250$. Measurements at the luminosities needed for the W-physics program will require rejection factors of $R>5000$.

The new first level muon trigger in PHENIX will be based on three fast trigger stations which will be added to each of the PHENIX muon spectrometers as shown in Fig.43. The trigger stations will use Resistive Plate Chamber (RPC) technology developed for the muon trigger in the CMS experiment at LHC. In addition new front end electronics for the existing muon tracker chambers will make it possible to introduce muon arm tracking information in the future muon trigger. Information from the three RPC stations and the muon tracker will be processed in standard

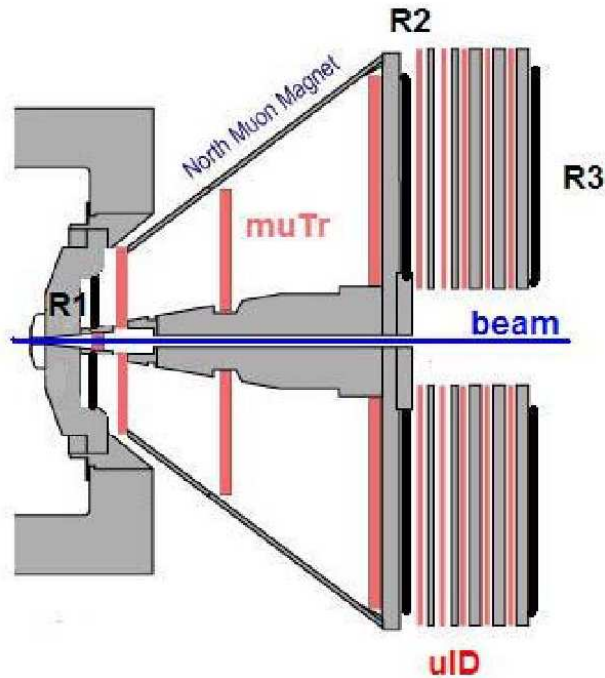


Figure 43: *The muon trigger upgrade layout. The existing muon tracker chambers and muon identifier planes are shown with the resistive plate chamber stations R1-R3.*

PHENIX first level trigger processor boards. The boards carry large Xilinx Fast Programmable Gate Arrays (FPGAs) and can carry out a fast online momentum measurement based on the tracking information from the RPCs and the muon trackers. In addition a timing cut will be applied in the RPC front-end electronics to remove beam backgrounds.

Detailed beam background measurements and beam-loss Monte Carlo simulations were carried out to confirm that the substantial steel absorbers in PHENIX introduce a large asymmetry in the incoming and outgoing beam backgrounds which can be exploited for triggering purposes. Overall the expected rejection power of the new muon trigger is expected to be well above the required level with $R > 10000$.

The possibility of NSF funding for the RPCs is being pursued. A proposal has been submitted to the NSF MRI program by a consortium of four University groups in January 2005: Abilene Christian University, UC Riverside, University of Illinois and Iowa State University. The funding requested from the MRI program is \$2.0M with an additional \$300k in institutional contributions from UCR, ISU and UIUC. The proposal is presently being reviewed. A funding decision is expected by summer 2005. Funding for the upgrade of the muon tracker front-end electronics, estimated at \$1M, is sought from Japanese sources. It is planned to complete the installation process in late 2008.

PHENIX Silicon Vertex Tracker

The PHENIX Collaboration proposes to construct a Silicon Vertex Tracker (VTX) in the next few years. The VTX will substantially enhance the physics capabilities of the PHENIX central arm spectrometer. Our prime motivation is to provide precision measurements of heavy-quark

production (charm and beauty) in A+A and p(d)+A collisions, and polarized p+p collisions. In addition, addition of a large acceptance central detector capable of monitoring multiplicities of hadronic final states along with their directions will enhance the PHENIX's capability to study Jets in hadron-hadron collisions. These are key measurements for the future RHIC program, both for heavy ion physics which intends to study the properties of dense nuclear medium created in their collisions, and for the exploration of the nucleon spin-structure through polarized pp collisions. While the detailed list of physics measurements possible with the VTX detector is discussed elsewhere [200], the principal measurements associated with polarized pp program are: (1) $\Delta g/g$ from charm and beauty production in polarized pp scattering and (2) x dependence of $\Delta g/g$ from γ -jet correlations Heavy quark production has been measured by PHENIX presently through the observation of inclusive (decay) electrons. These measurements are limited in accuracy by the systematic uncertainties resulting from possible large electron backgrounds originating from Dalitz decays and photon conversions. The measurements are statistical in nature, and one uses different models to distinguish between charm and beauty contributions. The VTX detector will provide tracking with a resolution of $< 50\mu\text{m}$ over a large coverage both in rapidity $|\eta| < 1.2$ and in azimuthal angle ($\Delta\phi \sim 2\pi$). A significantly improved measurement of heavy quarks in pp collisions is deemed possible over a wide kinematic range with the VTX.

The proposed VTX detector will have four tracking layers. For the inner two layers we propose to use silicon pixel devices with $50 \times 425 \mu\text{m}$ channels that were developed for the ALICE experiment at CERN/LHC. Our preferred technology for outer two detector layers is a silicon strip detector developed by the BNL Instrumentation Division which consists of $80\mu\text{m} \times 3 \text{ cm}$ strips layered to achieve an effective pixel size of $80 \times 1000 \mu\text{m}$. We plan to use SVX4 readout chip developed at FNAL for the strip readout. The main aim in using existing technology has been to reduce the cost and time for R&D that for such a project could ordinarily be rather high and long, respectively.

PHENIX proposes that the project will be mainly funded by two agencies: the DOE Office of Nuclear Physics and RIKEN Institute of Japan. While RIKEN funding of \$3M has been available since 2002, it is proposed that the \$4.3M for the Strip Layers will be available from DOE starting FY06. If the VTX is funded accordingly, it will built and commissioned in the RHIC - Run 8 which presently is expected to be a long Au+Au run.

PHENIX Nose Cone Calorimeter

A proposal for a forward spectrometer upgrade is being developed with the objective of greatly enhancing present capabilities for PHENIX in the forward direction. When completed, the detector will sit near the PHENIX magnet poletips, and will result in a nearly ten-fold increase in rapidity coverage for photons and to some extent for hadrons and jet detection, as well as better triggering capabilities. Newly acquired access to forward production of inclusive jets, direct photons or Drell-Yan pairs at large x_F in nucleon-ion collisions at RHIC will provide a new window for the observation of saturation phenomena expected at high parton number densities which is of importance in the evolution of the partonic distribution functions. In combination with the central arms, the possibility arises of detecting $\gamma + jet$ in polarized pp with a large rapidity gap, extending the x range over which PHENIX is sensitive to Δg .

The PHENIX Forward Upgrade is constrained by the existing muon spectrometer configuration including its wire chambers, hadron absorber walls and magnet yokes. The core element

of the proposed upgrade are compact tungsten calorimeters with silicon pixel readout and fine transverse and longitudinal segmentation built to identify and measure forward electromagnetic activity and provide jet identification and coarse jet energy measurements. The principal performance aspect of the NCC is its ability to run in the unassisted mode (without upstream tracking). The NCC is an extremely dense sampling calorimeter using tungsten absorber interleaved with silicon readout layers.

4.2 STAR

4.2.1 Recent spin-related upgrades

A cross-sectional view of the STAR detector, emphasizing the subsystems that have been added to the baseline detector [201] with the spin program as a primary driver, is shown in Fig. 44. The relative luminosity monitoring critical for the measurement of spin asymmetries is provided by Beam-Beam Counters (BBC) that have been added just to the east and west of the STAR magnet, at a distance of 3.5 m from the beam intersection point. The BBC's are plastic scintillating tile detectors for charged particles over the pseudorapidity range $3.3 < \eta < 5.0$. An east-west prompt coincidence, sensitive to nearly 90% of the total non-singly diffractive pp cross section at $\sqrt{s} = 200$ GeV, is used to discriminate beam collisions from beam-gas interaction background. The azimuthal segmentation of the scintillating tiles permits the measurement of left-right and up-down single-spin asymmetries. Comparison of the BBC asymmetries measured at STAR for hits in the inner BBC tiles with those measured simultaneously in the RHIC CNI polarimeters has revealed a small analyzing power ($A_N \approx 0.006$) suitable for use of the BBC's as a local polarimeter when the beam spin at STAR is transverse to its momentum. In particular, this functionality is important for tuning the STAR spin rotators: as shown in Fig. 45, one can adjust the rotator magnet currents to give longitudinal polarization at the IR by arranging for both (left-right and up-down) BBC transverse asymmetries to vanish.

The major STAR upgrades already installed for the spin program represent additions of electromagnetic calorimetry (EMC) for the detection of high-energy photons, electrons and π^0 over a broad range of pseudorapidity. The Forward Pion Detectors (FPD) are small lead-glass-based calorimeters placed to the left and right, and above and below, the beam lines 7.5 m to the east and west of the center of STAR. The FPD provides π^0 detection and identification at high $x_{Feynman}$ and forward rapidity ($3.3 < \eta < 4.1$), where large single-spin transverse asymmetries have been observed (see Figs. 6, 27). (The measurements reported in [60] were made with a precursor of the present FPD's that was a prototype section of the STAR Endcap EMC.) The FPD's will continue to be used to probe the origins of these large single-spin effects, and also to investigate gluon polarization via di-hadron coincidence measurements of the type discussed in Sec. 2.5. In addition, the FPD provides access in d+Au collisions at STAR to the low Bjorken- x regime where gluon saturation models predict, and the RHIC experiments have observed, the onset of significant suppression of moderate- p_T hadron production. A new calorimeter described below is planned to greatly expand the coverage of STAR's west-side FPD to enhance the above coincidence measurements in both p+p and d+Au runs.

The largest additions to STAR relevant to the spin program are the Barrel (BEMC [202]) and Endcap (EEMC [203]) calorimeters, funded by DOE and NSF, respectively. Each of these sub-

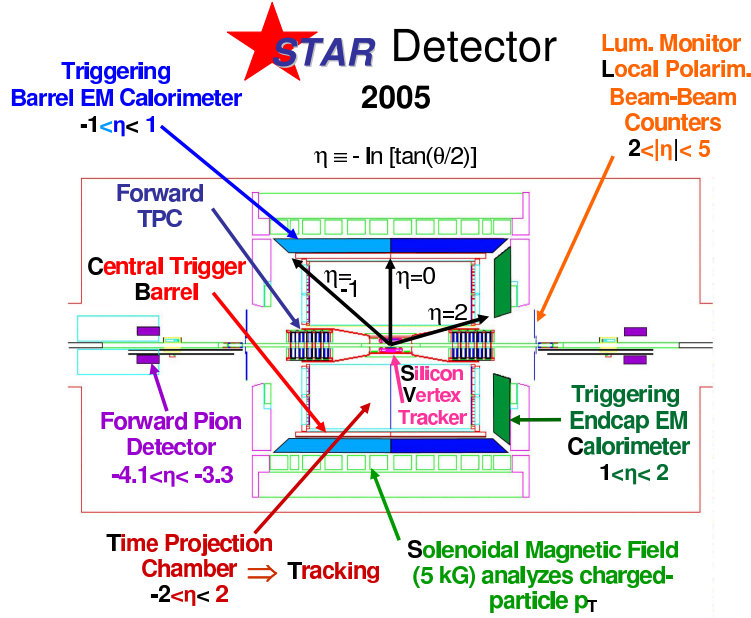


Figure 44: Cross sectional view of the STAR detector as installed for the 2005 RHIC run, emphasizing subsystems most relevant for the spin program, and their functions. Completion of the readout electronics for the barrel EMC during the 2005 run will make the detection subsystems used for $p+p$ fore-aft symmetric, except for the endcap EMC, which resides on the west side.

systems is a multi-layer sandwich of Pb radiator sheets and plastic scintillator with light collection via optical fibers. Each contains a fine-grained Shower-Maximum Detector (SMD – gaseous for BEMC, plastic scintillator for EEMC) for discriminating single photons from π^0 daughter photon pairs, by means of the transverse shape of the electromagnetic showers produced. Each also contains pre-shower layers, and the endcap adds a post-shower layer as well, to improve electron/hadron discrimination. As shown in Fig. 46, the fabrication and installation of both EMC's has been completed during 2004, although installation of final readout electronics for the east half of the BEMC is still anticipated to occur during February-March 2005. The EMC's provide critical detection and triggering capability for STAR studies of jets, photons, π^0 , W -bosons and J/ψ (as well as heavier quarkonium species), all of which play significant roles in the spin program described in earlier sections of this document. The broad pseudorapidity coverage ($-1 \leq \eta \leq 2$) permits, for example, study of γ -jet coincidences spanning a broad range of x -values for the participating gluons, while still maintaining large transverse momenta ($p_T > 5$ GeV/c) for the partonic scattering.

Both EMC's have performed well in partial installations for the 2003 and 2004 RHIC runs, enabling detector commissioning, optimization of online calibration and triggering, debugging of subtle electronics problems and initial extraction of physics results. The first paper based on BEMC transverse energy measurements for Au+Au collisions at STAR has already been published [204]; others, based on electron spectra measured with the BEMC, are in preparation. Figure 47 shows an event display for a dijet detected with STAR's TPC and BEMC, together with the spectrum of the ratio of BEMC/total transverse energy for jets reconstructed within the partial BEMC acceptance available during the 2004 $p+p$ RHIC run. Figure 48 shows a typical shower profile measured with the EEMC Shower-Maximum Detector for a π^0 candidate, together with

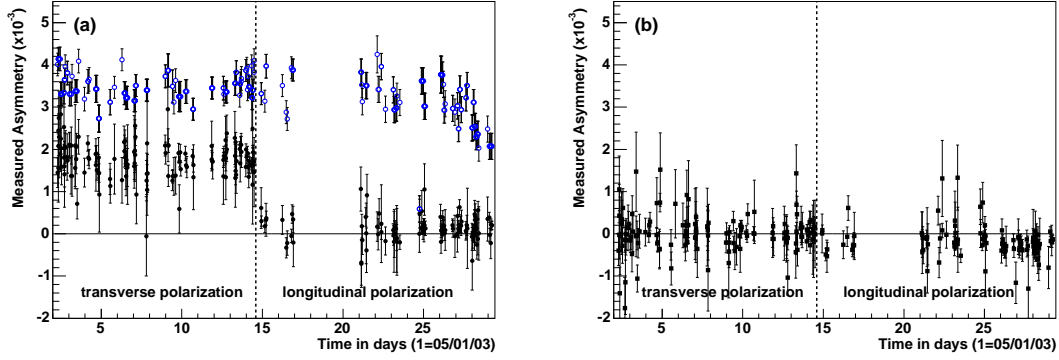


Figure 45: *Left-right (a) and up-down (b) single-spin asymmetries measured vs. time during the 2003 p+p run with the STAR BBC's (closed symbols) and the RHIC CNI polarimeters (open symbols). When the beam spin orientation at STAR was vertical, the left-right asymmetry was consistently about half that of the CNI polarimeters. Initial tuning of the STAR spin rotators to produce longitudinal polarization was carried out on day 14, by arranging for both BBC transverse asymmetries to vanish, while the CNI asymmetries remained sizable.*

an invariant mass spectrum reconstructed from the SMD and calorimeter tower information for all two-cluster combinations detected with the partial EEMC for several 2004 p+p runs. Analysis groups within STAR are actively working on optimizing the efficiency and background suppression in reconstruction algorithms for jets, π^0 and single photons, electrons and J/ψ . This work is aiming toward first EMC-based spin publications in the latter half of 2005 (based on 2003 and 2004 data) and toward readiness for prompt analysis of results from the anticipated long p+p run during 2005.

In addition to the above hardware upgrades, STAR has enhanced its spin program by the addition of new collaborators over the past few years. Prominent new groups with heavy interest in spin from MIT, LBNL, CalTech and Valparaiso University complement the groups from BNL, ANL, Indiana University, UCLA, Penn State, Texas A&M University, JINR Dubna and IHEP Protvino, who have been instrumental in launching STAR's spin program. With these hardware and manpower additions, the resources are in place to permit STAR to address many of the high priority spin physics goals described in Sec. 2, most prominently the delineation of gluon helicity preferences via a number of reaction channels. Learning curves, but no additional equipment, are anticipated for dealing most effectively with the TPC pileup and BBC occupancy problems that will arise as the p+p luminosity increases at RHIC, and for monitoring beam polarization locally at STAR when the beam spins are oriented longitudinally. For example, fine-grained shower-maximum detectors already installed in STAR's Zero Degree Calorimeters will still be useful for monitoring the beam polarization, via the neutron production asymmetries shown in Fig. 42, at much higher than present luminosity. It may be possible to monitor longitudinal beam polarization via the anticipated appreciable A_{LL} asymmetry for quark-quark scattering, which can be emphasized by requiring two high- p_T hadrons detected in STAR with a large rapidity interval between them. Additional upgrades are needed, however, to optimize W detection and the measurement of flavor-dependent sea antiquark polarizations in STAR, as described below.

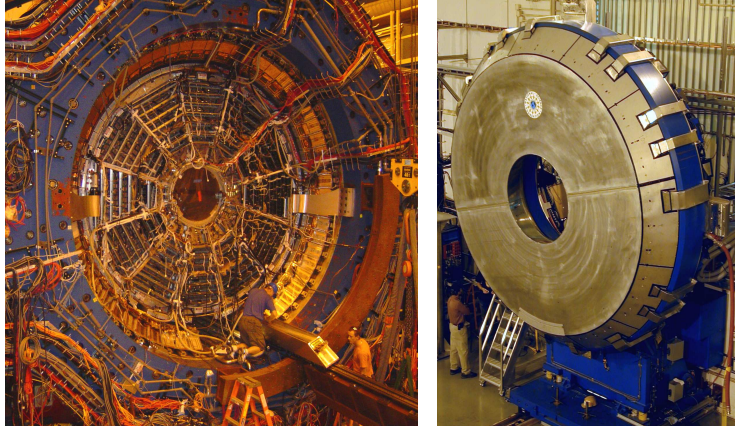


Figure 46: *Photographs showing insertion of one of the final barrel EMC modules into STAR (left) and the complete endcap EMC on the west poletip (right). With completion of these subsystems, STAR is ready to take full advantage of long polarized $p+p$ runs in the 2005-9 period.*

4.2.2 Future STAR upgrades relevant to the spin physics program

The W^\pm production studies central to the envisioned spin physics program at $\sqrt{s} = 500$ GeV strain the capabilities of STAR's Time Projection Chamber, which was designed for heavy-ion collisions to track charged particle momenta up to $p_T \sim 10$ GeV/c. The TPC provides very limited resolution for W daughter leptons up to p_T of 40 GeV/c, especially in the endcap region ($\eta > 1$), where the drifting electrons from charged particle tracks intercept a decreasing fraction of the readout pad rows. Fortunately, the EMC's provide measurements of electron transverse energy with a typical resolution $\sim 4\%$ for $p_T \approx 40$ GeV/c. But the EMC's alone cannot discriminate electrons from positrons, and charge sign determination for the parent W is critical to the physics goal of separating \bar{u} from \bar{d} polarizations in the proton sea (see Sec. 2.7). Furthermore, comparison of p_T measured from track curvature with E_T measured in the calorimeters provides a powerful method (over and above those available from the EMC's alone) to discriminate the low-rate W signal from a background of more abundant high- p_T charged hadrons. While STAR's present tracking capabilities are adequate for these tasks in the BEMC region, upgraded tracking is needed for W^\pm production in the endcap region, where the separation of \bar{u} from \bar{d} polarizations is kinematically cleanest (see Sec. 2.7).

The need for improved endcap tracking is demonstrated in Fig. 49 by simulations of 30 GeV/c pion tracks, whose sagitta in the middle of the endcap region is ≈ 2.5 mm. With the TPC alone, the charge sign is misidentified about 15-20% of the time. The addition of three space points measured with $\sim 50\mu\text{m}$ resolution near the vertex and two with $\sim 100\mu\text{m}$ resolution just in front of the endcap would completely remove the charge misidentification problem, and would provide 30% relative p_T resolution at the high momenta of relevance to the W production program. Improvements of this order are quite feasible with the arrangement of detectors outlined below, and would greatly enhance the physics impact of STAR's W measurements.

The conceptual designs presently under consideration for upgraded forward tracking in STAR are illustrated in Fig. 50. Space points near the vertex would be provided by an array of annular silicon strip detectors placed just downstream of STAR's vertex tracking devices, and inside the

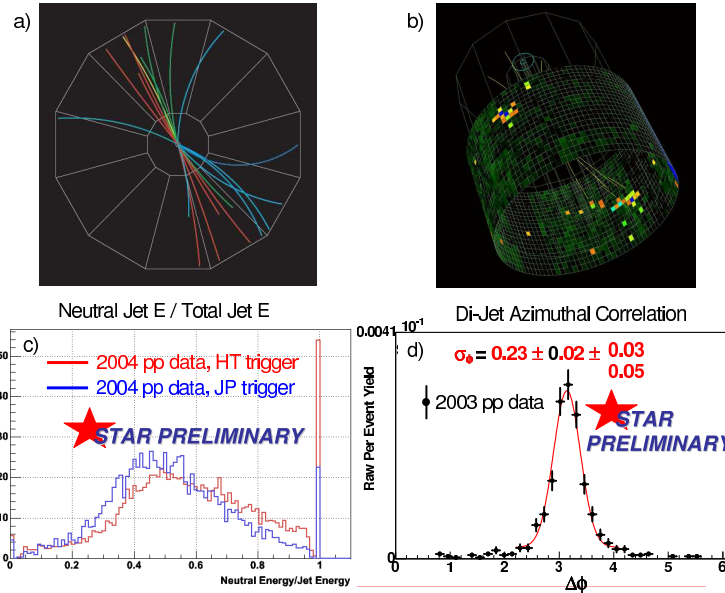


Figure 47: Event displays showing tracks reconstructed from a $p+p$ di-jet event in the STAR TPC (a) and from the TPC and BEMC (b). The events were collected during the 2004 run, when only the west half of the BEMC was functional. The lower frames show preliminary STAR $p+p$ jet physics results: (c) the spectrum of the ratio of BEMC to total (TPC+BEMC) energy measured for inclusive jets, for two different jet triggers; (d) the distribution of azimuthal angle differences between the reconstructed jet axes for di-jet events [205]. The differences between the two spectra in (c) reflect trigger biases (qualitatively consistent with simulations) that must be understood to extract reliable information concerning gluon polarization from measured jet two-spin asymmetries. The fit to the angular correlation in (d) is used to extract the mean transverse momentum $\langle k_T \rangle$ of the interacting partons before the hard scattering that produces the di-jet. STAR's results for $\langle k_T \rangle$ are consistent with the world data for $p+p$ at other collision energies [205].

TPC's inner field cage. Position would be measured just upstream of the EEMC in an array of 3-layer Gas Electron Multiplier (GEM) chambers [206] tiling the pseudorapidity region $1 < \eta \leq 2$, over the full azimuthal acceptance. The silicon disks would be integrated with and extend the coverage of a new barrel silicon-strip tracker envisioned to surround, and provide high-rate tracks pointing to, a high-resolution Advanced Pixel Sensor micro-vertex detector (the Heavy Flavor Tracker, HFT). The primary motivation for the latter two subsystems comes from the needs for high-quality measurements of slightly displaced vertices associated with heavy quark production in STAR heavy-ion collisions. Research and development on the type and size of GEM chambers that would be needed for the endcap tracker is ongoing in a collaboration between STAR and PHENIX. In addition to the ability to obtain the needed spatial resolution with thin chambers that would fit within the narrow space available in front of the EEMC, the GEM technology provides fast detectors whose tracking information would significantly alleviate ambiguities from pileup tracks in the TPC anticipated at the ultimate RHIC pp luminosities.

STAR groups from MIT and Lawrence Berkeley National Laboratory are leading a collaboration of several institutions (including ANL, BNL, IUCF, Yale and Zagreb) in planning the inner and endcap tracking upgrades. (The heavy-ion-driven HFT upgrade project is led by the LBNL

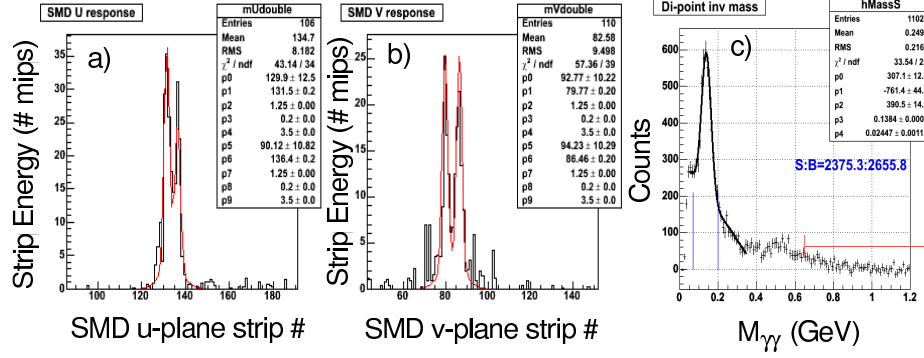


Figure 48: Elements of π^0 reconstruction with the STAR EEMC. Frames (a) and (b) show transverse electromagnetic shower profiles measured in two orthogonal SMD planes for a single event with a 14 GeV π^0 candidate detected during the 2004 RHIC p+p run (when one third of the SMD was functional). Frame (c) shows the invariant mass spectrum reconstructed for several p+p runs from all possible pairings of EEMC points in the calorimeter towers and SMD strips. The π^0 peak is prominent. Algorithm development to optimize reconstruction efficiency and resolution, and discrimination of single photons from π^0 is ongoing.

group.) The conceptual design of the silicon disks and GEM chambers is not yet complete, with still important open issues to address concerning the optimal tradeoffs between coverage and cost, the resolution impact of material in the endcap of the TPC, etc. The present plan is to proceed with this upgrade in two stages: first, the silicon barrel would be proposed, with the goal of fabricating and installing it in STAR in time for an FY09 RHIC run, when it would be needed to get optimal usage from the HFT (which is to be proposed on a slightly faster timeline); the silicon disks and GEM chambers would be proposed about a year later, with the goal of installation for a long 500 GeV pp run in FY10, when we would hope to collect a large fraction of the statistics needed for the W production A_L measurements. The rough funding scope anticipated for these two phases is \sim \$6M and \$5M, respectively, with contingency. Both DOE and NSF funding are likely to be sought to share the costs for the second phase. In addition, potential University based funding sources are being considered.

Additional planned STAR upgrades driven by the heavy-ion research program will also have significant benefits for the p+p spin measurements. An extension of STAR's forward electromagnetic calorimetry coverage beyond the EEMC, to $2.5 \lesssim \eta \lesssim 4$, has been proposed to the NSF in January 2005. This Forward Meson Spectrometer (FMS) (see Fig. 51) would be constructed from existing lead-glass counters to replace and expand the present Forward Pion Detector on STAR's west side. The primary motivation for the FMS is to probe the contributions of gluons to nuclear structure at very low Bjorken x (down to $x \sim 0.001$) in proton-nucleus or deuteron-nucleus collisions at RHIC. Gluon saturation models predict a suppression of hadron production at moderate p_T in this forward rapidity region, which can be tested by systematic measurements for mesons reconstructed from their daughter photons. Furthermore, Color Glass Condensate approaches to high-density QCD treat the gluons at such low x and at moderate momentum transfers as a classical field, from which parton scattering will result in mono-jet, rather than traditional di-jet, products. The FMS will allow searches for the onset of such mono-jet events as a function of the rapidity interval between correlated pairs of hadrons (e.g., π^0) detected in coincidence within STAR's extended EMC coverage.

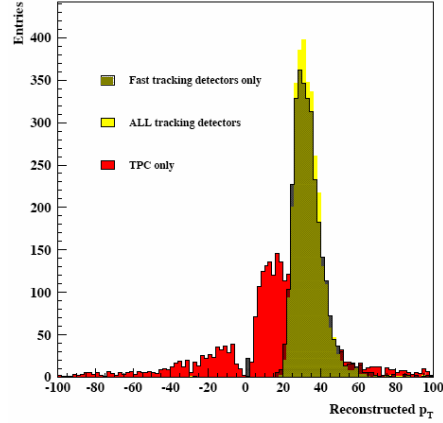


Figure 49: *Tracking simulations for the endcap pseudorapidity region ($1 < \eta < 2$) in STAR, showing the p_T response to 30 GeV/c thrown π^- under various assumptions of tracking detectors. With the TPC alone, at present performance levels, the p_T resolution is poor, and the charge sign is mistaken $\sim 20\%$ of the time. With a forward tracking upgrade the resolution will be sufficient for the W^\pm production program, and the charge sign errors will be removed. The simulation here assumes measurement of three space points with $50 \mu\text{m}$ resolution inside the TPC inner field cage and of two space points with $100 \mu\text{m}$ resolution just in front of the EEMC.*

Similar coincidences between leading hadrons in polarized p+p collisions permit study of parton-parton scattering spin sensitivities under conditions where one can vary the subprocess (qq vs. qg vs. gg) contributions in a controlled manner. As described in Sec. 2.4.1 of this document, A_{LL} measurements for such di-hadron events are part of the planned approach toward unraveling the polarization of gluons in a polarized proton. Furthermore, A_N measurements for mesons in the FMS, in coincidence with other jet fragments, will probe the origin of the large single-spin asymmetries already found (see Fig. 27) for forward π^0 production, as described in Sec. 2.5. Thus, the spin program would make substantial use of the FMS once it is installed in STAR.

It is hoped the FMS will be installed for the FY07 RHIC run, when STAR's present plans call for the next long d+Au collision run. Total funding needed for this project is about \$1M, with most of this sought from NSF. The project is being led by STAR physicists from Penn State University, BNL and IHEP Protvino, with additional participation by LBNL and Texas A&M University. The lead-glass cells would be taken from the existing STAR west-side FPD and from an available supply owned by the Protvino group.

The case for other STAR upgrades driven by the heavy-ion program is summarized in the STAR Decadal Plan [207]. An upgrade to the TPC front-end readout electronics and to the STAR Data Acquisition system will increase the event rate capability from the present ~ 100 Hz to ~ 1000 Hz, by 2007-8. This upgrade has two significant implications for the spin program: the FEE upgrade will free up space directly in front of the EEMC, needed for eventual installation of the endcap GEM tracker described above; the DAQ upgrade will permit collection of large data samples for abundant reaction channels, such as inclusive jet or π^0 production at moderate p_T , without introducing sizable and undesirable dead time for the rarer channels, such as direct photon production. The barrel Time-Of-Flight detector proposed to improve (by 2008)

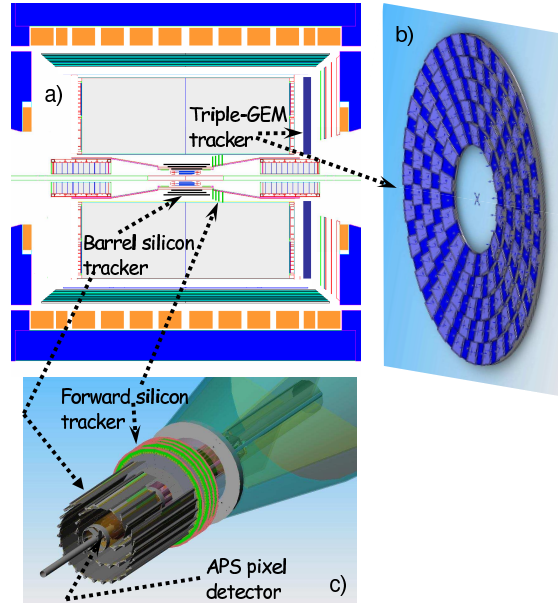


Figure 50: Schematic illustration of one layout of silicon and GEM detectors presently under consideration for STAR's tracking upgrades. In (a) the various components of the staged tracking upgrade are shown in their intended locations within the STAR detector. Frame (b) shows the layout of triple GEM chambers envisioned to tile the region in front of the EMC. Frame (c) shows the inner tracking region, including four silicon disks considered as part of the forward tracking improvement driven by the spin program. The other proposed subsystems highlighted in (c) – a fast barrel silicon tracker (supplanting STAR's current Silicon Vertex Tracker) and an Advanced Pixel Sensor micro-vertex detector – address needs for heavy flavor tracking in the heavy-ion program. The forward silicon tracker must be integrated with them and the associated changes they require in the beam pipe through the central region of STAR.

STAR's particle identification up to ~ 3 GeV/c in heavy-ion collisions will also aid the spin program, *e.g.*, in permitting clean identification of charged pions, and hence of the ρ -meson invariant mass region, for studies of transversity via interference fragmentation functions (see Sec. 2.5). The Heavy Flavor Tracker mentioned above, while again driven by studies of the unique matter produced in heavy-ion collisions, will also permit improved identification in STAR of the production of heavy quarks in p+p collisions, providing access to gluon polarization and to possible spin effects from the quark mass (explicit chiral-symmetry-breaking) terms in the QCD Lagrangian.

In summary, the completion of the barrel and endcap EMC's, following the addition of the Beam-Beam Counters and Forward Pion Detectors, has brought STAR to full readiness to exploit the anticipated long polarized pp collision runs during the 2005-9 period. A significant upgrade to STAR's forward tracking capabilities is still needed to optimize its W^\pm production program in 500 GeV pp runs anticipated for the 2009-12 period. Other STAR upgrades planned for the next several years, primarily to enhance its capabilities in studying heavy-ion collisions, will have significant side benefits for the spin program.

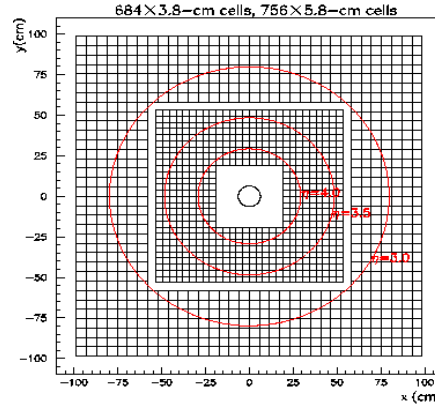


Figure 51: *Front view of the intended layout of Pb-glass counters comprising the proposed Forward Meson Spectrometer (FMS) at STAR. The detector would replace the current west Forward Pion Detector located 7.5 m from the center of STAR, greatly expanding acceptance for mesons decaying to photons and for meson coincidences in a kinematic region dominated by contributions from gluons at very low Bjorken x . This coverage is important to both the search for saturation of gluon densities in nuclei and to the STAR spin program. The pseudorapidity coverage is indicated by the red circles representing loci at $\eta = 3.0, 3.5$ and 4.0 .*

4.3 Other experiments

4.3.1 PP2PP

The pp2pp Experiment last took data in 2003, using silicon detectors in four Roman Pot stations that can remotely place the detectors close to the outgoing blue and yellow beams, measuring elastic scattering from collisions at IP 2. Results from this run are discussed in section 2. With a small modification requiring rotation of two stations to a horizontal orientation, the present experimental setup, see Fig. 52 is suitable for sensitive transverse spin measurements in an extended $|t|$ -range, $0.003 < |t| < 0.020$ (GeV/c)². This running would use accelerator optics of $\beta^*=20$ m. For $\sqrt{s}=500$ GeV, optics with $\beta^*=20$ m allows measurements up to $|t| \approx 0.12$ (GeV/c)². A proposal is being prepared, to run in 2006.

4.3.2 BRAHMS

The BRAHMS detector is well suited to explore the x_f and p_T dependence of the single spin asymmetries for identified charged hadrons. The forward spectrometer is operated at 2.3° and 4.0° for these measurements. The spectrometer has a total bending power of 7.2 Tm and a momentum resolution of $\delta p/p \approx 1 - 2\%$. The particle identification in the current setup using a Ring Imaging Cherenkov (RICH) detector allows for π^\pm identification for momenta up to 35 GeV/c. Operating the RICH at a lower pressure of the radiative gas of C_4F_{10} will allow for π identification up to ≈ 50 GeV/c. Identification of kaons is possible up to a somewhat lower momentum than π s due to the lower yields. During the 2004 run, a small sample of π^+ and π^- data were taken. Preliminary data are shown in section 2. The coverage in p_T vs x_f is shown in Fig. 53. Future measurements in 2005 and possibly in 2006 will extend this coverage towards larger x_f

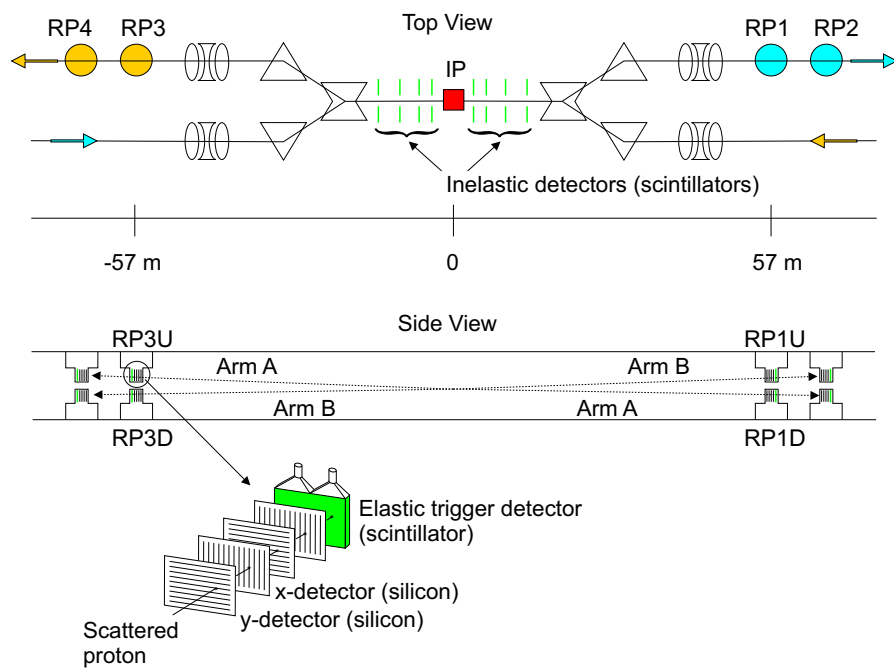


Figure 52: Layout of the $pp2pp$ Experiment. Note the detector pairs RP1, RP2 and RP3, RP4 lie in different RHIC rings. Scattering is detected in either one of two arms: Arm A is formed from RP3U and RP1D. Conversely, Arm B is formed from RP3D and RP1U.

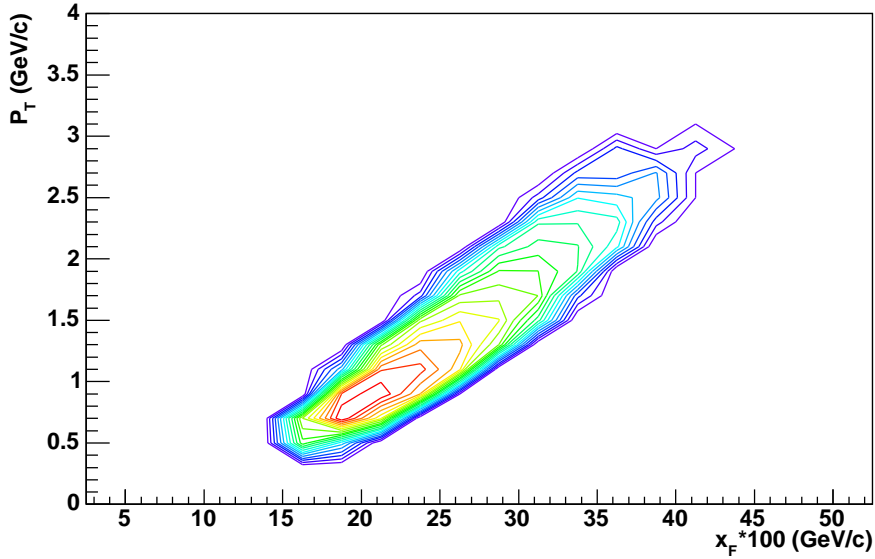


Figure 53: *BRAHMS* acceptance in x_F and p_T .

and p_T . The required delivered luminosity for such measurements is $2 - 4 pb^{-1}$.

4.3.3 Jet Target Experiment

With the addition of recoil detectors at more forward angles, covering 85° to 60° , and with forward detectors near the beam direction, the t range of the polarized atomic hydrogen jet target in RHIC can be substantially increased. The present detectors cover $-t=0.0015$ to 0.03 $(GeV/c)^2$ for polarimetry. A proposal is being considered to reach $-t=1$ $(GeV/c)^2$. The experiment would make precise measurements of the cross section and transverse spin asymmetries ($d\sigma/dt$, A_N , A_{NN}) for pp elastic scattering, from the Coulomb nuclear interference region to the intermediate t region dominated by Pomeron scattering, and into the diffraction dip region around $-t \sim 1$ $(GeV/c)^2$. With the use of additional RF transitions, the jet target can also produce deuteron beams. Deuterons would allow the study of polarized pd scattering, comparing the protons scattering from protons ($I=1$) to deuterons ($I=0$). Another attractive possibility with this facility is to scatter light ion beams from the polarized jet target. This allows the study of nuclear effects in polarized pA scattering.

4.3.4 Large Acceptance New RHIC Detector

A new comprehensive detector [165] has been discussed for RHIC II to measure and identify hadrons, electrons and muons, photons and jets over a large rapidity range and full azimuth. Such a comprehensive detector utilizing polarized p+p interactions at the RHIC II facility is an effective way to explore the structure and dynamics of the proton beyond the present RHIC spin program capabilities. The detector utilizes precision tracking and particle identification to large transverse momentum (20 GeV/c) in a 1.3 T solenoidal magnetic field with complete electromagnetic and

hadronic calorimetry and muon identification over $-3.5 < \eta < 3.5$. Further coverage forward ($3.5 < \eta < 4.8$) with tracking, electromagnetic and hadronic calorimetry is planned. High rate data-acquisition and triggering capabilities allow an investigation of rare processes, such as a possible parity violating interaction in the Standard Model (SM) and polarization of the QCD sea, that are complementary to a future dedicated eRHIC facility. RHIC II is in a unique position to explore aspects of physics beyond the SM in a region of phase space that is unconstrained by current or future experimental efforts at other collider facilities.

Some of the exciting spin physics topics that can be covered with a new comprehensive detector at RHIC II are the following: a) The polarization of strangeness in the sea can be probed by charm-tagged production at $\sqrt{s} = 500$ GeV in such a RHIC II detector. b) Gluons in the proton can be accessed directly through measurements of heavy-flavor production in various leptonic decay channels over a large kinematic range in the new detector. Measurements of heavy quarkonia will probe gluons in the proton at higher RHIC II luminosities. c) The transversity densities of quarks and anti-quarks will be accessible at RHIC, but can be probed with greater precision at RHIC II. The increased luminosity of RHIC II and the broad acceptance of the new detector will make possible double-transverse spin asymmetry (A_{TT}) measurements for high- p_T inclusive jets and the Drell-Yan process. d) Predictions for physics beyond the Standard Model (SM), e.g. new parity-violating interactions, may be discovered using spin measurements at RHIC II [173]. Here parity violation arises within the SM for quark-quark scattering through the interference of gluon- and Z^0 -exchange. Observation of a parity-violating single-spin asymmetry in inclusive single-jet production at RHIC II would signify quark compositeness [166]. Predicted deviations from the SM prediction are extremely small and increase with transverse jet energy, requiring the highest possible luminosities and data rates, and large coverage for jet measurements to the highest possible transverse energies. e) Although open charm production is fairly well understood, beauty production exhibits large discrepancies between theory [208] and recent data from HERA [209] and LEP [210]. This has led to an extensive discussion of physics beyond the Standard Model (SM) as an explanation for this discrepancy.vii RHIC II could play an important role in understanding this discrepancy through its ability to investigate energy- and spin-dependent charm and bottom production.

5 Spin plan schedule

In the charge, we were requested to consider two running schedules: 10 and 5 physics weeks for spin per year. These follow, showing *example* plans. We emphasize that the actual run plan will be developed from the experiment beam use proposals. Our consideration of these scenarios should not suggest that we advocate a change to this successful approach.

A key issue is the completion of experiment hardware to run the W physics program. The required hardware are the muon trigger improvements for PHENIX, and a forward tracker for STAR. The PHENIX muon triggering improvements are estimated to cost \$2.3M for resistive plate chambers and \$1M for muon tracker electronics. Planned completion is for the 2009 RHIC run. The STAR tracker (estimated \$5M) is planned to be proposed in 2006, and to be complete for the 2010 run.

The example plan below for the 10 physics week/year case is "technically driven". The plan assumes that the funding is received, and the work is completed as planned. For the 5 week plan, the delay in reaching luminosity goals for $\sqrt{s}=200$ GeV delays the start of the W running considerably, by greater than three years. An early completion of the W hardware is less of an issue for this case.

A second key issue is machine performance. We assume that we reach the polarization goal of 70% in 2006. For luminosity, we assume in the example plan that we reach 0.7 times the "maximum" luminosity (see section 3). This assumption is discussed there.

A third key issue is experiment availability, in which we include up time, live time, and the fraction of the collision vertex accepted by the experiment. This results in "recorded luminosity" for each experiment. We have taken the up time to be 70% for each experiment, as has been achieved. The live time for PHENIX is 90%, due to multi-event buffering; the live time for STAR is 50% for data-taking including the TPC, and 90% for data using fast detectors only. The online data selection adjusts thresholds, for example the lower p_T requirement, to reach these live time levels. The PHENIX vertex acceptance for the 200 GeV running is 50%, requiring the vertex to be within 30 cm of the IP. We have used this acceptance also for 500 GeV. The STAR vertex acceptance contains all collisions, with more restrictive vertex selection for certain processes. The overall factor for recorded/delivered luminosity for PHENIX is 32%, and for STAR is 35% (data with TPC) and 63% (fast detectors only). The physics sensitivities shown in section 2 also include apparatus acceptance and event selection acceptance.

Another factor in calculating sensitivities is the ratio of longitudinal to transverse spin running. STAR and PHENIX can choose this independently, and the actual split will be decided at the time. We have used 75% longitudinal and 25% transverse for 200 GeV running, and 100% longitudinal for 500 GeV running, for both experiments.

5.1 10 physics weeks

Table 6 shows the example spin plan for 10 physics weeks per year, with a *technically driven* schedule. The 200 GeV running continues through mid-2009, with a target total of 275 pb^{-1} delivered. By the year 2009, the PHENIX muon triggering improvements are complete, and the

STAR forward tracking is partially in place, and complete for the 2010 run. The year 2009 is split with both 200 GeV and 500 GeV running. By the completion of the year 2012, for 500 GeV, the target luminosity of 980 pb^{-1} is delivered. Polarization is taken as 0.7 from 2006, for both 200 GeV and 500 GeV running. These luminosities and polarizations provide the physics sensitivities presented in section 2.

Table 6: *RHIC spin example schedule, 10 physics weeks per year, technically driven. Luminosities are 0.7 times maximum.*

Fiscal year	Spin Weeks	CME(GeV)	P	L(pb^{-1})	Remarks
2002	5	200	0.15	0.5	First pol. pp collisions! Transverse spin
2003	4	200	0.3	1.6	Spin rotators commissioned, first helicity measurements
2004	3	200	0.4	3	New betatron tune developed, first jet absolute meas. P
2005	10	200	0.5	14	$A_{LL}(\pi^0, \text{jet})$, also 500 GeV studies
2006	10	200	0.7	32	AGS Cold Snake commissioned, NEG vacuum coating complete
2007	10	200	0.7	88	
2008	10	200	0.7	106	Direct γ
2009	5	200	0.7	35	target complete for 200 GeV;
	5	500	0.7	180	PHENIX μ trig.; W starts
2010	10	500	0.7	266	STAR forward tracker; W physics
2011	10	500	0.7	266	
2012	10	500	0.7	266	Completes 500 GeV target

5.2 5 physics weeks

Table 7 gives the example spin plan for 5 physics weeks per year, which we have interpreted to mean 10 physics weeks each two years to reduce the end effects. The programs are stretched out to over 6 years for the gluon polarization measurements at 200 GeV, and an additional 6 years or more for the W physics program. The proposed measurements would be completed in 2019 or later.

Table 7: *RHIC spin example schedule, average 5 physics weeks per year.*

Fiscal year	Spin Weeks	CME(GeV)	P	L(pb ⁻¹)	Remarks
2005	10	200	0.5	14	$A_{LL}(\pi^0, \text{jet})$, also 500 GeV studies
2006-2007	10	200	0.7	32	AGS Cold Snake commissioned, NEG vacuum coating complete
2008-2009	10	200	0.7	88	Direct γ
2010-11	10	200	0.7	106	
2012-13	5	200	0.7	35	200 GeV target complete;
	5	500	0.7	180	PHENIX μ trig.
2014-2015	10	500	0.7	266	STAR forward tracker; W physics
2016-2017	10	500	0.7	266	
2018-2019	10	500	0.7	266	Completes 500 GeV target

6 Summary

In this document we have described the RHIC spin research plan, responding to the request by the Department of Energy Office of Nuclear Physics. We were requested to cover 1) the science, 2) the requirements for the accelerator, 3) the resources that are needed and timelines, and 4) the impact of a constant effort budget to the program.

1) The science is presented in section 2. Here we have emphasized measuring gluon polarization and anti-quark polarization in the proton. RHIC will provide the first sensitive measurements of each. We believe this is an exciting program, which addresses the structure of matter.

2) The accelerator requirements are presented in section 3. We are well along in reaching the polarization requirement of 70%, and anticipate reaching this goal in 2006, for 200 GeV running. To reach this goal for 500 GeV running will require releveling the machine, which is planned. Reaching the luminosity goal will be challenging. We must store 2×10^{11} polarized protons in 110 rf bunches in each RHIC ring and collide them. RHIC at our luminosity will operate near or above previously achieved beam-beam parameters, and will be the first hadron collider in the strong-strong beam-beam regime. For the physics sensitivities presented, we have used a luminosity of 0.7 times the calculated maximum.

3) The required experiment resources are presented in section 4. The PHENIX and STAR detectors are complete for the gluon polarization program. Both need improvements to be ready for the W physics program. These are described in the section. For a "technically driven" program, where the improvements are funded and completed as proposed, the PHENIX detector will be ready for W physics in 2009, and the STAR detector in 2010.

There are also important planned upgrades for the heavy ion and spin programs that greatly extend the range of spin physics, and these are also described in section 4.

4) The impact of a constant effort budget is presented in section 5, where we compare the two plans, as requested in the charge to the RHIC Spinplan Group:

"I ask that you consider two RHIC Spin running scenarios: 1) 5 spin physics data taking weeks per year (averaged over two years using the combined fiscal year concept); 2) 10 spin physics data taking weeks per year. These two scenarios will give appropriate indications of the physics goals that can be met over a period of years without involving the Group in difficult funding and cost scenarios that are not central to the calculation of physics accomplishments over time." (Appendix A)

The plan with 10 spin physics weeks per year, the technically driven plan, completes the gluon polarization measurements and the W physics measurements by 2012.

The plan with 5 spin physics weeks per year completes this program in 2019 or later.

Acknowledgements

This report is based on work done over many years by accelerator physicists, experimenters and theorists in the RHIC Spin Collaboration and colleagues in the STAR, PHENIX, BRAHMS, and pp2pp experiments.

7 Appendix: the charge from DOE

CHARGE

to the RHIC Spin Plan Group

T. Kirk, ALD-HENP

November 9, 2004

The RHIC Spin Plan Group is charged with creating a written report that is responsive to the recommendation from the DOE S&T Review Committee in the Executive Summary section of the "Department of Energy Office of Nuclear Physics Report on the Science and Technology Review of the Relativistic Heavy Ion Collider (RHIC) at BNL - September 20, 2004." The recommendation made in that report was: "BNL should prepare a document that articulates its research plan for the RHIC spin physics program. A copy should be submitted to DOE by January 31, 2005." The text of the report goes on to identify appropriate objectives that the plan should encompass. I accept these objectives and transmit them to the RHIC Spin Plan Group here: "The plan should: (1) explain what science can be done at RHIC in the context of current and future capabilities world-wide (i.e. what will be the important measurements, what will be their significance and impact and will some of these be made elsewhere prior to RHIC, etc.), (2) explain what accelerator and detector performances are needed to make the measurements (i.e. what beam energies, intensities and polarizations, what detector capabilities, etc.), (3) identify the needed resources to implement the research plan and subsequent timeline with the significant technical and scientific milestones that will be achieved (assuming projected improvements in luminosity and polarizations, estimated time for developing the 500 GeV proton beam, estimated times to implement needed detector upgrades, what funding will be needed, etc.), and (4) explain the impact of a constant effort budget to the planned research program."

In addition to these objectives, I wish to supply some practical guidelines to the Group on the resource levels that should guide the outcome of the Plan. Specifically, I ask that you consider two RHIC Spin running scenarios: 1) 5 spin physics data taking weeks per year (averaged over two years using the combined fiscal year running concept); 2) 10 spin physics data taking weeks per year. These two scenarios will give appropriate indications of the physics goals that can be met over a period of years without involving the Group in difficult funding and cost scenarios that are not central to the calculation of the physics accomplishments over time. On the research efforts side, you should assume "constant effort" which means that inflation is compensated for the research budgets and staff is, therefore, not lost year by year.

You will also need the accelerator performance estimates provided by the accelerator physicists in the Collider-Accelerator Department and this will be provided to you. A knowledgeable member of the C-AD accelerator physics staff will be appointed to the RHIC Spin Plan Group to facilitate this purpose.

Finally, you should use the 20 Year RHIC Plan and the RHIC II planning process to integrate the spin parts of those activities with your report. The written report is due on January 31, 2005 for transmission to DOE Office of Nuclear Physics and should be reviewed by me prior to transmission to DOE.

References

- [1] M. Hirai, S. Kumano and N. Saito [Asymmetry Analysis Collaboration], Phys. Rev. D **69**, 054021 (2004) [arXiv:hep-ph/0312112].
- [2] M. Glück, E. Reya, M. Stratmann, and W. Vogelsang, Phys. Rev. **D63**, 094005 (2001).
- [3] For review, see: E. W. Hughes and R. Voss, Ann. Rev. Nucl. Part. Sci. **49**, 303 (1999).
- [4] B. Adeva *et al.* [Spin Muon Collaboration (SMC)], Phys. Rev. D **70**, 012002 (2004) [arXiv:hep-ex/0402010].
- [5] A. Airapetian *et al.* [HERMES Collaboration], Phys. Rev. Lett. **84**, 2584 (2000) [arXiv:hep-ex/9907020].
- [6] C. Schill, arXiv:hep-ex/0501056.
- [7] C. Bourrely, J. Soffer, Nucl. Phys. **B445**, 341 (1995).
- [8] T. Gehrmann and W.J. Stirling, Phys. Rev. **D53**, 6100 (1996).
- [9] I. Estermann, R. Frisch, O. Stern, Nature **132** (1933) 169;
see also: O. Stern, “The Method of Molecular Rays”, Nobel lecture 1946,
<http://nobelprize.org/physics/laureates/1943/stern-lecture.pdf>.
- [10] M. Gell-Mann, Phys. Lett. **8** (1964) 214; G. Zweig, CERN-TH-412.
- [11] O. W. Greenberg, Phys. Rev. Lett. **13** (1964) 598; M. Y. Han and Y. Nambu, Phys. Rev. **139** (1965) B1006.
- [12] E. D. Bloom *et al.*, Phys. Rev. Lett. **23**, 930 (1969); *ibid.* 935. For review see, for example: J. I. Friedman, H. W. Kendall, Ann. Rev. Nucl. Part. Sci. **22** (1972) 203; see also: H.W. Kendall, “Deep Inelastic Scattering: Experiments on the Proton and the Observation of Scaling”, Nobel lecture 1990, <http://nobelprize.org/physics/laureates/1990/kendall-lecture.pdf>.
- [13] J. D. Bjorken, Phys. Rev. **179**, 1547 (1969); R. P. Feynman, Phys. Rev. Lett. **23** (1969) 1415; J. D. Bjorken and E. A. Paschos, Phys. Rev. **185**, 1975 (1969).
- [14] C. G. . Callan and D. J. Gross, Phys. Rev. Lett. **22** (1969) 156.
- [15] J. G. H. de Groot *et al.*, Phys. Lett. B **82**, 292 (1979); *ibid.* 456; Z. Phys. C **1**, 143 (1979).
- [16] R. Brandelik *et al.* [TASSO Collaboration], Phys. Lett. B **86**, 243 (1979); C. Berger *et al.* [PLUTO Collaboration], Phys. Lett. B **86**, 418 (1979); W. Bartel *et al.* [JADE Collaboration], Phys. Lett. B **91**, 142 (1980).
- [17] R. Brandelik *et al.* [TASSO Collaboration], Phys. Lett. B **97**, 453 (1980); J. R. Ellis and I. Karliner, Nucl. Phys. B **148**, 141 (1979).
- [18] C. G. . Callan and D. J. Gross, Phys. Rev. D **8** (1973) 4383.

- [19] H. Fritzsch, M. Gell-Mann and H. Leutwyler, Phys. Lett. B **47** (1973) 365; D. J. Gross and F. Wilczek, Phys. Rev. D **8**, 3633 (1973); S. Weinberg, Phys. Rev. Lett. **31**, 494 (1973).
- [20] D. J. Gross, F. Wilczek, Phys. Rev. Lett. **30**, 1343 (1973); H. D. Politzer, *ibid.* 1346.
- [21] H. Georgi and H. D. Politzer, Phys. Rev. D **9** (1974) 416; Phys. Rev. D **14**, 1829 (1976).
- [22] S. D. Drell and T. M. Yan, Phys. Rev. Lett. **25**, 316 (1970) [Erratum-*ibid.* **25**, 902 (1970)].
- [23] S. M. Berman and M. Jacob, Phys. Rev. Lett. **25**, 1683 (1970); S. M. Berman, J. D. Bjorken and J. B. Kogut, Phys. Rev. D **4**, 3388 (1971); R. L. Jaffe, Phys. Rev. D **5**, 2622 (1972); R. P. Feynman, R. D. Field and G. C. Fox, Phys. Rev. D **18**, 3320 (1978).
- [24] S.B. Libby and G. Sterman, Phys. Rev. **D18**, 3252 (1978); R.K. Ellis, H. Georgi, M. Machacek, H.D. Politzer, and G.G. Ross, Phys. Lett. **78B**, 281 (1978); Nucl. Phys. **B152**, 285 (1979); D. Amati, R. Petronzio, and G. Veneziano, Nucl. Phys. **B140**, 54 (1980); Nucl. Phys. **B146**, 29 (1978); G. Curci, W. Furmanski, and R. Petronzio, Nucl. Phys. **B175**, 27 (1980); J.C. Collins, D.E. Soper, and G. Sterman, Phys. Lett. **B134**, 263 (1984); Nucl. Phys. **B261**, 104 (1985); J.C. Collins, Nucl. Phys. **B394**, 169 (1993).
- [25] G. Arnison *et al.* [UA1 Collaboration], Phys. Lett. B **122**, 103 (1983); G. Arnison *et al.* [UA1 Collaboration], Phys. Lett. B **126**, 398 (1983); M. Banner *et al.* [UA2 Collaboration], Phys. Lett. B **122**, 476 (1983); P. Bagnaia *et al.* [UA2 Collaboration], Phys. Lett. B **129**, 130 (1983).
- [26] C. Y. Prescott *et al.*, SLAC-PROPOSAL-E-095.
- [27] M. J. Alguard *et al.*, Phys. Rev. Lett. **37**, 1261 (1976).
- [28] J. Ashman *et al.* [European Muon Collaboration], Phys. Lett. B **206**, 364 (1988); Nucl. Phys. B **328**, 1 (1989).
- [29] see: D.L. Adams *et al.* [FNAL E704 Collaboration], Phys. Lett. B **261**, 201 (1991).
- [30] K. Krueger *et al.*, Phys. Lett. B **459**, 412 (1999), and references therein.
- [31] G. Bunce *et al.*, Phys. Rev. Lett. **36**, 1113 (1976); K. Heller *et al.*, Phys. Lett. **B68**, 480 (1977); S. A. Gourlay *et al.*, Phys. Rev. Lett. **56**, 2244 (1986).
- [32] For review, see: G. Bunce, N. Saito, J. Soffer and W. Vogelsang, Ann. Rev. Nucl. Part. Sci. **50**, 525 (2000) [arXiv:hep-ph/0007218].
- [33] L. De Nardo [HERMES Collaboration], Czech. J. Phys. **52**, A1 (2002) [Czech. J. Phys. **52**, C185 (2002)].
- [34] G. Altarelli and G. Parisi, Nucl. Phys. B **126**, 298 (1977).
- [35] SMC, B. Adeva *et al.*, Phys. Rev. **D58**, 112002 (1998); D. de Florian and R. Sassot, Phys. Rev. **D62**, 094025 (2000); G. Altarelli, R.D. Ball, S. Forte, and G. Ridolfi, Nucl. Phys. **B496**, 337 (1997); E. Leader, A.V. Sidorov, and D. Stamenov, Eur. Phys. J. **C23**, 479 (2002).
- [36] J. Blümlein and H. Böttcher, Nucl. Phys. **B636**, 225 (2002).

- [37] J.D. Bjorken, Phys. Rev. **148**, 1467 (1966); *ibid.* **D1**, 1376 (1970).
- [38] R. L. Jaffe and A. Manohar, Nucl. Phys. B **337**, 509 (1990).
- [39] X. D. Ji, Phys. Rev. Lett. **78**, 610 (1997).
- [40] B. L. G. Bakker, E. Leader and T. L. Trueman, Phys. Rev. D **70**, 114001 (2004) [arXiv:hep-ph/0406139].
- [41] G. Altarelli and G. G. Ross, Phys. Lett. B **212**, 391 (1988).
- [42] R. L. Jaffe, Phys. Lett. B **365**, 359 (1996) [arXiv:hep-ph/9509279]; L. Mankiewicz, G. Piller and A. Saalfeld, Phys. Lett. B **395**, 318 (1997) [arXiv:hep-ph/9611326]; V. Barone, T. Calarco and A. Drago, Phys. Lett. B **431**, 405 (1998) [arXiv:hep-ph/9801281]; H. J. Lee, D. P. Min, B. Y. Park, M. Rho and V. Vento, Phys. Lett. B **491**, 257 (2000) [arXiv:hep-ph/0006004].
- [43] B. Dressler, K. Goeke, M. V. Polyakov and C. Weiss, Eur. Phys. J. C **14**, 147 (2000) [arXiv:hep-ph/9909541]; Eur. Phys. **C18**, 719 (2001).
- [44] F. G. Cao and A. I. Signal, Phys. Rev. D **68**, 074002 (2003) [arXiv:hep-ph/0306033].
- [45] P. Amaudruz *et al.*, [NMC], Phys. Rev. Lett. **66**, 2712 (1991); M. Arneodo *et al.*, [EMC], Phys. Rev. **D 50**, R1 (1994).
- [46] A. Baldit *et al.* [NA51 Collab.], Phys. Lett. **332**, 244 (1994); E.A. Hawker *et al.* [E866 Collab.], Phys. Rev. Lett. **80**, 3715 (1998).
- [47] K. Ackerstaff *et al.*, [HERMES Collab.], Phys. Rev. Lett. **25**, 5519 (1998).
- [48] S. Kretzer, F. Olness, J. Pumplin, D. Stump, W. K. Tung and M. H. Reno, Phys. Rev. Lett. **93**, 041802 (2004) [arXiv:hep-ph/0312322].
- [49] G. P. Zeller *et al.* [NuTeV Collaboration], Phys. Rev. Lett. **88**, 091802 (2002) [Erratum-*ibid.* **90**, 239902 (2003)] [arXiv:hep-ex/0110059].
- [50] X. D. Ji, J. P. Ma and F. Yuan, Nucl. Phys. B **652**, 383 (2003) [arXiv:hep-ph/0210430]; S. J. Brodsky, D. S. Hwang, B. Q. Ma and I. Schmidt, Nucl. Phys. B **593**, 311 (2001) [arXiv:hep-th/0003082].
- [51] J. P. Ralston and D. E. Soper, Nucl. Phys. B **152**, 109 (1979).
- [52] R. L. Jaffe and X. D. Ji, Phys. Rev. Lett. **67**, 552 (1991).
- [53] H.-X. He and X. D. Ji, Phys. Rev. D **52**, 2960 (1995) [arXiv:hep-ph/9412235].
- [54] A. Airapetian *et al.*, Phys. Rev. Lett. **84**, 4047 (2000); Phys. Lett. B **535**, 85 (2002); **562**, 182 (2003).
- [55] A. Airapetian *et al.* [HERMES Collaboration], Phys. Rev. Lett **94**, 012002 (2005).
- [56] D. W. Sivers, Phys. Rev. **D41**, 83 (1990); Phys. Rev. D **43**, 261 (1991).
- [57] J. Qiu and G. Sterman, Phys. Rev. **D59**, 014004 (1999).

- [58] S. Kretzer, Phys. Rev. **D62**, 054001 (2000); B. Kniehl, G. Kramer and B. Pötter, Nucl. Phys. **B582**, 514 (2000); Nucl. Phys. **B597**, 337 (2001); L. Bourhis, M. Fontannaz, J.P. Guillet, M. Werlen, Eur. Phys. J. **C19**, 89 (2001).
- [59] S.S. Adler *et al.* [PHENIX Collaboration], Phys. Rev. Lett. **91**, 241803 (2003).
- [60] J. Adams *et al.* [STAR Collaboration], Phys. Rev. Lett. **92**, 171801 (2004); G. Rakness [STAR Collaboration], arXiv:nucl-ex/0501026.
- [61] B. Jäger, A. Schäfer, M. Stratmann, W. Vogelsang, Phys. Rev. **D67**, 054005 (2003) [arXiv:hep-ph/0211007].
- [62] D. de Florian, Phys. Rev. **D67**, 054004 (2003) [arXiv:hep-ph/0210442].
- [63] F. Aversa, P. Chiappetta, M. Greco and J. P. Guillet, Nucl. Phys. B **327**, 105 (1989).
- [64] J. Pumplin *et al.* [CTEQ Collaboration], JHEP **0207**, 012 (2002).
- [65] V. Guzey, M. Strikman and W. Vogelsang, Phys. Lett. B **603**, 173 (2004) [arXiv:hep-ph/0407201]; S. Kretzer, arXiv:hep-ph/0410219.
- [66] K. Okada [PHENIX Collaboration], arXiv:hep-ex/0501066.
- [67] L.E. Gordon and W. Vogelsang, Phys. Rev. **D48**, 3136 (1993); *ibid.* D **50**, 1901 (1994).
- [68] P. Aurenche *et al.*, Phys.Lett. B140, 87 (1984); Nucl.Phys. B297, 661 (1988); H. Baer *et al.*, Phys.Rev. D42, 61 (1990); Phys.Lett. B234, 127 (1990).
- [69] L. Apanasevich *et al.*, Phys. Rev. D **59**, 074007 (1999) [arXiv:hep-ph/9808467]; P. Aurenche, M. Fontannaz, J. P. Guillet, B. A. Kniehl, and M. Werlen, Eur. Phys. J. C **9**, 107 (1999) [arXiv:hep-ph/9811382]; *ibid.* C **13**, 347 (2000) [arXiv:hep-ph/9910252]; U. Baur *et al.*, arXiv:hep-ph/0005226; C. Bourrely and J. Soffer, Eur. Phys. J. C **36**, 371 (2004) [arXiv:hep-ph/0311110].
- [70] C. Adler *et al.* [STAR Collaboration], Phys. Rev. Lett. **90**, 082302 (2003) [arXiv:nucl-ex/0210033].
- [71] D. de Florian, S. Frixione, A. Signer, and W. Vogelsang, Nucl. Phys. **B539**, 455 (1999).
- [72] B. Jäger, M. Stratmann and W. Vogelsang, Phys. Rev. D **70**, 034010 (2004) [arXiv:hep-ph/0404057].
- [73] A.P. Contogouris, B. Kamal, Z. Merebashvili, and F.V. Tkachov, Phys. Lett. **B304**, 329 (1993); Phys. Rev. **D48**, 4092 (1993); A.P. Contogouris and Z. Merebashvili, Phys. Rev. **D55**, 2718 (1997).
- [74] S. Frixione and W. Vogelsang, Nucl. Phys. **B568**, 60 (2000).
- [75] L. E. Gordon, Phys. Lett. B **406**, 184 (1997) [arXiv:hep-ph/9609403]; S. Chang, C. Coriano and L. E. Gordon, Phys. Rev. D **58**, 074002 (1998) [arXiv:hep-ph/9709496].
- [76] C. Coriano and L. E. Gordon, Phys. Rev. D **54**, 781 (1996) [arXiv:hep-ph/9602297].
- [77] I. Bojak and M. Stratmann, Phys. Rev. D **67**, 034010 (2003) [arXiv:hep-ph/0112276].

- [78] P.G. Ratcliffe, Nucl. Phys. **B223**, 45 (1983);
 A. Weber, Nucl. Phys. **B382**, 63 (1992);
 B. Kamal, Phys. Rev. **D57**, 6663 (1998);
 T. Gehrman, Nucl. Phys. **B534**, 21 (1998).
- [79] V. Ravindran, J. Smith, and W.L. van Neerven, Nucl. Phys. **B647**, 275 (2002);
 see also: S. Chang, C. Coriano, and R.D. Field, Phys. Lett. **B403**, 344 (1997); Nucl. Phys.
B528, 285 (1998);
 S. Chang, C. Coriano, R.D. Field, and L.E. Gordon, Nucl. Phys. **B512**, 393 (1998);
 E. L. Berger, L. E. Gordon and M. Klasen, Phys. Rev. D **62**, 014014 (2000) [arXiv:hep-
 ph/9909446].
- [80] V. Ravindran, J. Smith and W. L. van Neerven, Nucl. Phys. B **682**, 421 (2004) [arXiv:hep-
 ph/0311304].
- [81] D. L. Adams *et al.* [E704 Collaboration], Phys. Lett. B **261**, 197 (1991).
- [82] M. Glück, E. Reya, and A. Vogt, Eur. Phys. J. **C5**, 461 (1998) [arXiv:hep-ph/9806404].
- [83] S. S. Adler *et al.* [PHENIX Collaboration], Phys. Rev. Lett. **93**, 202002 (2004) [arXiv:hep-
 ex/0404027]; Y. Fukao [PHENIX Collaboration], arXiv:hep-ex/0501049.
- [84] H.-L. Lai *et al.* [CTEQ Collaboration], Eur. Phys. J. **C12**, 375 (2000).
- [85] A. D. Martin, R. G. Roberts, W. J. Stirling and R. S. Thorne, Eur. Phys. J. C **28**, 455 (2003)
 [arXiv:hep-ph/0211080]; *ibid.* C **35** (2004) 325 [arXiv:hep-ph/0308087].
- [86] M. Stratmann and W. Vogelsang, Phys. Rev. D **64**, 114007 (2001) [arXiv:hep-ph/0107064].
- [87] M. Anselmino, A. Efremov, E. Leader, Phys. Rep. **261**, 1; E: **281**, 399 (1997); H.-Y. Cheng,
 Int. J. Mod. Phys. **A11**, 5109 (1996); arXiv:hep-ph/0002157; B. Lampe, E. Reya E, Phys.
 Rep. **332**, 1 (2000); S.D. Bass Eur. Phys. J. **A5**, 17 (1999).
- [88] H.J. Lipkin, Phys. Lett. **B256**, 284 (1991); Phys. Lett. **B337**, 157 (1994); J. Lichtenstedt,
 H.J. Lipkin, Phys. Lett. **B353**, 119 (1995).
- [89] M. Glück, E. Reya, M. Stratmann, W. Vogelsang, Phys. Rev. **D53**, 4775 (1996).
- [90] A. Airapetian *et al.* [HERMES Collaboration], Phys. Rev. D **71**, 012003 (2005) [arXiv:hep-
 ex/0407032].
- [91] N.S. Craigie, K. Hidaka, M. Jacob, F.M. Renard, Phys. Rep. **99**, 69 (1983); C. Bourrely, J.
 Soffer, E. Leader, Phys. Rep. **59**, 95 (1980).
- [92] C. Bourrely, J. Soffer, Phys. Lett. **B314**, 132 (1993); Nucl. Phys. **B423**, 329 (1994); P.
 Chiappetta, J. Soffer, Phys. Lett. **B152**, 126 (1985).
- [93] L. C. Bland [STAR Collaboration], talk presented at the “Circum-Pan-Pacific RIKEN
 Symp. High Energy Spin Phys. (Pacific Spin 99)”, RIKEN Rev. **28**, 8 (2000) [arXiv:hep-
 ex/0002061].
- [94] T. Sjöstrand *et al.*, Computer Physics. Commun. **82**, 74 (1994); *ibid.* **135**, 238 (2001).

- [95] C. Balazs, C.-P. Yuan, Phys. Rev. **D56**, 5558 (1997).
- [96] P.M. Nadolsky, C.-P. Yuan, Nucl. Phys. **B666**, 3 (2003).
- [97] F. Abe *et al.* [CDF Collaboration], Phys. Rev. Lett. **74**, 850 (1995); *ibid.* **81**, 5754 (1998).
- [98] K. Gottfried, Phys. Rev. Lett. **18**, 1174 (1967).
- [99] H.L. Lai *et al.* [CTEQ Collaboration], Phys. Rev. **D55**, 1280 (1997).
- [100] A.D. Martin, R.G. Roberts, W.J. Stirling, R.S. Thorne, Eur. Phys. J. **C14**, 133 (2000).
- [101] V. Barone, A. Drago and P. G. Ratcliffe, Phys. Rept. **359**, 1 (2002).
- [102] K. Chen, G. R. Goldstein, R. L. Jaffe and X. D. Ji, Nucl. Phys. B **445**, 380 (1995) [arXiv:hep-ph/9410337].
- [103] V. Barone, Phys. Lett. B **409**, 499 (1997) [arXiv:hep-ph/9703343].
- [104] W. Vogelsang, Phys. Rev. D **57**, 1886 (1998) [arXiv:hep-ph/9706511].
- [105] A. Hayashigaki, Y. Kanazawa and Y. Koike, Phys. Rev. D **56**, 7350 (1997) [arXiv:hep-ph/9707208]; S. Kumano and M. Miyama, Phys. Rev. D **56**, 2504 (1997) [arXiv:hep-ph/9706420].
- [106] J. Soffer, Phys. Rev. Lett. **74**, 1292 (1995); D. W. Sivers, Phys. Rev. D **51**, 4880 (1995).
- [107] see, for example: Stefano Capitani, Nucl. Phys. **B597**, 313 (2001).
- [108] J. C. Collins, Nucl. Phys. **B396**, 161 (1993).
- [109] B.E. Bonner *et al.*, Phys. Rev. Lett. **61**, 1918 (1988); A. Bravar *et al.*, *ibid.* **77**, 2626 (1996); **264**, 462 (1991); Z. Phys. C **56**, 181 (1992).
- [110] C.E. Allgower *et al.*, Phys. Rev. D **65**, 092008 (2002).
- [111] A. Bravar *et al.*, Nucl. Phys. Proc. Suppl. **79**, 520 (1999).
- [112] G.L. Kane, J. Pumplin, and W. Repko, Phys. Rev. Lett. **41**, 1689 (1978).
- [113] J. W. Qiu and G. Sterman, Phys. Rev. Lett. **67**, 2264 (1991); Nucl. Phys. B **378**, 52 (1992).
- [114] A. V. Efremov and O. V. Teryaev, Phys. Lett. B **150**, 383 (1985); Sov. J. Nucl. Phys. **36**, 140 (1982) [Yad. Fiz. **36**, 242 (1982)]; Yad. Fiz. **39**, 1517 (1984).
- [115] Y. Koike, AIP Conf. Proc. **675**, 449 (2003).
- [116] M. Burkardt, Phys. Rev. D **69**, 091501 (2004).
- [117] Matthias Burkardt, Phys. Rev. D **66**, 114005 (2002).
- [118] J. C. Collins, S. F. Heppelmann, G. A. Ladinsky, Nucl. Phys. **B420**, 565 (1994); A. V. Efremov, L. Mankiewicz and N. A. Tornqvist, Phys. Lett. **B284**, 394 (1992).

- [119] M. Anselmino, M. Boglione, U. D’Alesio, E. Leader and F. Murgia, Phys. Rev. D **71**, 014002 (2005) [arXiv:hep-ph/0408356]; arXiv:hep-ph/0412236; U. D’Alesio and F. Murgia, arXiv:hep-ph/0412317.
- [120] B. Jaffe *et al.*, Phys. Rev. D **57**, 5920 (1998); J. Tang, arXiv:hep-ph/9807560, and J. Tang, Thesis, MIT (1999).
- [121] P. B. van der Nat and K. Griffioen [the HERMES Collaboration], arXiv:hep-ex/0501009.
- [122] X. D. Ji and F. Yuan, Phys. Lett. B **543**, 66 (2002).
- [123] A. V. Belitsky, X. D. Ji and F. Yuan, Phys. Rev. D **69**, 074014 (2004).
- [124] D. Boer, AIP Conf. Proc. **675**, 479 (2003).
- [125] J. C. Collins and A. Metz, Phys. Rev. Lett. **93**, 252001 (2004) [arXiv:hep-ph/0408249].
- [126] X. D. Ji, J. p. Ma and F. Yuan, Phys. Rev. D **71**, 034005 (2005); Phys. Lett. B **597**, 299 (2004) [arXiv:hep-ph/0405085].
- [127] D. Boer and W. Vogelsang, Phys. Rev. D **69**, 094025 (2004).
- [128] M. Anselmino, M. Boglione and F. Murgia, Phys. Lett. B **362**, 164 (1995) [arXiv:hep-ph/9503290].
- [129] M. Anselmino, M. Boglione and F. Murgia, Phys. Rev. D **60**, 054027 (1999) [arXiv:hep-ph/9901442].
- [130] R. D. Klem *et al.*, Phys. Rev. Lett. **36** (1976) 929; W. H. Dragoset *et al.*, Phys. Rev. D **18** (1978) 3939; S. Saroff *et al.*, Phys. Rev. Lett. **64** (1990) 995; B. E. Bonner *et al.*, Phys. Rev. D **41** (1990) 13.
- [131] A. Ogawa [STAR Collaboration], Proceedings of the 16th International Spin Physics Symposium, arXiv:hep-ex/0412035.
- [132] C. Aidala [PHENIX Collaboration], Contribution to the “12th International Workshop on Deep Inelastic Scattering (DIS 2004)”, arXiv:hep-ex/0410003.
- [133] A. Metz, Invited talk at the “16th International Spin Physics Symposium”, arXiv:hep-ph/0412156.
- [134] U. D’Alesio and F. Murgia, private communication; U. D’Alesio and F. Murgia, Phys. Rev. D **70**, 074009 (2004).
- [135] M. Boglione, E. Leader, Phys. Rev. D **61**, 114001 (2000).
- [136] T. Henry, J. Phys. G **30**, S1287 (2004).
- [137] X. Artru, J. Collins, Z. Phys. C **69**, 277 (1996); D. Boer, R. Jakob, P. J. Mulders, Phys. Lett. B **424**, 143 (1998).
- [138] M. Grosse Perdekamp, A. Ogawa, K. Hasuko, S. Lange, V. Siegle, Nucl. Phys. A **711**, 69 (2002).

- [139] M. Anselmino, V. Barone, A. Drago, N. N. Nikolaev, Phys. Lett. **B594**, 97 (2004).
- [140] M. Anselmino, M. Boglione, U. D’Alesio, E. Leader, F. Murgia, Phys. Rev. **D70**, 074025 (2004).
- [141] M. Anselmino, M. Boglione, and F. Murgia, Phys. Rev. D **60**, 054027 (1999); M. Boglione and E. Leader, Phys. Rev. D **61**, 114001 (2000).
- [142] M. Anselmino, M. Boglione, and F. Murgia, Phys. Lett. B **362**, 164 (1995); M. Anselmino and F. Murgia, *ibid.* **442**, 470 (1998); U. D’Alesio and F. Murgia, AIP Conf. Proc. **675** 469 (2003).
- [143] O. Martin, A. Schafer, M. Stratmann and W. Vogelsang, Phys. Rev. D **57**, 3084 (1998) [arXiv:hep-ph/9710300]; *ibid.* Phys. Rev. D **60**, 117502 (1999) [arXiv:hep-ph/9902250].
- [144] A. Mukherjee, M. Stratmann and W. Vogelsang, Phys. Rev. **D67**, 114006 (2003).
- [145] E. S. Ageev [COMPASS Collaboration], arXiv:hep-ex/0501073.
- [146] C. Bernet [COMPASS Collaboration], arXiv:hep-ex/0405073.
- [147] see: <http://www.jlab.org/sciprogram.html>
- [148] S. B. Gerasimov, Sov. J. Nucl. Phys. **2** (1966) 430 [Yad. Fiz. **2** (1966) 598]; S. D. Drell and A. C. Hearn, Phys. Rev. Lett. **16** (1966) 908.
- [149] see: http://www.jlab.org/div_dept/physics_division/talks/
- [150] B.Z. Kopeliovich and L.I. Lapidus, Sov. J. Nucl. Phys. **19**, 114 (1974).
- [151] N. Buttimore, B. Kopeliovich, E. Leader, J. Soffer and L. Trueman, Phys. Rev. **D59**, 114010 (1999).
- [152] C. Bourrely, J. Soffer, D. Wray, Nucl. Phys. **B91**, 33 (1975).
- [153] M.G. Ryskin, Yad. Fiz. **46**, 611 (1987); Sov. J. Phys. **46**, 337 (1987).
- [154] B. Z. Kopeliovich, B. G. Zakharov, Phys. Lett. **B 226**, 156 (1989).
- [155] B.G. Zakharov, Sov. J. Nucl. Phys. **49**, 860 (1989).
- [156] O. Jinnouchi *et al.*, arXiv:nucl-ex/0412053.
- [157] B.Z. Kopeliovich and T.L. Trueman, Phys. Rev. D **64**, 034044 (2001).
- [158] H. Okada, talk presented at the Spin 2004 Symposium, Trieste, Italy, to appear in the Proceedings.
- [159] N. Akchurin *et al.* [E581/704 Collaborations.], Phys. Rev. D **48** (1993) 3026.
- [160] I. Alexeev *et al.*, “Measurement of A_N in Elastic PP-Scattering with Small Momenta Transfers at $\sqrt{s} = 200\text{GeV}$ at RHIC”, to appear in the Proceedings of the Spin 2004 Symposium, Trieste, Italy.

- [161] P.D.B. Collins PDB, E.J. Squires, *Springer Tracts in Modern Physics* 44, Springer-Verlag, Berlin (1968); J.R. Forshaw, D.A. Ross, *Lecture Notes in Physics* 9, Cambridge University Press (1997).
- [162] T. L. Trueman, Contribution to the Spin 2004 Symposium, arXiv:hep-ph/0412242.
- [163] P.Gauron, E. Leader and B. Nicolescu, Phys. Rev. Lett. 54, 2656 (1985); A. Donnachie and P.V. Landshoff, Nucl. Phys. B267, 690 (1986).
- [164]
- [165] Expression of Interest for a Comprehensive New Detector at RHIC II, P. Steinberg et al., http://www.bnl.gov/henp/docs/pac0904/bellwied_eoi_r1.pdf
- [166] P. Taxil, J.M. Virey, Phys. Lett. B364, 181 (1995); Phys. Rev. D55, 4480 (1997).
- [167] J. D. Lykken, Snowmass 1996, eds. D. G. Cassel, L. Trindle Gennari, R. H. Siemann, p. 891; J. L. Lopez, D. V. Nanopoulos, Phys. Rev. **D55**, 397 (1997); K. S. Babu, C. Kolda, J. March-Russell, Phys. Rev. **D54**, 4635 (1996); A. E. Fraggi, M. Masip, Phys. Lett. **B388**, 524 (1996).
- [168] K. Agashe, M. Graesser, I. Hinchliffe, M. Suzuki, Phys. Lett. **B385**, 218 (1996); H. Georgi, S. L. Glashow, Phys. Lett. **B387**, 341 (1996).
- [169] E. J. Eichten, K. D. Lane and M. E. Peskin, Phys. Rev. Lett. **50**, 811 (1983).
- [170] F. Abe *et al.* [CDF Collaboration], Phys. Rev. Lett. **68**, 1104 (1992); *ibid.* **77**, 438 (1996).
- [171] M. Cvetič *et al.*, Phys. Rev. **D56**, 2861 (1997).
- [172] P. Taxil, J. M. Virey, Phys. Lett. **B383**, 355 (1996); Phys. Lett. **B441**, 376 (1998).
- [173] T. Gehrmann, D. Maitre and D. Wyler, Nucl. Phys. B **703**, 147 (2004) [arXiv:hep-ph/0406222].
- [174] J. Soffer, Nucl. Phys. (Proc. Suppl.) **64**, 143 (1998).
- [175] D. Boer, Phys. Rev. **D62**, 094029 (2000).
- [176] S. Kovalenko, I. Schmidt, J. Soffer, Phys. Lett. **B503**, 313 (2001).
- [177] G. L. Kane, G. A. Ladinsky, C.-P. Yuan, Phys. Rev. **D45**, 124 (1992).
- [178] A. Ogawa, V. L. Rykov, N. Saito, Proc. of the 14th Int. Symp. on Spin Physics, AIP Conf. Proc **570**, ed. T. Nakamura, p. 379 (2000); V. L. Rykov, arXiv:hep-ex/9908050.
- [179] R. Escrivano, E. Masso, Nucl. Phys. **B429**, 19 (1994).
- [180] A. Deshpande, Nucl. Physics **B105** (Proc. Suppl.), 178 (2002); G. Raedel and A. De Roeck *ibid.*, 90; J. Lichtenstadt *ibid.*, 86.
- [181] M. Stratmann, W. Vogelsang, Phys. Lett. B **386**, 370 (1996) [arXiv:hep-ph/9606346]; contribution to “Whitepaper on Electron Ion Collider”, February 2002, BNL-68933-02/07-REV.

- [182] S.D.Bass, Nucl. Physics **B105** (Proc. Suppl.), 56 (2002).
- [183] I. Abt, A. Caldwell, X. Liu and J. Sutiak, “A Detector for Forward Physics at eRHIC: Feasibility Study”, arXiv:hep-ex/0407053.
- [184] T. Roser, W. Fischer, M. Bai, F. Pilat, “RHIC Collider Projections (FY2005-FY2008)”, <http://www.rhichome.bnl.gov/RHIC/Runs/RhicProjections/pdf> (Last update on 16 August 2004).
- [185] T. Roser et al., “Acceleration of Polarized Beams Using Multiple Strong Partial Siberian Snakes”, Proceedings of European Particle Accelerator Conference, Lucerne, Switzerland, 2004.
- [186] J. Tojo et al., Phys. Rev. Lett. **89**, 052302 (2002).
- [187] O. Jinnouchi et al., RHIC/CAD Acc. Phys. Note 171 (2004).
- [188] T. Wise et al., and H. Okada et al., Proceedings of the Spin 2004 Symposium, Trieste, Italy, to be published; talks in <http://www.ts.infn.it/events/SPIN2004/>.
- [189] K. Adcox *et al.* [PHENIX Collaboration], Nucl. Instrum. Meth. **A499**, 469 (2003).
- [190] M. Allen *et al.* [PHENIX Collaboration], Nucl. Instrum. Meth. **A499**, 549 (2003).
- [191] L. Aphecetche *et al.* [PHENIX Collaboration], Nucl. Instrum. Meth. **A499**, 521 (2003).
- [192] K. Adcox *et al.* [PHENIX Collaboration], Nucl. Instrum. Meth. **A499**, 489 (2003).
- [193] M. Aizawa *et al.* [PHENIX Collaboration], Nucl. Instrum. Meth. **A499**, 508 (2003).
- [194] S. Adler [PHENIX Collaboration], arXiv:hep-ex/0502006.
- [195] S. S. Adler *et al.* [PHENIX Collaboration], arXiv:nucl-ex/0409028.
- [196] H. Akikawa *et al.* [PHENIX Collaboration], Nucl. Instrum. Meth. **A499**, 537 (2003).
- [197] S. S. Adler *et al.* [PHENIX Collaboration], Phys. Rev. Lett. **92**, 051802 (2004).
- [198] A. Bazilevsky *et al.*, AIP Conf. Proc. 675, 584 (2003).
- [199] C. Adler *et al.*, Nucl. Instrum. Meth. **A470**, 488 (2001).
- [200] The Proposal for a Silicon Vertex Tracker (VTX) for the PHENIX Experiment, <http://www.phenix.bnl.gov/plans.html>.
- [201] K.H. Ackermann, *et al.*, Nucl. Instrum. Methods **A499**, 624 (2003).
- [202] M. Beddo, *et al.*, Nucl. Instrum. Methods **A499**, 725 (2003).
- [203] C. Allgower, *et al.*, Nucl. Instrum. Methods **A499**, 740 (2003).
- [204] J. Adams, *et al.* [STAR Collaboration], Phys. Rev. **C70**, 054907 (2004).
- [205] T. Henry [STAR Collaboration], J. Phys. **G30**, S1287 (2004).

- [206] F. Sauli and A. Sharma, *Annu. Rev. Nucl. Part. Sci.* **49**, 341 (1999).
- [207] STAR Collaboration Decadal Plan, September 2003,
<http://www.star.bnl.gov/STAR/smd/whitepaper-18.pdf>.
- [208] E. Asakawa, J. i. Kamoshita, A. Sugamoto and I. Watanabe, *Eur. Phys. J. C* **14**, 335 (2000)
[arXiv:hep-ph/9912373].
- [209] K. H. Klimek [H1 Collaboration], arXiv:hep-ph/0305266.
- [210] M. Acciarri et al. [L3 Collaboration], *Phys. Lett. B* **503**, 10 (2001).